



Development of a Soft Robotics Diaphragm to Simulate Respiratory Motion

J. (Jeroen) van Dorp

MSc Report

Committee:

dr.ir. H. Naghibi Beidokhti
dr.ir. M. Abayazid
dr.ir A.Q.L. Keemink
prof.dr.ir. G.J.M. Krijnen

July 2019

024RAM2019
Robotics and Mechatronics
EE-Math-CS
University of Twente
P.O. Box 217
7500 AE Enschede
The Netherlands

Summary

The respiratory-induced motion of the liver introduces challenges in the medical field. This motion makes it difficult to do needle insertions at the right position and to aim the radiation beam at for example a tumour in the liver. Nowadays MRI is increasingly used for guidance during the aforementioned procedures, because it gives improved contrast on soft tissues and can therefore aid the navigation of the needle or radiation beam.

In this project a device is made that can simulate this respiratory-induced motion of the liver. This is done with the purpose that other robotic systems can be tested on it and that clinicians can practice procedures on the device. The device is made such that it is MR compatible and can fit inside an MRI machine.

For the design of the device close attention is paid to the human diaphragm. This resulted in a soft robotics diaphragm incorporating two different types of actuators. With these actuators it is able to simulate motion comparable to those of the human diaphragm. These actuators have first been designed and characterized. After that they have been implemented in the diaphragm, which has again been characterized. Next to the diaphragm a liver phantom and a stand to support the diaphragm have been designed.

Based on the characterization of the diaphragm a model has been made that can predict the behaviour of the diaphragm. Also a controller has been made that can set different motion profiles for the diaphragm. The main focus has been simulating AP and SI motion. For both it is able to generate a motion within a realistic range and speed.

Preface

I would like to thank my supervisors Hamid and Momen for, first of all, introducing me to 'the world of soft robotics', with which I was not familiar. I would also like to thank them for the fruitful discussions about this project and their advice. The technicians Sander and Henny must also be thanked for their input on the design of the molds for the actuators and the other parts that have been custom made for this project. Without that advice the fabrication of the actuators would have taken a considerable longer time. Someone I should also thank is Jan Lenssen for designing and fabricating the Arduino shield that I and a lot of other students used to control the pressure regulators.

Jeroen van Dorp
Enschede, 24th of June 2019

Contents

1	Introduction	1
1.1	Background of the project	1
1.2	Anatomy	1
1.3	Research question and sub questions	3
2	Approach and conceptual designs	4
2.1	Requirements	4
2.2	Approach and assumptions	4
2.3	Initial concept	5
2.4	Soft robotics	5
2.5	Elasticity of the lungs	8
2.6	MR compatibility and safety	8
2.7	Concepts	9
2.8	Dimensions	11
2.9	Controller, software and user interface	11
2.10	Summary and next step	12
3	Design, production and testing of actuators	13
3.1	Pneumatic artificial muscle	13
3.2	Pneunet bending actuator	16
3.3	Vacuum actuated muscle inspired structure	20
3.4	Summary and next steps	29
4	Design, production and characterization of the diaphragm	30
4.1	Stand	31
4.2	Liver phantom	31
4.3	Design, analysis and production of the diaphragm	32
4.4	Testing	37
4.5	Characterization for the models	41
4.6	Summary and next steps	51
5	Model of the diaphragm and control	52
5.1	Model	52
5.2	Control	55
5.3	Validation of control	57
5.4	Summary	60
6	Conclusion and recommendations	62

6.1	Discussion of the specifications	62
6.2	Recommendations for future work	63
6.3	Answers to the research questions	64
7	Appendix	66
7.1	Schematic drawings of actuators	66
7.2	Code in the 20-sim controllers	69
	Bibliography	73

1 Introduction

1.1 Background of the project

The motion of the liver due to respiration during procedures introduces some challenges in the medical field. For example a tumour in the liver moves with respiration (Rohlfing et al., 2004). Inserting a needle at the right spot or aiming a radiation beam (Shirato et al., 2004) can therefore be rather difficult and requires the right timing for needle insertion and some practice in order to do it correctly.

In this thesis the research and development of a soft robotics diaphragm that can simulate the motion of the liver caused by respiration will be described. Such a system can be specifically interesting for testing other robotics systems such as robotic needle insertion devices and they can help in training clinicians for image guided percutaneous needle intervention for treatment and diagnostic purposes, such as ablation and biopsies. MR imaging is increasingly used for interventional procedures as it gives improved contrast compared to other imaging methods on soft tissues (more than for example ultrasound) and can therefore help with the 'navigation' during these procedures. Next to that MR imaging is non-invasive.

Previous work

There was already a device available to simulate this motion at the Robotics and Mechatronics group at the University of Twente, but there is the need for a more realistic and improved version. The device that was already available moves a liver phantom on a plate in 2 dimensions, this was done with help of soft-actuators and was MRI compatible (Naghbi et al., 2018). Also other work has been done to create respiratory simulators for liver motion. However, the motion was limited (Müller et al., 2007), it was not MR compatible (Abayazid et al., 2018) or motion itself was correct, but not dynamic (Lee et al., 2010). A complete new design will be made where the liver phantom is moved by a soft robotics diaphragm, similar to what would happen in the human body, where a large part of the respiration is facilitated by the motion of the diaphragm (Marieb and Hoehn, 2007). The human body will therefore be the main source of inspiration for the design of the device. For this reason the anatomy of the human diaphragm will be briefly explained next.

1.2 Anatomy

1.2.1 Liver

The liver is the largest internal organ of the human body (Marieb and Hoehn, 2007) and hepatic cancer has been one of the leading causes of cancer deaths (Bray et al., 2018).

The liver can have different shapes and dimensions, but it is at least sex and age related and some data suggests it is also region, BMI and/or alcohol consumption related (Wolf, 1990; Chouker et al., 2004; Verma et al., 2010; Kratzer et al., 2003). Different data can be found, but the average volume of the liver should be 1086 cm^3 and 1006 cm^3 for respectively male and female. Whereas an unhealthy liver can be much larger, cases of livers with a volume of almost 4000 cm^3 can be found for patients with Chronic Hepatitis for example (Nagasue et al., 1987). The diameter measured from left to right is somewhere between 10.6 cm and 25.3 cm, for back to front that is somewhere between 6.2 cm and 20 cm and the height is somewhere between 13.8 cm and 24.9 cm (Verma et al., 2010).

1.2.2 Diaphragm

The diaphragm separates the pleural cavity from the abdomen. The liver is right underneath the diaphragm, as can be seen in figure 1.1, and it is partially attached to it with ligaments.

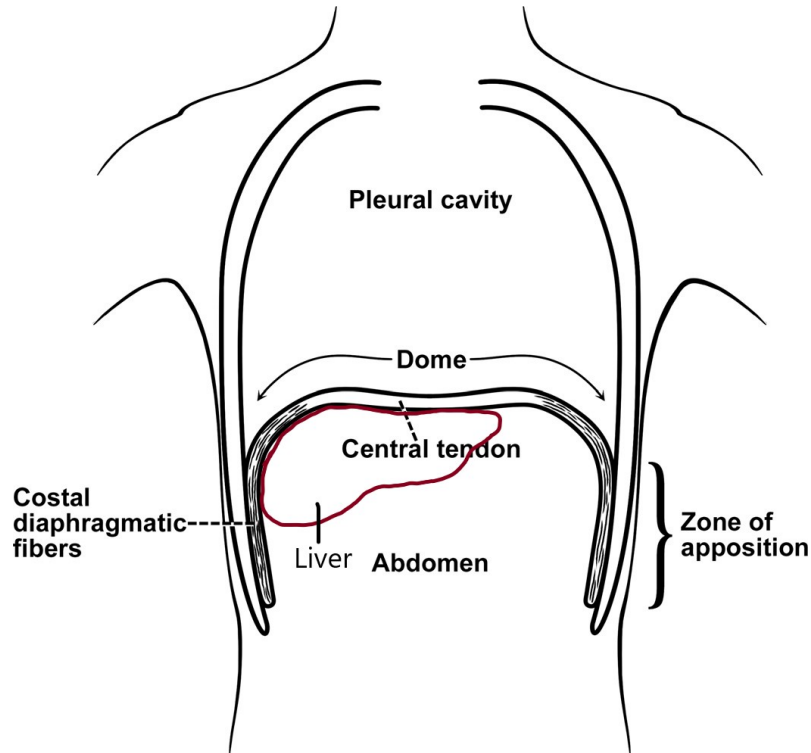


Figure 1.1: Schematic drawing of the diaphragm (Troyer and Wilson, 2016) and the liver

Two muscle groups can be identified in the diaphragm, the costal muscles that are on the sides attached to the ribcage (the zone of apposition) and the crural muscles that are around the esophagus (Pickering and Jones, 2002). For respiration they work synchronously together, but for example during swallowing they do not. By contracting the costal muscles the diaphragm can move downward. Relaxing those muscles again will cause the diaphragm to move upward again. This is due to the elasticity of the lungs. A motion of the ribcage can also be identified which helps facilitating the motion of the diaphragm and respiration in general. For the design of the soft robotics system only the diaphragm itself will be looked into, the motion of the ribcage will be neglected.

1.2.3 Motion of the liver

The motion of the liver is mainly caused by the motion of the diaphragm. The diaphragm moves downwards to expand the pleural cavity, such that the lungs can be filled with more air, and while doing this it pushes the liver downwards. Due to this and the surrounding tissue and organs of the liver a three dimensional motion can be distinguished for the liver. Often more relevant in the medical field, especially when looking at liver cancer treatment, is the fact that this also causes a tumour in the liver to move. The motion that can be identified is somewhere between 0 mm to 8 mm, 4 mm to 14 mm and 2 mm to 8 mm respectively for left-right (ML), up-down (cranial-caudal or SI) and front-back (anterior-posterior or AP). With a frequency between 0.25 Hz to 0.3 Hz (Kitamura et al., 2003). An example of this motion can be seen in figure 1.2. These directions are assuming the patient in upright position. Important is that the motion in anterior-posterior direction really differs for different locations in the liver. Towards the middle of the abdomen the motion can be factor two larger compared to the side of the abdomen (Hu et al., 2017). Also others factors like heartbeats and the motion of the stomach can cause significant motion (in AP and SI direction on average 2 mm), as mentioned in some studies into the motion of the liver (Shirato et al., 2004; Kitamura et al., 2003).

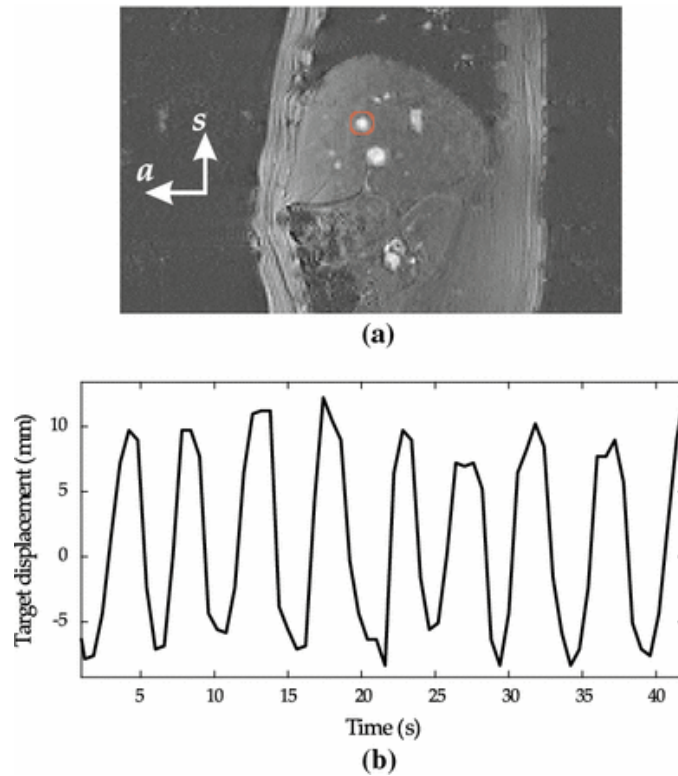


Figure 1.2: SI motion of a tumour in the liver, indicated by the red circle (Abayazid et al., 2018)

1.3 Research question and sub questions

The main research question is: How to develop an MR compatible liver phantom that is actuated by a bio-inspired diaphragm to simulate respiratory-induced motion? Several sub questions that need to be answered are:

- How can the device be made MR compatible?
- How can the diaphragm be inspired by the human anatomy?
- What kind of actuators can be used to develop this diaphragm?
- How can a realistic respiratory motion be generated?
- How can the device be made such that it can be used for testing purposes of robotic systems and training purposes for clinicians/surgeons?

By answering these questions it should be possible to develop a device that simulates the respiratory motion of the liver.

2 Approach and conceptual designs

The starting point of the design will be the human diaphragm. By identifying what kind of mechanisms the human diaphragm uses to achieve its motion inspiration for the design of the robotic diaphragm can be acquired. Eventually the goal for the robotic diaphragm is to mimic the respiration motion and perhaps similar mechanisms can be used for that.

2.1 Requirements

Based on the research that has been done the requirements for the robotic diaphragm can be determined. The physical aspects, safety and usability are important for the device. Taking this into account the following requirement can be derived:

- The robot needs to be MR safe and sufficiently MR compatible
 - The part that goes inside the scanner bore should not cause artefacts that can obscure the region of interest
 - The system needs to fit inside a scanner with a bore of 50 cm, which is assumed to be the smallest MRI scanners that is commonly used for this application
- The motion of the liver needs to be accurate
 - Between 0 mm to 8 mm in left-right (ML) direction
 - Between 4 mm to 14 mm in up-down (SI) direction
 - Between 2 mm to 8 mm in front-back (AP) direction with preferably the possibility of creating a difference between left and right
 - Frequency that should be achievable is 0.25 Hz to 0.3 Hz
 - *Optional: taking into account the motion of for example heartbeats*
- The set-up will represent a patient in supine position
- The design of the set-up will be inspired by the human anatomy
- The user interface should be such that it is usable by clinicians

2.2 Approach and assumptions

With the requirements set the approach is to first explore the possibilities for actuators that can be used for the diaphragm, where the main focus will be soft robotics because of the MR compatibility and compliance. Based on this concepts for the diaphragm will be thought of to give a direction for the design of the actuators. This will lead to the design of the actuators which will be used to realize the diaphragm. These actuators can be tested and characterized to get an insight in if and how they will function in the diaphragm. First focus will lie on developing the device for one directional motion. Thus allowing the liver phantom to be moved up and down (SI motion) in a manner that is similar to what happens in the human body. After that is accomplished the device will be developed further to be able to move the liver phantom in all directions. The approach for further development of the device such that it functions in more directions will be determined based on the results of the first design. Next focus will lie on improving the control of the motion and making a user interface that is easy to operate, also for clinicians.

It is decided to only look at the diaphragm itself and not the motion of the ribcage to limit the design options. Also external forces on the liver will not be taken into account from for example

the surrounding tissues. The diaphragm itself will already give a lot of design freedom as will become clear in the following chapters.

2.3 Initial concept

It has been identified that the human diaphragm is in a dome shape when it is in a relaxed state and that it is in a more flattened shape when contracted. So for the soft robotics diaphragm actuators to reach these two states need to be present. Useful actuators to look into are therefore actuators that can bend (to go into the relaxed dome shape) and actuators that can contract (to flatten the diaphragm). Since the device also needs to be MR compatible actuators without metal are preferred, this makes soft robotics, ideal as will be explained next.

2.4 Soft robotics

Soft robotics have been around for some time already, but definitely not all possibilities of them have been explored yet (Trivedi et al., 2008). What distinguishes soft robotics from 'normal' robotics is the fact that the actuators are soft. Most soft robotics actuators do not require any metal for example, which is often the case for most other actuators. The fact that it does not require any metal means that it is more easily possible to create MR compatible robots. That is what makes it particularly interesting in the case of designing a soft robotics diaphragm which needs to be used inside an MRI device. Another advantage of soft robotics is the compliance, which most soft robotics actuators have. This makes it ideal for interaction with humans (Agarwal et al., 2016; Yap et al., 2017), but it can also be beneficial for the development of the soft robotics diaphragm as the real human diaphragm has some compliance. Several types of soft robotics actuators that can be interesting for the design of the soft robotics diaphragm are looked into. They will be introduced and explained next.

2.4.1 McKibben actuators or pneumatic artificial muscles

A soft robotics actuator that has been in use for multiple purposes for quite some time is the McKibben muscle, also known as the pneumatic artificial muscle (PAM). A schematic drawing of an artificial muscle can be seen in figure 2.1.

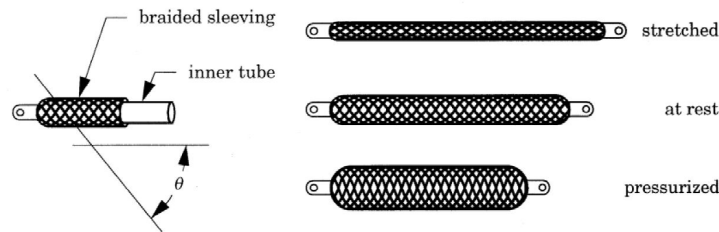


Figure 2.1: Schematic drawing of an artificial muscle (Daerden and Lefeber, 2002)

In the 1950's and 1960's it was developed in artificial limb research (Chou and Hannaford, 1996; Pritts and Rahn, 2004). These actuators are built up out of an expanding tube surrounded by braided cords. When the tube expands by applying pressure to it (via some kind of pump) it pushes against the braided cords/mesh, which cannot expand. This causes the whole 'muscle' to contract. Several factors influence the working of the artificial muscles, such as the friction of the mesh on the bladder, the type of material of the bladder and the geometry of the mesh. In general it can be said that when non uniformity of the mesh and friction is neglected and thin walls are chosen real world actuators can be described by equation 2.1 (Obiajulu et al., 2013).

$$F = P \frac{\pi D_0^2}{4} (3 \cos^2 \theta - 1) \quad (2.1)$$

Where D_0 is the initial diameter of the mesh and θ being the angle of the mesh as can be seen in figure 2.1, which can be further defined as.

$$\text{contraction} = \frac{l_0 - l}{l_0} = 1 - \frac{\cos(\theta)}{\cos(\theta_0)} \quad (2.2)$$

This means force is depended on the actual pressure in the actuator, but also the current state/elongation/angle of the mesh, which means that the actuator is somewhat compliant, making precise open loop control hard. Based on this important design parameters are:

- Diameter of the bladder
- Angle of the mesh in unactuated state
- Length in unactuated state

The fact that these actuators contract makes them ideal to simulate muscles. Examples of their use are robotic hands (Faudzi et al., 2018) and cardiac compression devices (Obiajulu et al., 2013).

2.4.2 Fluidic elastomer actuators

Fluidic elastomer actuators can be made in different shapes and sizes, but the essence is usually the same. It is a soft stretchable material with compartments in it that can filled with air (or some other fluid), and example can be seen in figure 2.2. By controlling how much every compartment is filled with air it is possible to extend and bend these actuators in different directions. It is usually only possible to bend and extend these actuators, contracting with a positive pressure of the fluid inside can only be done by McKibben-like actuators (Suzumori et al., 1992; Marchese et al., 2015). Some examples of their use are replicating a manta (fish) (Suzumori et al., 2007), caterpillars (Trimmer et al., 2006) or assistive gloves for rehabilitation (Yap et al., 2017). The way in which they move and the forces and torques they can generate depend on the design of the actuator. In general can be said that with thicker walls smaller forces and torques can be generated with the same pressure inside the actuator. However due to the fact that larger pressure can be applied before extreme ballooning or rupturing the actuator when the walls are thicker, usually the maximum force and/or torque an actuator can apply becomes larger with a larger wall thickness, but this again largely depends on the design/geometry of the actuator. Also the Youngs modulus of the material that is used makes a difference. (Sun et al., 2013).

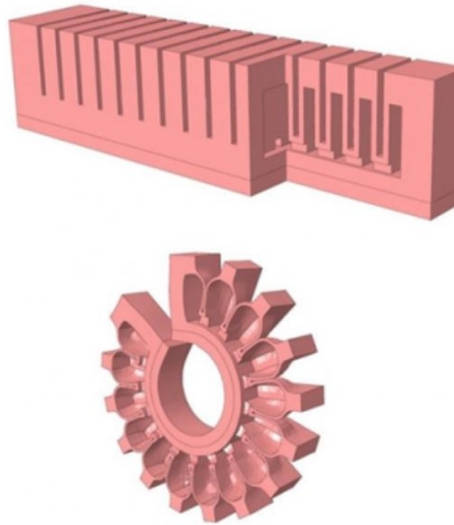


Figure 2.2: An example of a fluidic elastomer actuator, a Pneunet bending actuator (SoR, 2018)

2.4.3 Vacuum actuated muscle inspired pneumatic structures

Vacuum actuated muscle inspired pneumatic structures (VAMPS or vacuum actuators) differ from the previously mentioned actuators in the way that they are actuated. Whereas the other two that are mentioned are actuated by positive pressure (compared to the surroundings) a VAMPS is actuated with a vacuum. They are mostly based on the principle of mechanical instability and contract with a vacuum applied to them because of buckling of their internal structure. Their internal structure is also key in the way they buckle. For example contraction in a linear manner can be created, but also buckling causing a rotation in the actuator can be created by different structures. Previous research has shown that the actuation stress is in the same order of magnitude as that of human muscles and that as long as the geometric feature ratios are kept the same the behaviour of the actuator will stay the same. This means scaling up or scaling down a design should be fairly easy, making it ideal to work with (Yang et al., 2016, 2015). An example of a contracting VAMPS can be seen in figure 2.3.

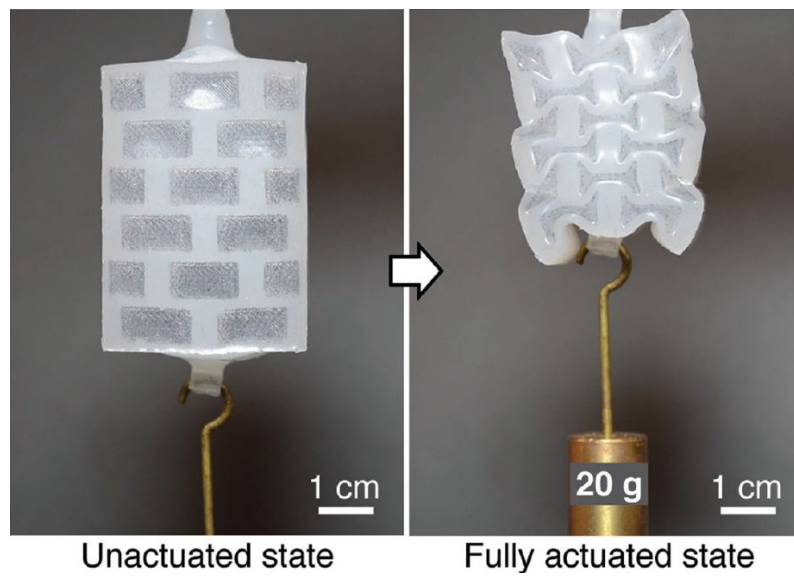


Figure 2.3: Example of a vacuum actuated muscle inspired pneumatic structure (Yang et al., 2016)

The maximum loading stress is a function of the geometric features and the Young's modulus of the material that is used where it linearly scales with the Young's modulus. In general it can be said that the force (T) the actuator can generate is linearly dependent on the pressure (P) and the cross sectional area (A) of the active chambers in the actuator in perpendicular plane of actuation (equation 2.3). The strain (s) of the actuator (equation 2.4) is a function of the differential pressure (ΔP) and the loading stress (σ). This strain is roughly linearly dependent on the differential pressure up until some critical pressure that is determined by the geometric features and that is again linearly dependent on the Young's modulus of the material used. At this critical pressure the actuator is almost completely buckled, hence increasing the pressure difference will barely result in any motion.

$$T = PA \quad (2.3)$$

$$s(\Delta P, \sigma) = \frac{L(\Delta P, \sigma) - L(0, \sigma)}{L(0, 0)} \quad (2.4)$$

The mentioned relation between Young's modulus, geometric features and differential pressure give at least the following design parameters:

- For the same geometric features, differential pressure and Youngs modulus the output force of the actuator scales with the cross-sectional area of the actuator.
- The critical pressure with the same geometric features can be altered by choosing a different Youngs modulus.
- In general the behaviour of the actuator can be changed by changing the geometric features.

VAMPS have some advantages over the positive pressure actuators; they are safer, since there is a smaller/virtually no chance on rupturing/exploding actuators. They are robust, because small holes may close themselves due to the negative pressure and they can be compacter. The last one is especially true when compared to the McKibben muscles which expands in radial direction when contracting, vacuum actuators just contract without expanding in any direction, at least in the ideal case. Some research is being done into these actuators, but positive pressure actuators are found more often than VAMPS (Li et al. (2017)), which makes it interesting, but also more difficult, to look at for the robotic diaphragm.

2.5 Elasticity of the lungs

At rest the human diaphragm has a dome shape, because it is pulled upward by the elasticity of the lungs. So, it might be interesting to look at elastic materials that are MR compatible that can help replicate this elasticity of the lungs. If for example the soft robotics diaphragm would only be realized by contracting actuators getting the diaphragm into that dome shape might be difficult. An elastic material that is preformed in a dome shape could be useful for this. A material that might be used for this application is nitinol. Nitinol is a shape memory alloy, which means that the material can be deformed and stay in the deformed shape, but upon heating it will return to its old shape. Heating without it disturbing the MR image will be hard, so this is not ideal to use in the robotic diaphragm, but actuators have been made based on this principle (Jani et al., 2014). Some of these alloys also demonstrate super elasticity, which means that they can easily deform when a force is applied to it, but it can go back to its old form when it is released (Szold, 2006). It is an alloy that is often used in medical instruments and for example stents that can be placed in blood vessels. Even though they can introduce some artifacts on the MR image, often nitinols are MR compatible (Fischer et al., 2004; Holton et al., 2002). This superelastic material can also be used the other way around, so to flatten the diaphragm again. If for example only bending actuators are used it is possible to use the superelastic material that was preformed into a straight/stretched state to let the diaphragm go back to that state.

2.6 MR compatibility and safety

MR safety and compatibility of the robotic diaphragm will be essential as it will be used in an MRI device by clinicians. Next to that it is desired that a needle insertion device can be tested inside an MRI machine side by side with the robotic diaphragm.

MR safe usually refers to the device being usable in a MR environment without introducing any extra danger for patients or people working near it (MRS, 2008). MR compatibility goes one step further, since there it is also defined what else the device might cause, besides any safety issues. There are several degrees of MR compatibility ranging from usable inside the scanner near the area of interest when it is turned on to only being used outside the scanner (Yu and Riener, 2006; Tsekos et al., 2008). In this case the robot needs to be able to be inside the scanner while it is scanning. It is allowed to cause some artefacts, but they are not allowed to be near/obscure the tumor in the liver phantom. Since the whole system will be close to the tumor, as the tumor will be inside it this needs to be taken into account. Next to all this there will also be a size constraints as the device actually needs to be able to fit inside a scanner bore and preferably

it should not take up more space than an average human. This should allow for the 'normal' instruments and tools to fit inside the machine just like when there would be a patient inside.

2.7 Concepts

Previously some potentially useful actuators and materials were identified. As mentioned two states of the diaphragm can be identified. Both can be seen in figure 2.4; the bend/dome state at the top (exhalation) and the straight/contracted state at the bottom (inhalation).

Designs made of only fluidic elastomer actuators are potentially an option, since the dome shape can be created with that. Straightening the diaphragm with only fluidic elastomer actuators is difficult however, as they can only actively elongate or bend. For straightening the diaphragm PAM's or VAMPS are potentially usable. Assuming the diaphragm is already in a dome shape it can be straightened by letting those actuators contract. The downside of PAM's and VAMPS is that it is not possible to actively bend them. Thus getting the diaphragm back in a dome shape will be more difficult with those actuators. Getting the diaphragm back in the dome shape is something that can potentially be done with help of superelastic materials. If that material is pre-shaped in a dome shape, they can while the diaphragm is at 'rest' keep it in a dome shape, but when the diaphragm is straightened it can deform with it. Based on these ideas several concepts have been chosen to further pursue and potentially develop.

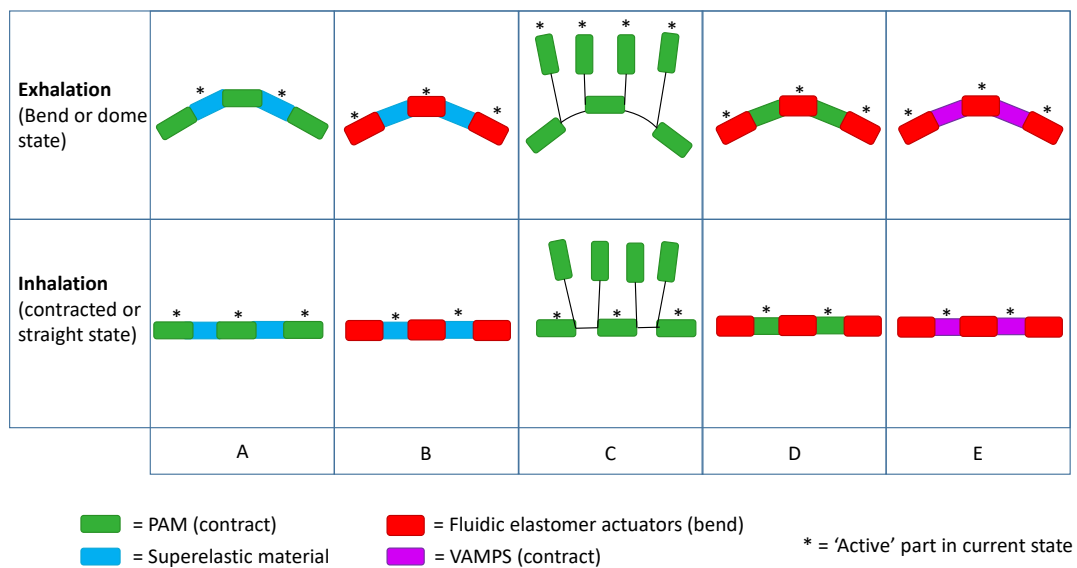


Figure 2.4: Multiple for the soft robotics diaphragm with different configurations of actuators. The diaphragm is represented the same way as it is in figure 1.1

2.7.1 Combination of PAM and superelastic material

This design is more or less inspired by the human body, it can be seen in figure 2.4 as A. It will feature PAM's to straighten the diaphragm, comparable with the costal muscles. Superelastic material embedded in the diaphragm will make sure it will move into the dome shape once it is relaxed. There are some issues that might cause problems for this design. The first being that the elastic material might not be able to exert enough force to get the diaphragm back in dome shape while also moving the liver phantom. Another thing is the fact that the superelastic material might cause artefacts on the MR image. Also, incorporating artificial muscles into a diaphragm might be difficult, due to the mesh.

2.7.2 Combination of fluidic elastomer actuators and superelastic material

This design will be in principle the opposite of the previously mentioned concept where PAM and superelastic material are combined. In this case the fluidic elastomer actuators (in figure 2.4 B) will make the diaphragm bend and the superelastic material will generate the elasticity with which the diaphragm will move downwards. The downside of this design is that the force with which the diaphragm contracts cannot be well controlled. The advantage of this design is that is probably easy to produce. It should be a sheet with on top of that bending actuators and in the sheet there should be superelastic material.

2.7.3 Only PAM

This design probably has the most flexibility in terms of controllability, it can be seen in figure 2.4 as C. It will have only pneumatic artificial muscles, again those that are embedded in the diaphragm which can straighten the diaphragm, representing costal muscles. In order to get the diaphragm in the dome shape there is another set of PAM's. These will simulate the elasticity of the lungs. The advantage of this design is that the going into dome shape is well controllable as well and it is possible to do that with some force. This last part is a real advantage since the phantom liver needs to be attached to the diaphragm in order for it to move with the diaphragm. This will require some force which can be generated by the PAM's at the top. Assuming for both the straightening PAM's and the PAM's that will pull the diaphragm back into its dome shape it should be possible to control all PAM's individually. Resulting in good controllability in all directions that even makes it possible to move the diaphragm asymmetrically.

2.7.4 Combination of PAM and fluidic elastomer actuators

Another option (D in figure 2.4) is combining the PAM's with fluidic elastomer actuators. Where the PAM's will, like in the other designs, be used to straighten the diaphragm and thus push the liver phantom. Embedded in the diaphragm will be fluidic elastomer actuators which will allow it to bend, thus letting it go into the dome shape. Pneumatic bending actuators are potentially suitable for this (SoR, 2018). A downside might be that it will be hard to manufacture this diaphragm as it requires PAM's and fluidic elastomer actuators to be combined and the other issue is that it requires more pumps. For a smooth operation it would be desired to be able to control the PAM's and pneumatic actuators simultaneously, but that requires at least two pumps and preferably even more to control different groups of the PAM's and pneumatic actuators separately simultaneously, which might be a necessity to be able to get controllability in three dimensions.

2.7.5 Combination of VAMPS and fluidic elastomer actuators

This option is comparable to where the PAMs and fluidic elastomer actuators are used, but the PAMs are replaced by VAMPS (see E in figure 2.4). An advantage of this is that it should be easier to combine the two types of actuators into one diaphragm. All actuators can be made from one piece of elastomer and do not require any other materials in them. The downside for this type of diaphragm is that also vacuum regulators and a vacuum pump are necessary, which are not necessary for all the other concepts.

2.7.6 Issues for all designs

In all designs there is the issue that the liver can be pushed by the diaphragm, but it also needs to move back with the diaphragm. So a spring-like effect is needed for that. An option would be attaching it to the diaphragm or maybe have rubber bands pushing it back into the diaphragm. An issue with this might be that the phantom liver might deform in some unwanted way and it will also influence the motion of the diaphragm. What might be an option as well is hanging the liver in a stand such that gravity and the constraints always push it against the diaphragm. This

is something that will be looked into when the design of the diaphragm is made. Another issue with soft robotics is the compliance of the actuators. Constraints and external loads largely influence the behaviour of the actuators and eventually the diaphragm. This will make it difficult to test the actuators and predict what they will do when used in a diaphragm. It will also be difficult to compare the final diaphragm design with a human diaphragm based on anything else than motion. Defining anything like a mechanical impedance of the human diaphragm itself is nearly impossible as that depends on the muscles in the diaphragm, the state these muscles are in, the thorax and its muscles, the lungs, etc. For the soft robotics diaphragm this will depend on the constraints of the diaphragm, manufacturing errors, perhaps some hysteresis, etc. A straight comparison based on force or impedance will therefore be hard.

2.8 Dimensions

As mentioned previously the dimensions of the device should not exceed that of a normal human, since it should not take up more space in an MRI. A stand needs to be designed holding the diaphragm in place. This needs to be sturdy such that no unwanted motions come from the stand. This design will be made based on the experience of the production of the actuators and the results of the experiments with them.

2.9 Controller, software and user interface

In order to control the actuators and eventually the diaphragm hardware and software is needed. In order to control the pressure and vacuum in the actuators pressure and vacuum regulators are needed. Also hardware to interface between the software and the regulators is needed. From previous projects at the Robotics and Mechatronics group Festo pressure regulators are available. These are VEAB-L26-D7-Q-V1-1R1 and VEAB-L-26-D2-Q4-V1-1R1 for positive pressure and VEAB-L-26-D14-Q4-V1-1R1 for vacuum. Next to that MHE2-M2H-3/26-QS-4 solenoid valves from Festo are available. These can be used to split the output of the regulators over multiple tube and thus actuators. This however does only allow for sequential control of actuators that are connected to the same regulators via a solenoid valve. Also an Arduino shield is already available (figure 2.5) that allows for four regulators to be controlled and read-out simultaneously and four solenoid valves to be controlled.

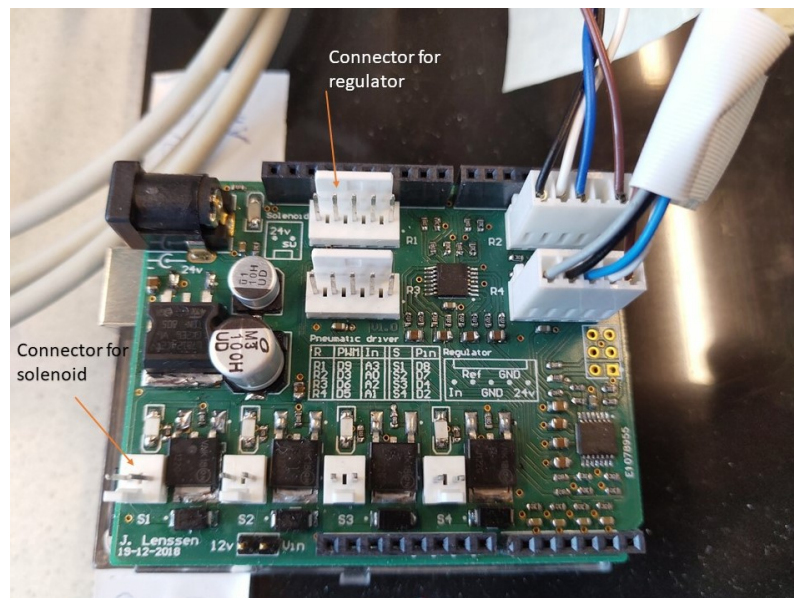


Figure 2.5: The Arduino shield, with two regulators connected

Schematically this set-up is depicted in figure 2.6. Since the control is essentially done by an Arduino there are multiple options to make the software. Especially useful if this set-up is going to be used in for example hospitals. Eventually a user interface will be made such that it can run without the need of Matlab or any programming skills for the user. Customizable breathing loops should be possible.

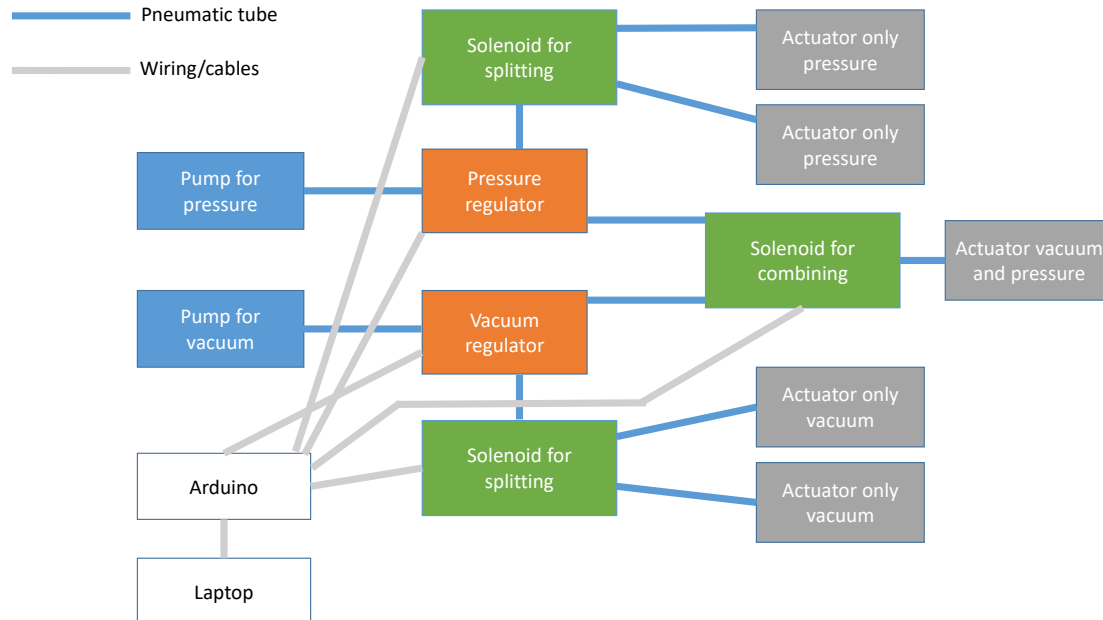


Figure 2.6: Control set-up depicting several options of controlling several types of actuators via an Arduino with a laptop. Blue lines depicting air hoses and grey lines depicting signal wiring.

2.10 Summary and next step

Several potentially useful actuators have been identified in this chapter, these are the pneumatic artificial muscle, the fluidic elastomer actuator and vacuum actuated muscle inspired structures. In the next chapter these actuators will be designed and characterized with the requirements and assumption that are set and done in mind. Based on the outcome of that a decision will be made about which concepts of the diaphragm will be pursued.

3 Design, production and testing of actuators

In this chapter the design of the actuators, their FE models, molds, the production and testing will be discussed. The process from design to characterization will be explained for one actuator completely, after which this is done for the next actuator. The first assumption for the diaphragm is that it is around 200 mm by 300 mm when contracted, based on this several actuators are made as a proof of concept. These dimensions are chosen based on the liver phantom size and the maximum dimensions the final device should have. The start for every actuator is that it is modelled and an FE model is made from that, if that is feasible. Based on the outcome of the FE model dimensions can be adjusted. Next the actuator can be fabricated and characterized to get an insight in how they can be used in the diaphragm. For all actuators there is chosen to make them out of Ecoflex 00-50 and 00-30, because at the lab there was already experience with this material and this material is also often used in designs found in literature (Yang et al., 2016; SoR, 2018). Eventually mostly Ecoflex 00-50 is used, because this is easier to work with than Ecoflex 00-30 due to the higher viscosity.

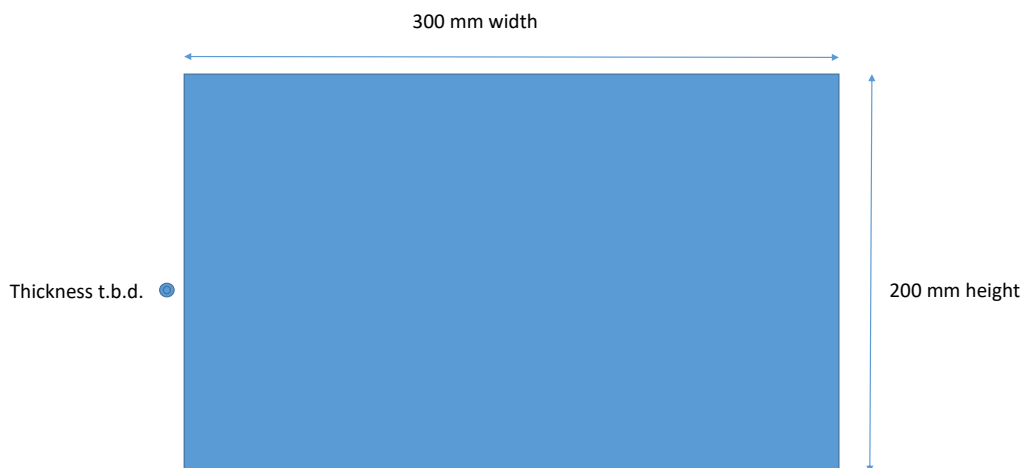


Figure 3.1: The initial dimensions chosen for the diaphragm as well as the naming of the dimensions

3.1 Pneumatic artificial muscle

The purpose of this actuator is that it is able to contract. It can then be used to either let the diaphragm go into the dome shape (see figure 2.4 C) or to let the complete diaphragm contract and straighten (see figure 2.4 A, C and D). The important design parameters were previously identified as:

- Diameter of the bladder
- Angle of the mesh in unactuated state
- Length in unactuated state

3.1.1 Actuator design

The most important part of this actuator is the bladder. This is a bladder that can be made from an elastomer and is schematically represented in figure 3.2. In this case there is chosen for Ecoflex 00-50 and Ecoflex 00-30. The starting point of this design is previous research (Obiajulu et al., 2013) where a wall thickness of 2 mm is suggested. The length of the bladder is chosen such that two of these actuators could be combined with other actuators in the final diaphragm and is set to be 93.75 mm, with the assumption of around 20% contraction this should result in a muscle of 75 mm. This means the first important design parameter, the length in unactuated state, is set.

Another design parameter is the diameter of the actuator. This is based on the mesh that is already available in the lab, which is 15 mm. The diameter of the bladder is therefore taken to be 14 mm. This also sets the last design parameter, because the mesh that is already available has an angle of 30 degrees. The force the actuator can generate is at first not the most important design parameter, because of two reasons. The first one being that if one actuator is not strong enough it should be possible to incorporate multiple actuators in parallel. Next to that it is hard to determine what the minimum required force would be when the actuator is incorporated in the diaphragm.

Furthermore the ends of the bladder are chosen to be 5 mm thick such that these do not expand much and one side has an opening for a pneumatic tube to be attached to. The actual attachment of the mesh can be done with a combination of wire and tape.

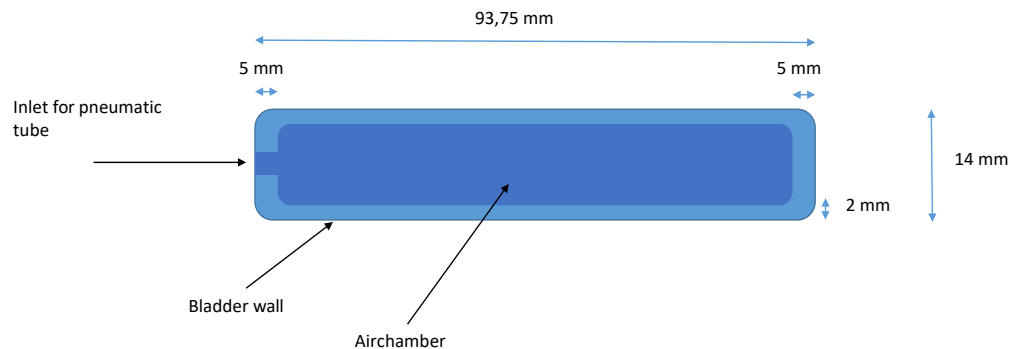


Figure 3.2: The bladder of the artificial muscles schematically represented

Making a representative finite element model for an artificial muscle including mesh and bladder is a rather difficult task and not as straightforward as for the other actuators. Simulating the interaction between the mesh and bladder is difficult. This can be simplified, but to create a meaningful model interaction between the mesh and bladder need to be taken into account as was also suggested in previous research (Tondur, 2012). Simplification of the model can be done by first characterizing the artificial muscle and afterwards fitting the FE model to it, but that defeats the design testing purpose of the model. So it has been decided not to further look into making a model for the artificial muscle, but instead focus on designing more actuators.

3.1.2 Mold and fabrication

Based on previous knowledge and insights from the technicians at the Robotics and Mechatronics group a mold has been designed. Based on the dimensions previously mentioned a CAD model in Solidworks has been made that could be 3D-printed by an Objet 3D printer. The mold consists out of three parts. Two for the outside of the bladder, these are translucent such that it can be seen how far the Ecoflex has already filled the mold and one for the inside of the bladder which is attached to the top of the mold. The mold with at the bottom of the image the fabricated bladder can be seen in figure 3.3.

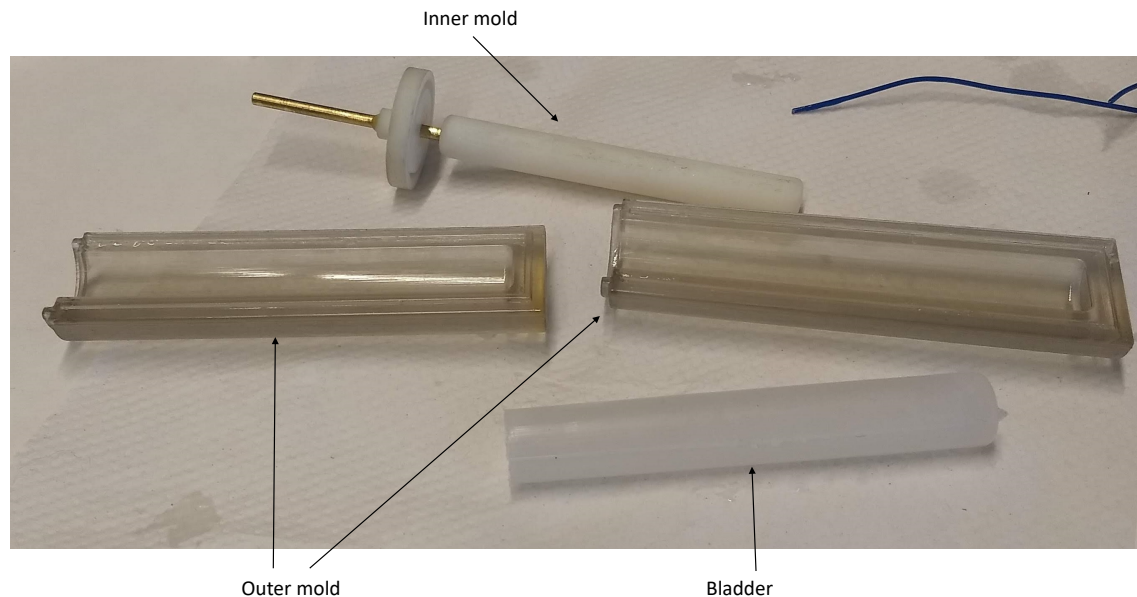


Figure 3.3: The mold of the Pneumatic artificial bladder with a finished bladder

Fabrication is done in several steps; Seal the mold with tape, prepare the Ecoflex as described on the packaging and pour it in the mold. It is essential that more than enough Ecoflex is prepared and that the degassing of the Ecoflex is done sufficiently. Next to that there is a small difference in how to make the actuator with Ecoflex 00-50 and Ecoflex 00-30. Ecoflex 00-50 cures faster than Ecoflex 00-30 and does not leak from the mold, whereas Ecoflex 00-30 does leak. Ecoflex 00-30 needs to cure for 20 min minutes before it is poured into the mold, this causes the viscosity of Ecoflex 00-30 to be higher and prevents leaking from the mold. After that the process is the same for both. The pneumatic hose can be attached with help of wire and duct-tape. The design of the mold does have an issue. The top does have some play and since the walls are thin it can happen that the wall thickness is not homogeneous. With the mesh around it this is not really an issue any more however. The implication for the design is however that if the basic design of the mold is kept the same it is almost impossible to have thinner walls, because chances are the walls will not fully close.

3.1.3 Characterization

The aim of this characterization is to find the relation between applied pressure to the artificial muscles and the contraction while unconstrained. This is done by applying pressure in steps of 0.1 bar up to the pressure where the muscles start leaking a lot of air. For every pressure step the length of the actuator is measured, see figure 3.4. Comparing the initial length of the actuator to the contracted length of the actuator results in the contraction.

For all artificial muscles holds that this design starts leaking at the part where the air hose is inserted and this leaking starts at around 0.6 bar, differing 0.1 more or less depending on the

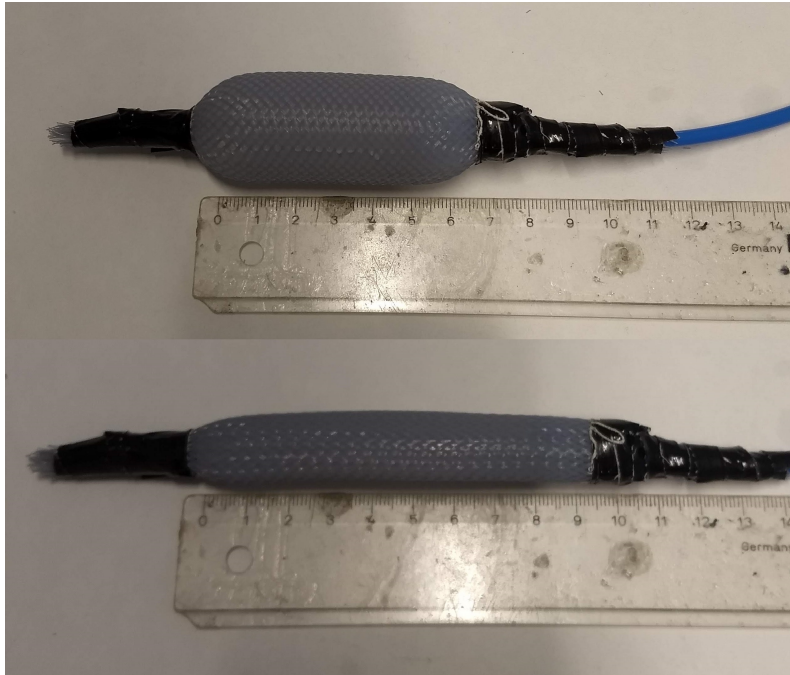


Figure 3.4: The finished PAM, at the top contracted and at the bottom relaxed

specific actuator. All actuators show a contraction of 20-25% (absolute contraction of the actuator compared to the bladder of 97.5 mm) before leaking does not allow for an increase in pressure any more. Contraction versus pressure can be seen in figure 3.5 for three different actuators with the same design. Contraction is virtually instant after applying the pressure. It was possible to lift a 500 g weight of the ground by just contracting the muscle, with only a slight reduction of the contraction that could be achieved. What can be seen is that there is definitely a difference between several individual actuators. This is most probably due to the fact that it is difficult to attach the wire and tape in the same manner every time. This might be something to look into in the future, even though maximum contraction is comparable it is desired to also have contraction at the same pressure to be more similar for multiple artificial muscles. This would allow for better feed forward control as the behaviour is more predictable in that case. When looking at the difference between Ecoflex 00-50 and Ecoflex 00-30 there is only a slight difference at low pressures. Since Ecoflex 00-50 is easier to work with this is the best choice to make the material of the bladder from.

3.2 Pneunet bending actuator

The purpose of the pneunet bending actuator is to bend. As can be seen in figure 2.4 B,D and E. As fluidic elastomer actuator there are several design parameters as previously discussed. These are:

- The shape of the actuator and the air chambers in it
- Youngs modulus of the material of the actuator
- Wall thickness of the air chambers

3.2.1 Actuator design

The basic design of this actuator is based on the Pneunets bending actuators (see figure 2.2) as can be found on the soft robotics toolkit website (SoR, 2018). It has been chosen because it is easily scalable and it can be used to generate the dome shape of the diaphragm. This design

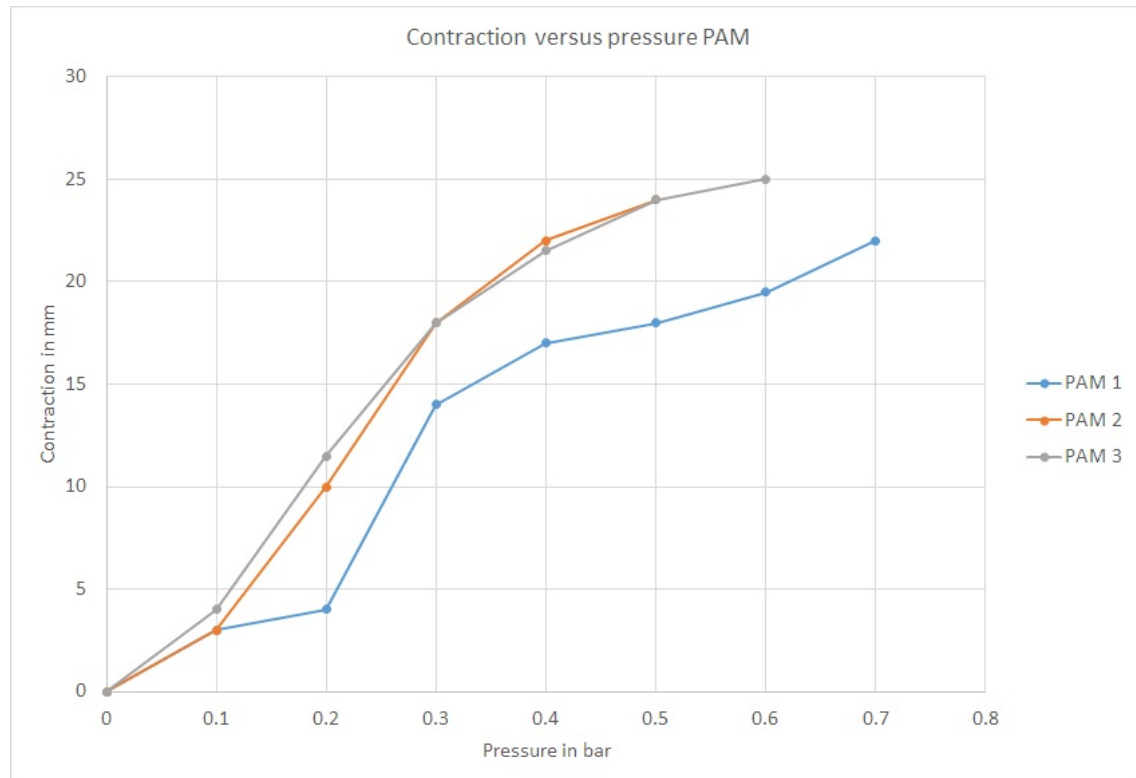


Figure 3.5: Contraction versus pressure for three different, but in design identical, PAM's.

has been shortened and widened such that it is more suitable to be used in a diaphragm in terms of outer dimensions of the actuator. The width now is 200 mm, which is the same as the height of the diaphragm to be designed. The width is 50 mm, such that 3 in combination with 2 artificial muscles would give a width of the diaphragm of approximately 330 mm.

The forces that need to be generated and how to measure them such that they are representative for the final application in the diaphragm is hard to determine. Eventually a load (the liver phantom) will be distributed over a large part of the diaphragm and thus actuator. For this reason again outer dimensions and potential displacement/deformation (which needs to be in the range of the requirements of SI motion) as well as manufacturability are mainly taken into account in this design. If necessary adjustments to the design will be made based on simulations and test results from where the actuator is loaded with different weights.

A schematic drawing of the design with the most important parameters can be seen in figure 7.1 in chapter 7. Four air chambers can be found in every actuator with the 'active' walls having a thickness of 2 mm. These walls will bulge outwards when pressure is applied to the actuator. This means that walls will start touching and push the air chambers away from each other. Because the bottom of the actuator is one sheet of Ecoflex the actuator is not able to expand there. The result is that it will start to bend, because the top of the actuator is not constrained. With this the shape of the actuator and the wall thickness is set. As for the Young's modulus of the material of the actuator, there is chosen for Ecoflex 00-50, which has a Young's modulus of 2.17 MPa.

A CAD model has been made with Solidworks of the actuator before production. This in order to easily create a mold, but also to be able to simulate the behaviour of the actuator before production would start.

With Abaqus the finite element model has been constructed for this actuator to verify its functioning. It has been modelled as a hyperelastic material with the Yeoh model.

3.2.2 Mold and fabrication

The design of the mold is also derived from the soft robotics toolkit website (SoR, 2018). Additions to that design have been made, such as an opening for a pneumatic hose and notches to put a screwdriver in the mold to make demolding easier. This mold consists of three parts, the first two to make the top of the actuator and the last one to make the bottom of the actuator (see figure 3.6).

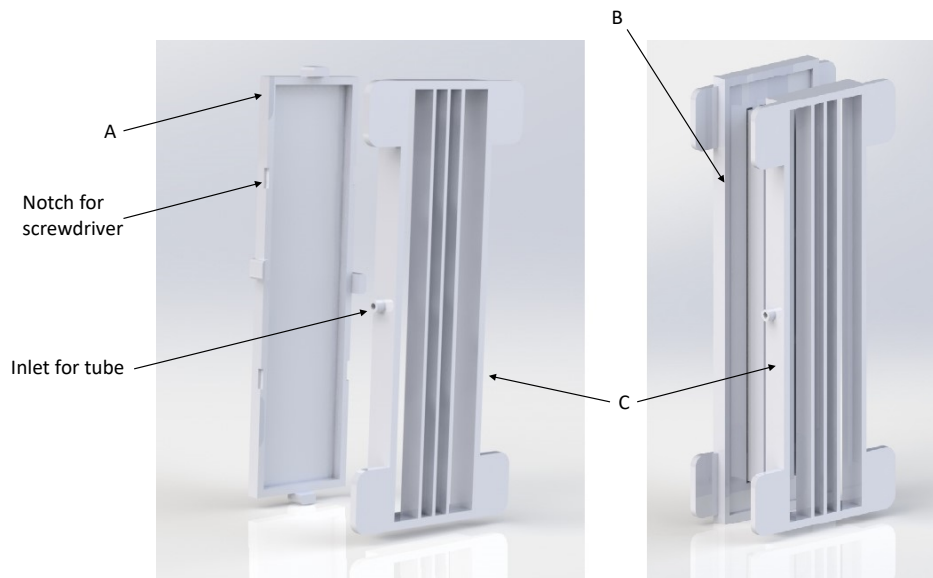


Figure 3.6: Mold for the pneumatic actuator. With A and C the bottom can be made and with part B and C the top of the actuator can be made

Fabrication of this actuator is straightforward. It is made from Ecoflex 00-50. First the top part containing the air chambers and interconnecting channels is made. Once that is cured the bottom can be attached to the top, which will seal off the actuator. For this type of actuator there are two difficulties while producing it. It can happen that some of the air channels between the chambers are closed off while placing the top on the bottom, which makes it impossible to actuate all chambers. This can be solved by cutting the actuator open and making the air channels free of Ecoflex after which the parts can be put together again with some new Ecoflex. Another issue is the fact that the opening for the pneumatic tube sometimes gets filled with Ecoflex. This can be fixed by puncturing it with a screwdriver after the Ecoflex has cured. Although this needs to be done carefully in order not to puncture any other parts of the actuator.

3.2.3 Characterization

Characterization of this actuator has been done in an as free as possible state. Which has been done by measuring several points on the actuator and looking at their displacement while applying different pressures in steps of 0.01 bar to the actuator as can be seen in figure 3.7. This has been done by taking photos of the actuator in every state and processing that data with ImageJ software. The actuator has been put on top of a smooth surface that has oil applied to it in order to reduce friction. The goal is to find the relation between the displacement of the red dot (middle of the actuator) and the input pressure.

Measuring any force from the actuator will always be difficult as clamping it will deform the actuator, which will influence the measurement again. What has been done is putting a weight on top of the actuator and check whether it is able to lift that weight and measure the displacement

of the weight. A weight of 500 g and 1000 g including a plate of 110 g to support the weights on top of the actuator could be lifted, respectively 8 and 4 mm in vertical direction from its starting position. The lifting of the 1000 g weight can be seen in figure 3.8. Which led to the conclusion that the actuators incorporated into a diaphragm might also generate enough force/displacement to be able to move a phantom liver, at least the force that it is able to generate would most probably be adequate. Eventually this will all still depend on the constraints of the diaphragm.

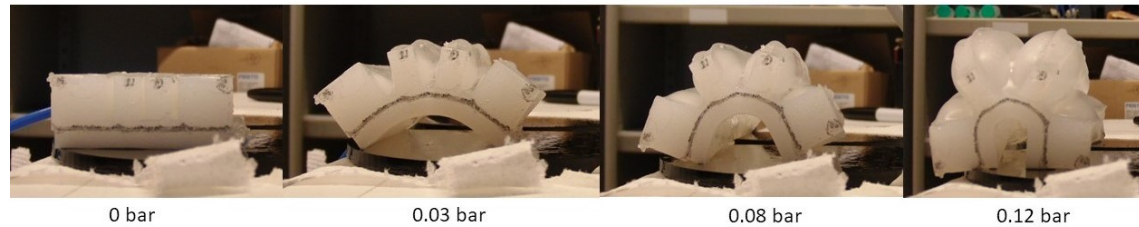


Figure 3.7: Testing the pneunet actuator in a free state. Increasing pressure from left to right

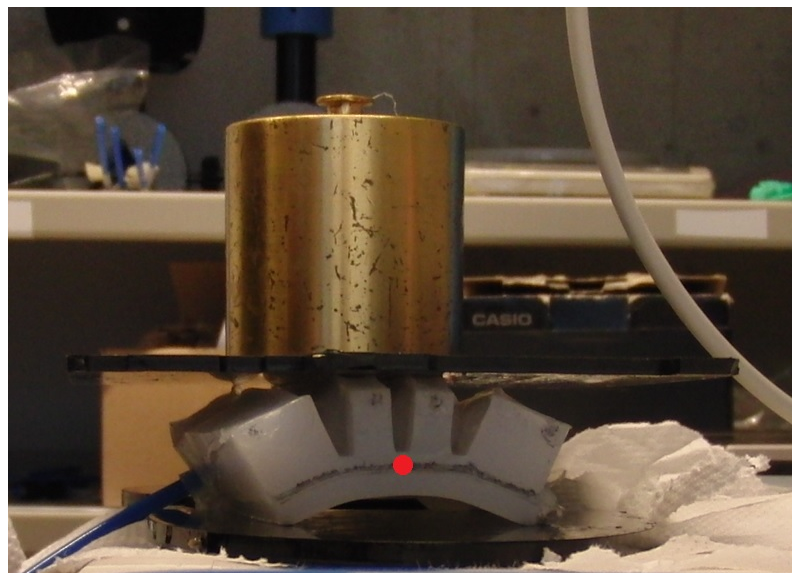


Figure 3.8: Loading and testing the actuator. The displacement of the red dot is measured in vertical direction

The results of the characterization can be seen in figure 3.9. It is clear that the external forces on the actuator have a large influence on the behaviour of the actuator. Whereas the actuator in the unloaded case almost behaves linearly, this is for the loaded cases not the case. This means characterization needs to be done again when the design of the diaphragm is made to find out what the behaviour is under those conditions.

3.2.4 Comparison between FEM and characterization

Also a comparison between the FE model and the real actuator can be made. The main difference between the two is the fact that the support and gravity play a role in the motion of the physical actuator whereas this does not influence the FE model. That is where the bump around 0.03 bar comes from in the graph of the physical actuator, whereas the FE model stays smooth. Other than that displacement versus pressure is comparable in the whole pressure range. This means that for further design iterations of this actuator the FE simulations could be used for quick design iterations.

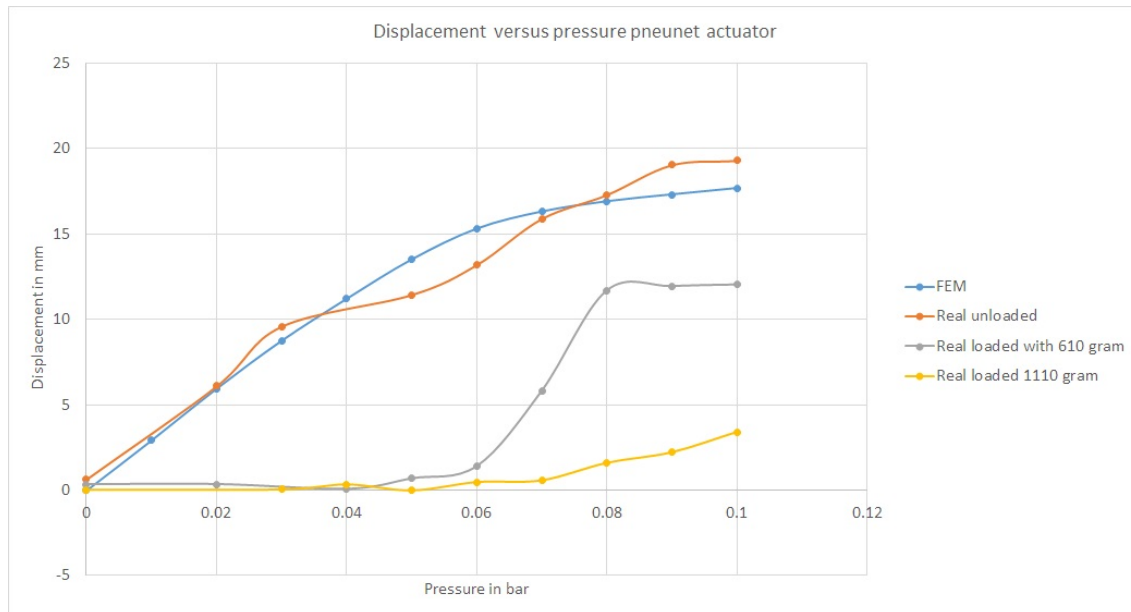


Figure 3.9: The displacement of the same point in the middle of the actuator in a FEM simulation and the real actuator.

3.3 Vacuum actuated muscle inspired structure

For the vacuum actuated muscle inspired structure several design iterations were done. Although they were consecutive steps in the design process they will all be explained simultaneously. As they are comparable for the different versions of the design. The purpose of this actuator is to contract the diaphragm as can be seen in figure 2.4 E. Important design parameters have been earlier identified as:

- The cross-sectional area of the actuator in direction of actuation
- Youngs modulus of the material being used
- Geometric features of the different parts of the actuator

3.3.1 Actuator design

Version 1

The main principle of working of this actuator is contracting in one direction caused by buckling of the internal structure while a vacuum is applied to the actuator, as was explained in section 2.4.3. The actuator will be made fully out of Ecoflex 00-50, because this should make it easier to combine with the other actuators that are made out of Ecoflex 00-50. This also means that the Youngs modulus of the material of the actuator is already set.

For the geometric features of the design not much information could be found in literature, but the design is based on the literature that was available (Yang et al., 2016). This design has been chosen as starting point, because at the critical pressure contraction of this design is about 40%. So even when the actuator contracts less then expected still a contraction comparable to that what is expected for the artificial muscle should be reachable, which was 20 to 25%. The internal layout of chamber in the actuator is 1 row of 4 chambers, then 1 of 3 chambers in the middle and 1 of 4 chambers on the outside again. With a width of 28.58 mm and a height of 48.5 mm This means that the geometric features are set for this design.

A cut through of the design can be seen in figure 3.10. Outer dimensions of the actuator are chosen such that they match the initial ideas of the diaphragm and the ratio of width and length

of the internal chambers. The ratio length over width is about 0.55 of the chambers. The width is 93.75 mm, just as the artificial muscles. The height of the actuator is slightly higher than 200 mm (the desired height of the diaphragm) in order to make sure the width is correct and the ratio of the dimensions of the chambers as well. The thickness of the whole actuator is 37 mm. The thickness of the walls is taken 4 mm for the short walls of the cells and 2 mm for the long walls. Logically when buckling will happen this will earlier lead to buckling of the long thin walls than buckling of the short thick walls. Thus promoting contraction in just one direction. With the outer dimensions set also the cross-sectional area in direction of actuation has been set, namely 37 mm \times 200 mm. Also for this actuator a Solidworks model has been made for this actuator.

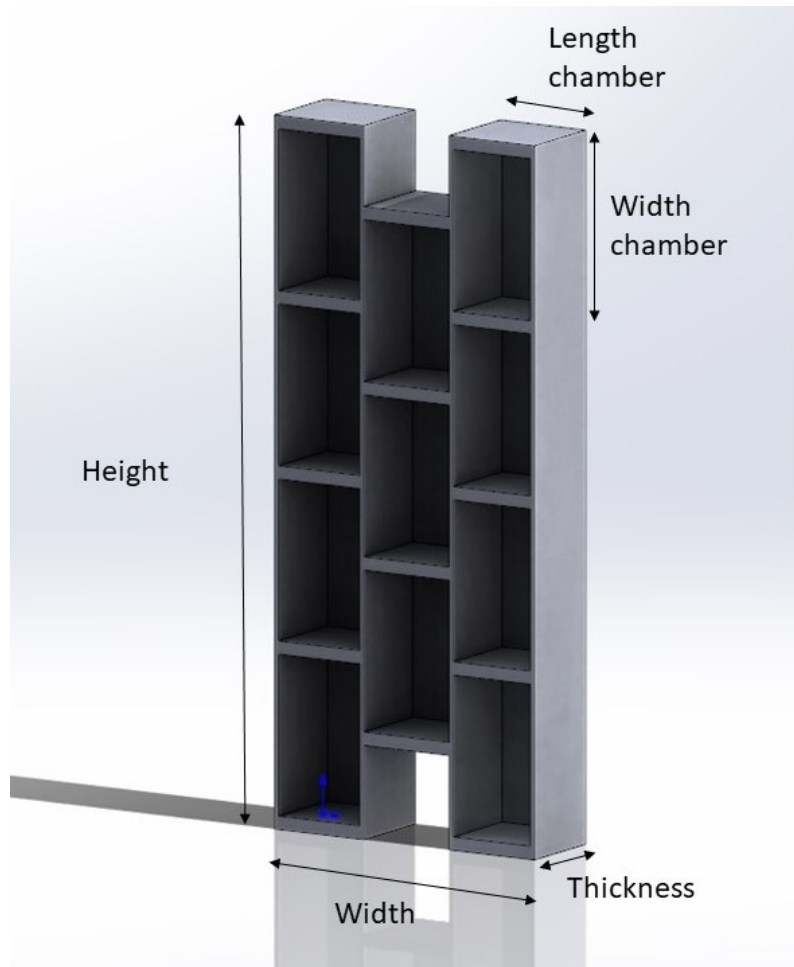


Figure 3.10: The design of the first version of the actuator. The interconnecting channels are not shown. The naming used for the different dimensions is given as well.

Version 2

The first version of the vacuum actuated muscle inspired structure was difficult to produce, dimensions did not completely match with the Pneunet bending actuators and actuation was slow due to its large volume, as will be explained further later on. For this reason a second version is made.

The basic design stayed the same, however the volume is largely reduced by making the chambers less thick. Going from a thickness of 37 mm (which came from literature) to 20 mm, which is also the height of the bending actuators, thus allowing the actuators to 'flush' when on the diaphragm. This does mean that the ratio of the geometric features is altered, but the assump-

tion is that the thickness of the actuator does not really contribute in the buckling motion. Also the height is slightly altered to match the dimensions of the Pneunet actuators. The height of the internal cells is now 45 mm and the width is 28.6 mm, thus resulting in a different ratio, 0.64 instead of 0.55, which is the result of keeping the inner configuration with the amount of chambers the same and changing the outer dimensions of the actuator. What the exact difference will be in behaviour is not known, but the assumption is that the internal walls are still considerably small compared to the size of the chambers and that this would not limit the buckling.

Version 3

The second version of this actuator type failed because it was too flat and the first did function, but actuation was too slow, the right combination of the two could result in a desired actuator. Based on the first actuator the ratio between the width, thickness and length of the internal structure was derived, which was then downscaled to approximately fit in the outer dimensions of the second version. This should result in the same behaviour as for version 1. Where version 1 has internal blocks with a size of $48.5 \text{ mm} \times 28.58 \text{ mm} \times 37 \text{ mm}$ (LxWxT), version 2 has them of $45 \text{ mm} \times 28.58 \text{ mm} \times 20 \text{ mm}$. Both with a wall thickness of 4 mm in the length direction of the chambers and 2 mm in the width direction of the chambers and an arrangement of the internal chambers of a row of 4 then a row of 3 which is skewed by exactly half a chamber and then a row of 4 again. In version 3 the internal structure has been rescaled to come close to the ratio in version 1 with a thickness of 20 mm. This results in internal cell dimensions of $20.5 \text{ mm} \times 11.1 \text{ mm} \times 16 \text{ mm}$ with the cells in 4 rows of 8 in length direction with in between 3 rows of 7 in length direction that are exactly skewed half a cell. This can be seen in figure 3.11 at the bottom right as the cube design. Wall thickness has stayed the same, as decreasing that would probably cause problems during production.

Based on this cubed structure that was used previously also other structures were designed, these can be seen in figure 3.11. All having the same outer dimensions and all having the same total area of cells of roughly 12.000 mm^2 . The cube design is most probably the easiest to fabricate, due to the simple geometry, but if one of the other geometry shows a bigger maximum contraction and more contraction at the same pressure than the other designs in simulation it might be worth to look into this design.

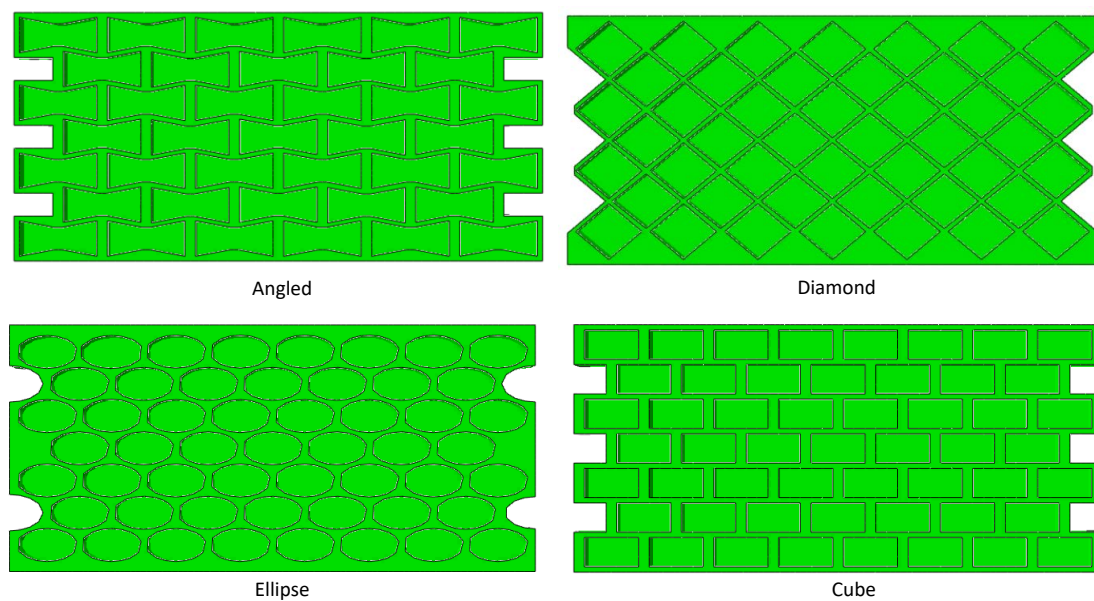


Figure 3.11: The different designs for version 3 of the VAMP that were simulated.

3.3.2 FE model

For all actuator designs described previously an FE model has been made. Ecoflex has been modelled as hyperelastic material with the Yeoh model. All of them have been tested for contraction behaviour to verify whether the actuator behaves as expected or not. This was done by constraining the bottom of the actuator, as can be seen in figure 3.19 and then looking at the displacement at the top. For version 1 and 3 the simulations were done before the actuators were fabricated, but due to time constraints the second actuator was only simulated after the actuator was already fabricated. In hindsight not the right decision, because after fabrication it became clear that version 2 was not a working design. For version 3 the comparison between the different structures led to the decision to go with the cubed structure. The contraction versus the applied differential pressure/vacuum can be seen in figure 3.12. The angled geometry did show more contraction with the same pressure than the cube design. This might be explained by the fact that this geometry is 'pre-buckled'. For the ellipse and diamond design the contraction at the same pressure was less when compared to the cube actuator. Simulations stopped at different pressures, because at those pressures lateral buckling started to occur in simulation. Even though the angled design has more contraction with the same pressure in simulation the fact that the cubic design seemed easier to fabricate due to its straight walls and thicker walls it was decided to fabricate just the cube version.

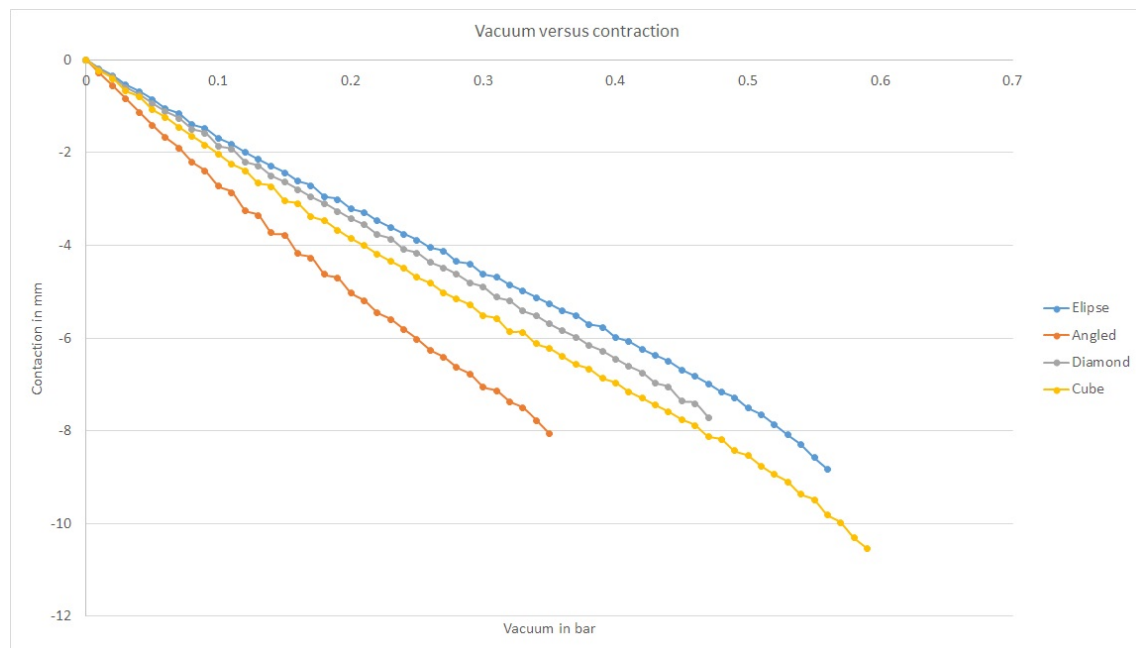


Figure 3.12: FE results for the different geometries that were tested.

3.3.3 Mold and fabrication

Version 1

Since not much information was available for the design of a mold this had to be made from scratch. There need to be internal chambers and they need interconnected, but in the end the whole actuator needs to be closed of. This makes that the actuator needs to be molded in two parts. First creating the internal structure after which the parts that are necessary to mold that internal can be removed (figure 3.13) and the actuator can be closed of (figure 3.14). Because there will be considerable small parts in the actuator, some parts are just 2 mm thick, and Ecoflex is viscous there is a large chance of trapping air bubbles when producing the actuator. On top of that there is the chance that it is not possible to fill all parts of the mold with Ecoflex before it starts curing, due to this viscosity. To mitigate these issues a fill opening at the bot-

tom of the mold has been made to insert a tube with a funnel to. This would allow the mold to be filled from the bottom. Air relief holes are made at the top such that trapped air can escape.

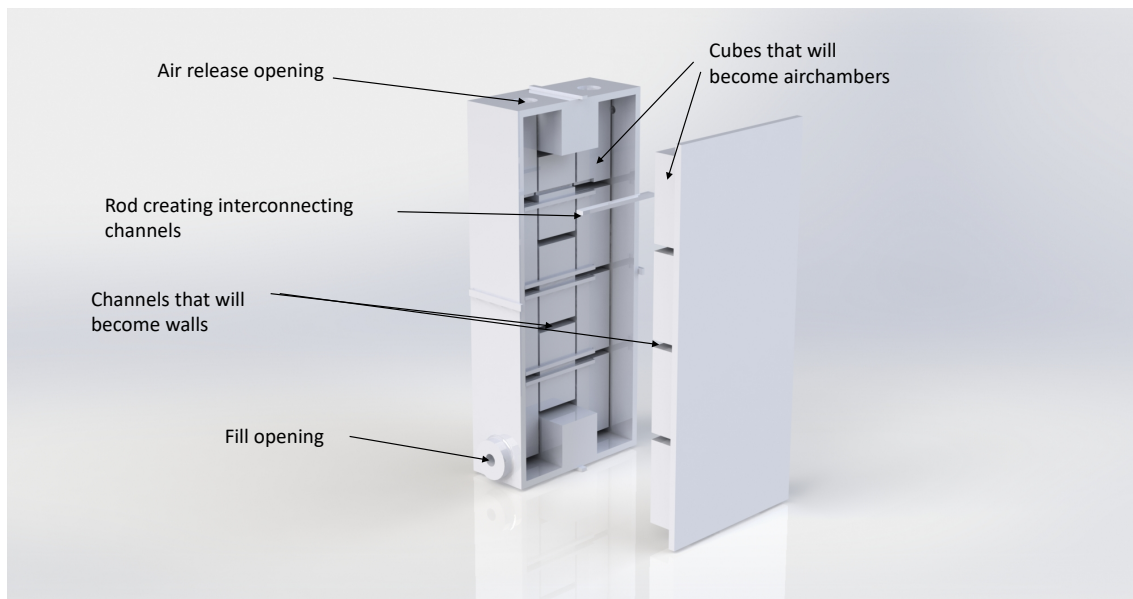


Figure 3.13: A Solidworks render of the mold for the VAMP. Two parts that create the internal chambers, with rods that fit in there to create the interconnecting channels and one outer rim where the other parts fit in.

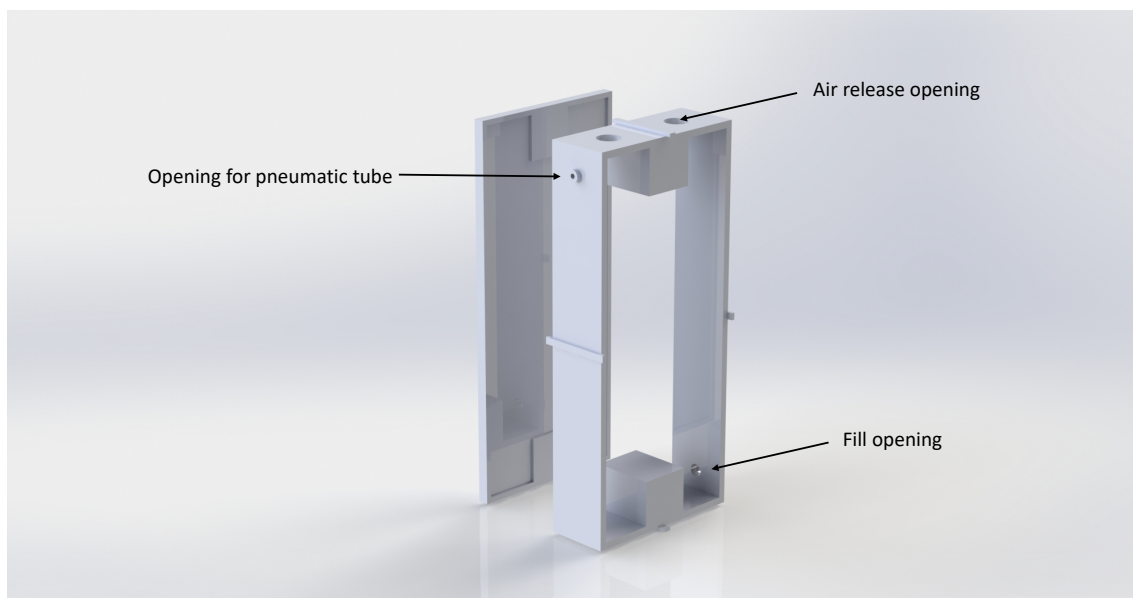


Figure 3.14: Second part of the VAMP mold. This part is used to close the actuator of on both sides. First on one side, then on the other.

The mold did not work as was intended, because the viscosity of the Ecoflex was too high/the channels were too small. As can be seen in 3.15. Large parts of the actuator were not filled with Ecoflex and there were defects at the part where it was filled.

With another approach the same mold could be used in a different way. The air holes were sealed of as well as the insert for the tube. Placing the mold on its side, just as depicted in figure 3.15 and attaching just one side of the mold that is responsible for the internal structure and filling the mold then worked better. Once it was sufficiently filled and most air bubbles got out the other side of the mold responsible for the other half of the internal structure was put on top. This approach worked, but came with other issues. Because the mold is closed of and the Ecoflex works as a seal it is nearly impossible to open up the mold after the curing is done. This was only possible by breaking the mold at several spots.

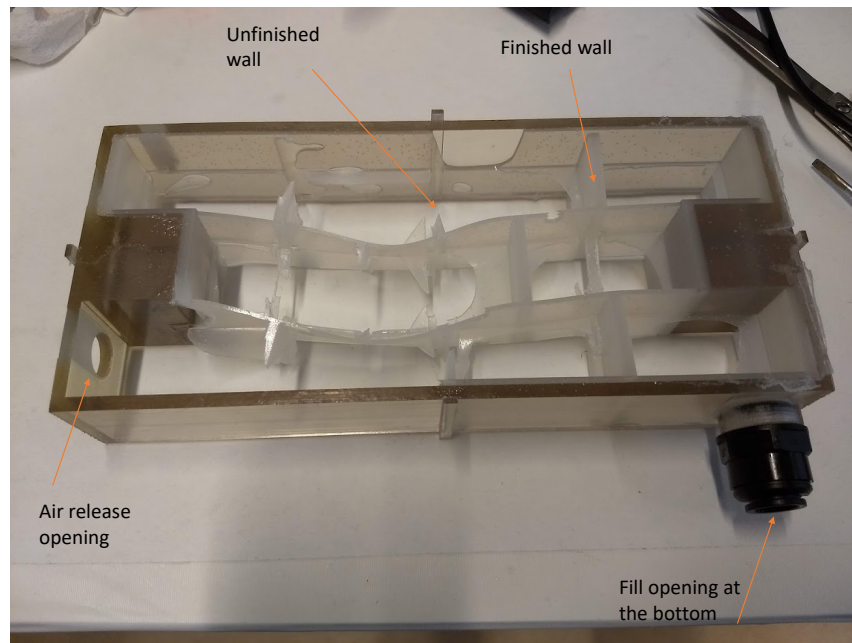


Figure 3.15: The mold is only filled partially. It should have filled up from bottom (on the right) to the top (on the left) and eliminating air bubbles this way. The channels were too small however, as can be seen there are wall that are not completely filled with Ecoflex

Version 2 and 3

For the mold design of version 2 and 3 a different approach was taken, since the previous version was difficult to produce and consistency was hard as well. The molding steps have been reduced from three steps to two. The chambers will now be formed by blocks that are suspended in the mold, this allows in one step the molding of the chambers and closing of one side of the actuator. Also the removal of the blocks responsible for the inner structure should be easier, since the mold is not completely closed of anymore. Also all blocks can be pulled out separately instead of all at once, which should simplify this a lot. On top of that the top of the mold is open, so air bubbles that are still present in the Ecoflex, even after correct degassing, can escape the mold and will not be an issue in the actuator. The mold can be seen in figure 3.16, this is the same for version 2 and 3, only the dimensions are changed between those two.

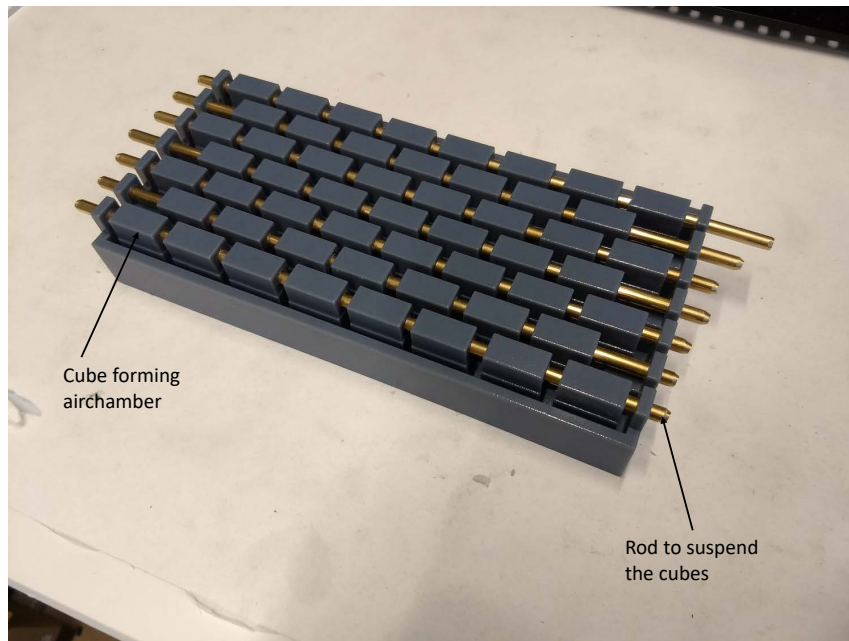


Figure 3.16: Mold for version 3 before pouring in the Ecoflex for step 1. A different mold design was used then for version 1. The blocks are suspended in the Ecoflex in order to close of one side of the actuator and create the internal chambers in one step.

3.3.4 Characterization

For all actuators the same characterization has been done. The goal is to determine the relation between vacuum and contraction. A vacuum is applied in incremental steps after which the average length of the actuator is measured. Comparing the length for every pressure step with the initial length of the actuator allows to determine the contraction of the actuator. The bottom of the actuator is constrained, the top is not as can be seen in figure 3.19.

Version 1

With this actuator several issues were identified while testing. First of all since the thickness of the walls is not precisely the same everywhere a slight inhomogeneous motion can be seen. Next to that with the available hardware (vacuum pump, solenoid valves and vacuum pressure regulator) the time to contract more than 5 mm takes more than five seconds. Initial requirements that were set would need full contraction to be possible in around 1.5 s (full breath cycle would be around 3 s), thus actuation was not quick enough. Contraction versus pressure can be seen in 3.17. The critical pressure is at 0.02 bar.

Version 2

Immediately during the first test it became clear that the chosen dimensions do not work. Due to the 'flattening' of the actuators the side walls come in contact with each other when deflating the actuator. They do this before the actuator starts actually buckling, this means there is virtually no contraction. This means this design is unusable.

Version 3

Version 3 works as desired. Two actuators are made and tested for contraction. Absolute contraction is about 2.5 cm for both of them, which is a contraction of around 25%. Which is less than what was expected from literature where almost 40% was reached with a comparable structure, but not an issue, because it is still comparable to the contraction of the artificial muscles as was aimed for. The critical pressure is between 0.6 bar and 0.7 bar, which is in line

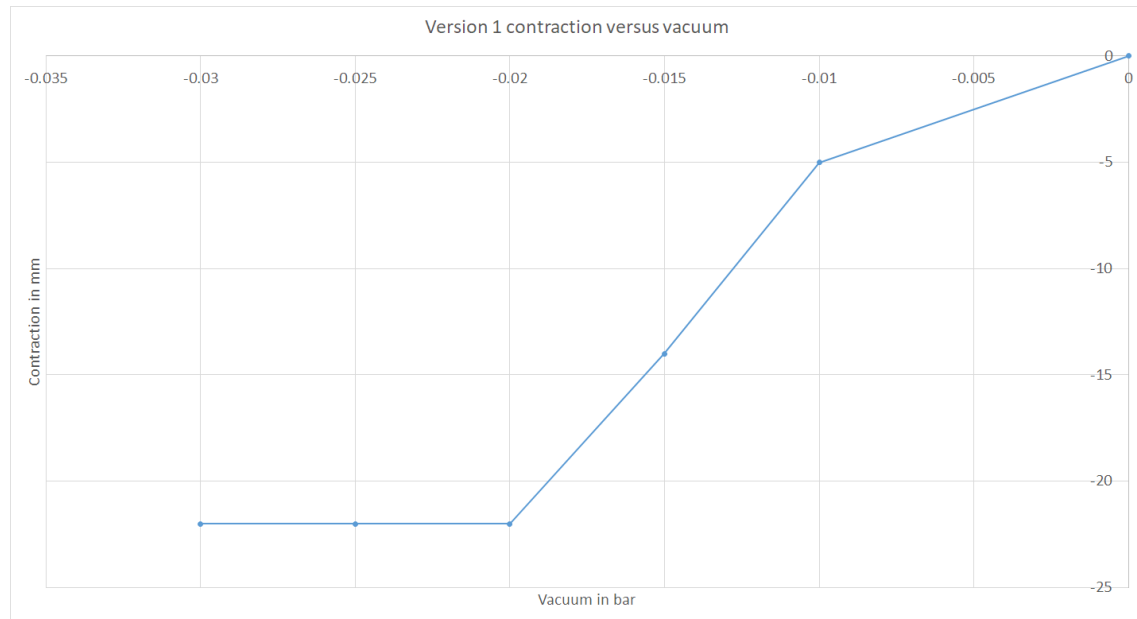


Figure 3.17: Average contraction for free contraction of the first version

with other literature where Ecoflex 00-30 is used and the critical pressure is around 0.4 bar. With a higher Young's modulus a higher critical pressure is expected. What can also be said is that the contraction versus pressure curve is more or less linear up until the critical pressure, as was predicted based on previous literature.

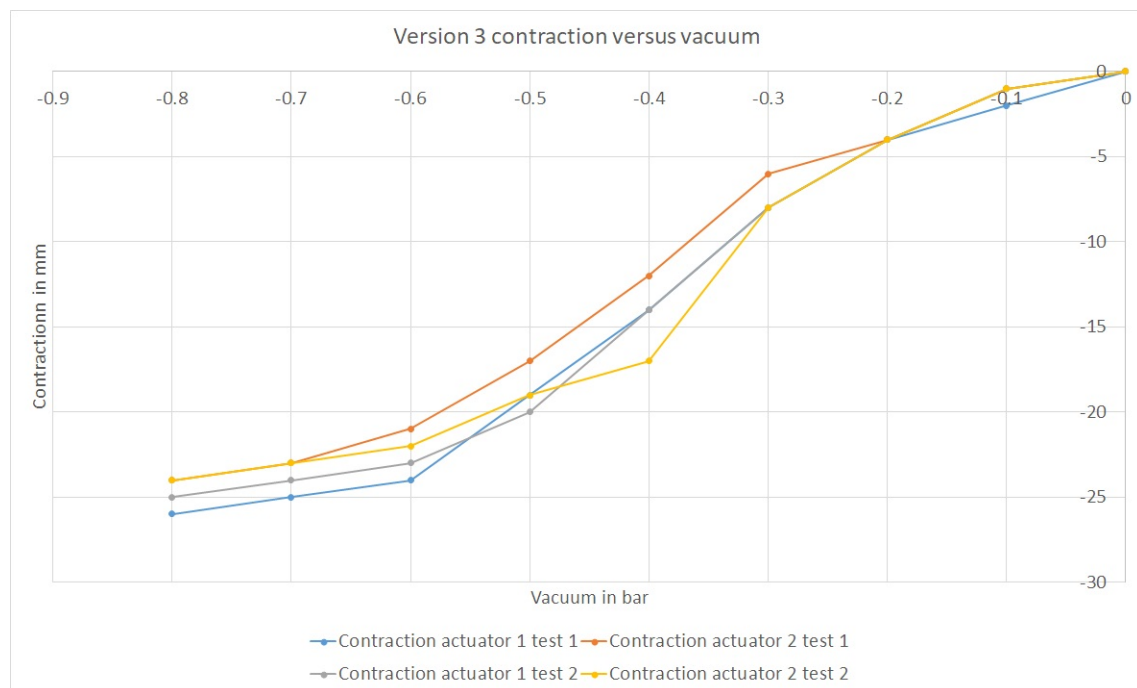


Figure 3.18: Contraction versus pressure for version 3 of the actuator. Tested twice for two actuators

3.3.5 Comparison between FEM and characterization

Version 1

The first thing that can be said is that the overall motion of the actuator in simulation is real life is comparable, at least when comparing them in static cases as can be seen in figure 3.19. Dif-

ferences that can be seen are due to the lack of gravity and a pneumatic tube in the simulation. The pneumatic tube causes the real actuator to contract a bit skewed, there is a slight load of the tube on the actuator. Gravity causes the real actuator to contract/buckle more at the bottom of the actuator than at the top due to the weight of the actuator itself. Another difference between the simulation and the real actuator is the constraint at the bottom. In the simulation the whole bottom face is constraint. For the real actuator it is not easily possible to do this the same way. Tape has been used to constrain it, without further influencing the motion of the actuator, but as can be seen in figure 3.19 the bottom of the actuator still starts buckling, which is definitely not the case in the simulations.

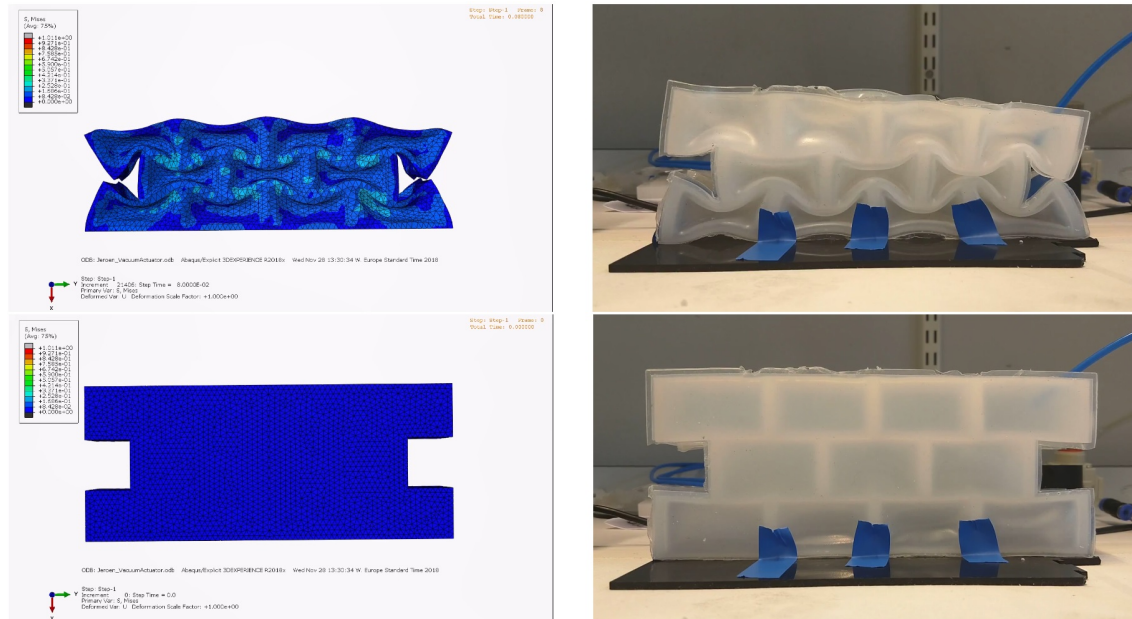


Figure 3.19: The FE model (left) and real actuator (right) side by side. On top the contracted state and at the bottom the 'relaxed' state.

Version 2

Both simulation and real testing give the same results. The actuator shows virtually no contraction.

Version 3

In figure 3.20 the simulation versus the real actuator can be seen. What is clear is that up until 0.2 bar the same contraction can be seen, however after that the contraction of the real actuator is more than in simulation. What can be seen is that the critical pressure for the real actuator is around the same pressure as where in simulation lateral buckling can be seen. The fact that simulation and physical actuator deviate from each other from 0.2 bar on most probably has to do with the constraints not being exactly the same. In the simulation the bottom is constrained in all directions and the top is only unconstrained in the direction of desired contraction as this allows for a better comparison between the different designs for just the contraction that is desired. This is difficult to realise outside simulation where only the bottom is constrained by tape and the top is unconstrained. Non-uniform deformation can happen there, meaning internal walls can tilt slightly, leading to more contraction with the same pressure.

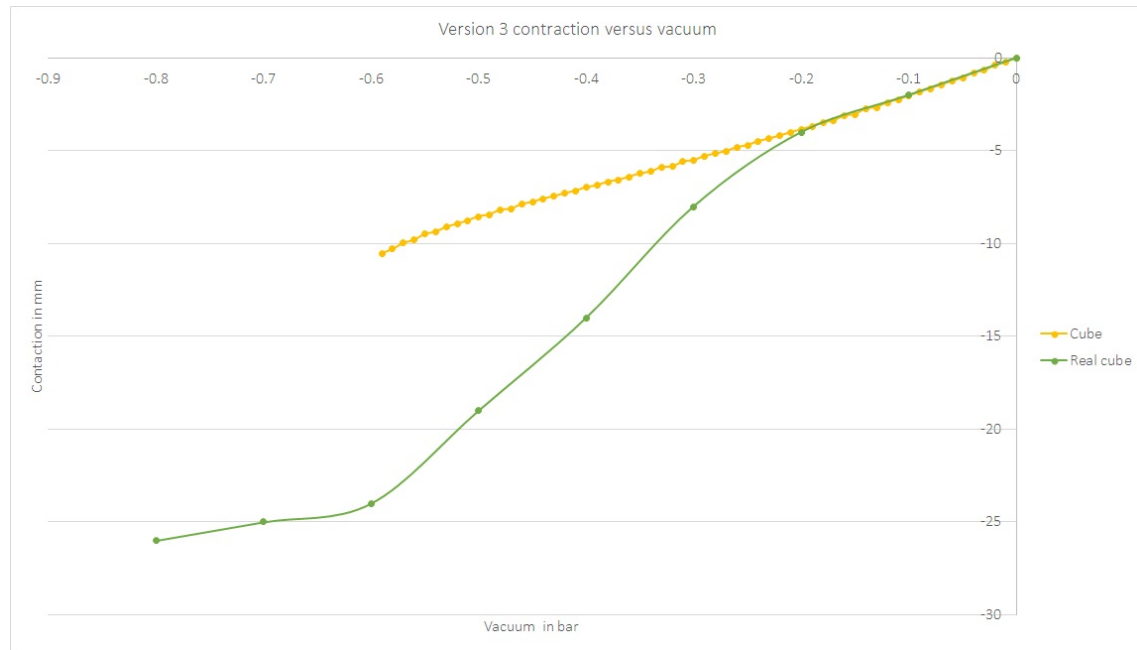


Figure 3.20: Data of the contraction versus vacuum for the simulation and real actuator version 3

3.4 Summary and next steps

Three types of actuators have been designed and characterized. For all three designs have been made that behave comparable to previous literature and that can be used in the design of the diaphragm. This design of the diaphragm will be made and explained in the next chapter.

For the Pneunet bending actuator an FE model has been made that corresponds well with the behaviour of the physical actuator and can probably therefore be used to evaluate different designs of this actuator and know their behaviour before production. The FE model for the VAMPS can only be used for evaluation between different designs before production as the contraction of the physical actuator is different than what can be seen in simulation.

4 Design, production and characterization of the diaphragm

In this chapter the design, analysis, production and characterization of the diaphragm will be discussed. The diaphragms described here are build up out of the actuators that were introduced in chapter 3. The actuators that will be used for the diaphragm are the Pneunet bending actuator and the vacuum actuated muscle inspired structure version 3. The reason the pneumatic artificial muscles are not used in the diaphragm is because the vacuum actuated muscle inspired structures are potentially easier to incorporate into a fully Ecoflex diaphragm. Both the artificial muscles and the vacuum actuated muscle inspired structures would fulfil the same role, thus the vacuum actuator is chosen. The pneumatic artificial muscles will be used to change the orientation of the diaphragm, as will be explained later on.

Furthermore, superelastic material will be used, because it can aid in keeping the diaphragm in shape and it is possible to vary the compliance of the diaphragm with.

The concepts that will be pursued are the ones explained in section 2.7.2, from now on diaphragm version 1, as well as the one explained in section 2.7.5, from now on referred to as diaphragm version 2. Both will be made with and without superelastic material. First, diaphragm version 1 is made where it is possible to insert superelastic material in the diaphragm. The step from diaphragm version 1 to version 2 is the addition of vacuum actuators to version 1.

In order to test the diaphragm, a stand is made to support it and a liver phantom is made to be able to test the diaphragm with a realistic load. The stand and liver phantom will also be explained in this chapter. In chapter 5 two models are explained, the characterization on which those two models are based is explained at the end of this chapter.

The requirements that need to be taken into account for the design of the diaphragm, stand and liver phantom are:

- The robot needs to be MR safe and sufficiently MR compatible
 - The part that goes inside the scanner bore should not cause artefacts that can obscure the region of interest
 - The system needs to fit inside a scanner with a bore of 50 cm, which is assumed to be the smallest MRI scanner that is commonly used for this application
- The motion of the liver needs to be accurate
 - Between 0 mm to 8 mm in left-right (ML) direction
 - Between 4 mm to 14 mm in up-down (SI) direction
 - Between 2 mm to 8 mm in front-back (AP) direction with preferably the possibility of creating a difference between left and right
 - Frequency that should be achievable is 0.25 Hz to 0.3 Hz
 - *Optional: taking into account the motion of for example heartbeats*
- The set-up will represent a patient in supine position
- The design of the set-up will be inspired by the human anatomy

Where first the focus will lie on the SI motion and after that the other requirements.

4.1 Stand

In order to support/hang the diaphragm a stand is necessary. The stand must be able to hold the diaphragm and it needs to have space for the liver phantom. First, the aim is to only focus on SI motion, thus the liver can simply be supported by a plate over which it is sliding. Later on, this support for the liver can be changed to also allow motion in AP and ML direction.

The stand can be seen in figure 4.1, the support plate for the liver phantom and the liver phantom itself are not shown there. In that figure also the names of the direction of motion are shown. SI motion is up and down, when a person is standing up right. AP is back and front when a person is up right. Since the stand is representing someone lying down on its back that is rotated 90 degrees, as depicted in figure 4.1. The angle under which the diaphragm is hung can also be seen there, this is θ .

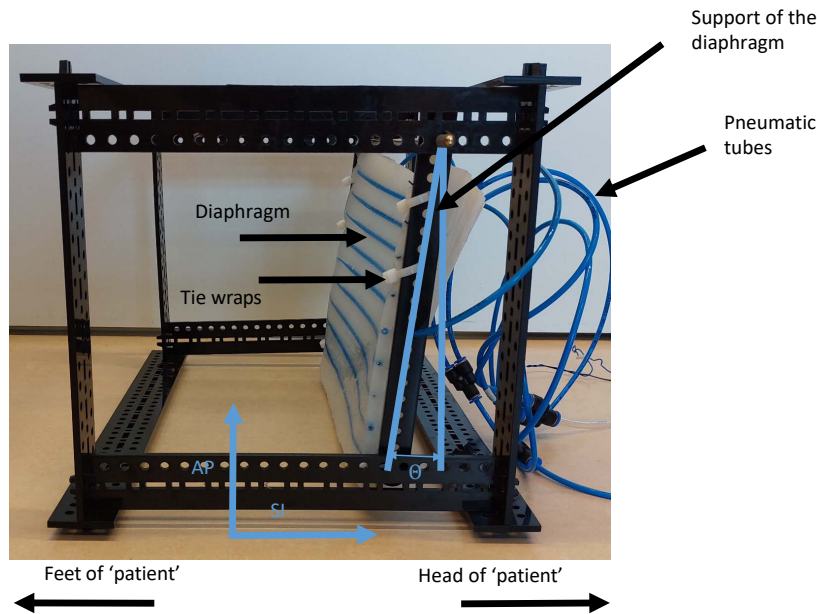


Figure 4.1: The designed stand with the names of the directions of motion

The stand has been made such that it can be produced quickly and the diaphragm, wiring and tubing can be attached to it. Next to that it is made such that dimensions can quickly be changed and it is already MRI compatible, apart from one brass rod, which is used to attach the support of the diaphragm to. This should still be changed before the stand goes into a MR scanner. It is made from Delrin of 4 mm thick from pieces that can be laser-cut. The connector pieces are all such that they can be assembled without tools, useful when assembly has to be done near an MRI scanner. Next to that it is possible to put the stand together in different configurations. Along every stud holes have been made such that wiring, tubing etc. can be attached there.

The diaphragm will be attached to the stand with help of tie wraps. As this allows for the diaphragm to be attached and detached easily and also in different ways if necessary. This can also be seen in figure 4.1.

4.2 Liver phantom

For previous projects a gelatin liver phantom has been made at the research group. The material for this liver had been chosen such that the elasticity of the liver was the same as it would be for a real liver. This however started to degrade after a few days. So a new liver phantom has been made from Ecoflex. This does not degrade in a period of a few days and it is also MR

compatible. To make this the same mold has been used as for the aforementioned projects. The weight (approximately 1300 g) and shape are correct, the elasticity is not, but for the testing that is neglected. The fact that the weight is the same as for a real liver means that this allows for comparable loads on the diaphragm. The gelatin liver with the right elasticity and the Ecoflex liver with the right weight can be seen in figure 4.2.

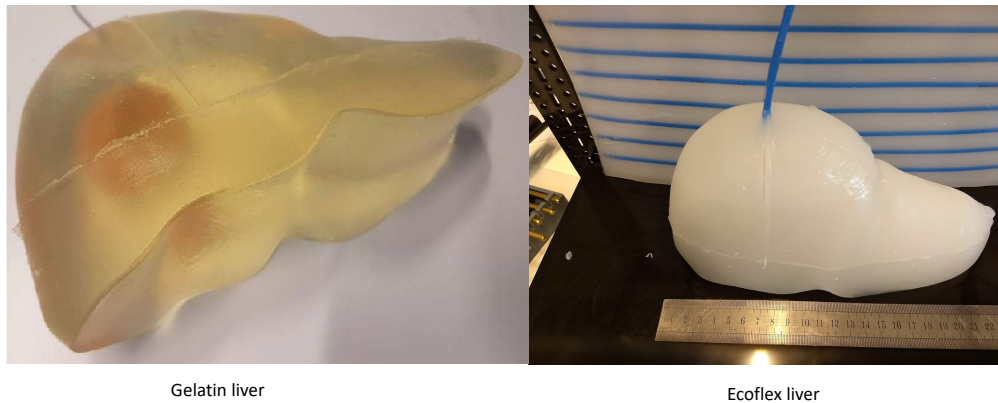


Figure 4.2: On the left is gelatin liver on the right is the Ecoflex liver, both are made with the same model. Elasticity and weight differ between the two.

4.3 Design, analysis and production of the diaphragm

4.3.1 Diaphragm version 1

The first iteration of the diaphragm only contains the Pneunet bending actuators. These are placed with an equal spacing across the diaphragm (see figure 4.6). The diaphragm consists of a 5 mm thick sheet of Ecoflex 00-50 of approximately 200 mm × 337 mm. Inside that sheet inserts are made such that nitinol wires can be easily inserted and removed. A schematic drawing of this can be seen in figure 4.3. The diaphragm will be free on the top and bottom to move, but will be attached to the stand on the left and right side. When looking at the top view, the middle diaphragm will move downwards when the actuators are actuated.

This layout has been tested for its motion in FE simulations, which can be seen in figure 4.4. The deflection of the middle of the diaphragm when it is constrained at both sides and when it is constrained on one side can be seen in figure 4.5. The real diaphragm behaviour should be somewhere in between those simulations, since it will be attached on two sides to the stand, but due to the compliance of Ecoflex it will be difficult to make this a rigid connection/constraint. With both ends constrained an SI motion of up to 12 mm can be seen, which is in the desired range. Assuming that this would be the worst case scenario led to the decision to pursue this concept and fabricate it.

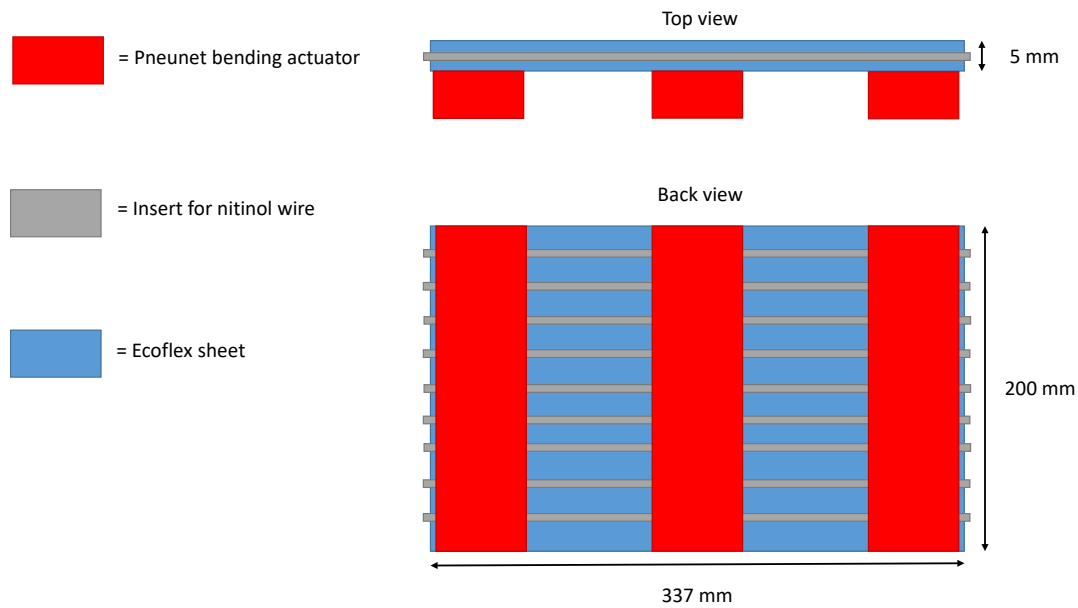


Figure 4.3: Schematic drawing of version 1 of the diaphragm, this is the diaphragm in unactuated state. The Pneunet bending actuator will bend the diaphragm into a dome shape. The nitinol wire will add some elasticity to the diaphragm which should help it flatten again.

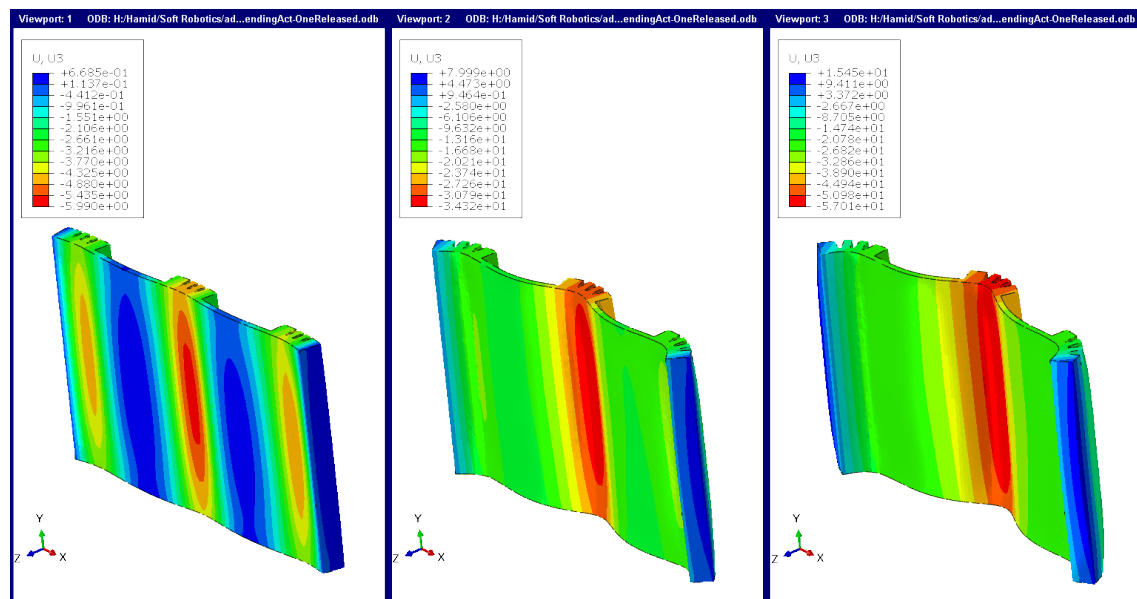


Figure 4.4: FE simulation of version 1 of the diaphragm. The bending actuators are attached on the back with an equal spacing. From left to right more pressure is applied to the bending actuators. The colours represent the motion in SI direction, where from left to right the motion is a maximum of 5 mm, 34 mm and 57 mm can be seen

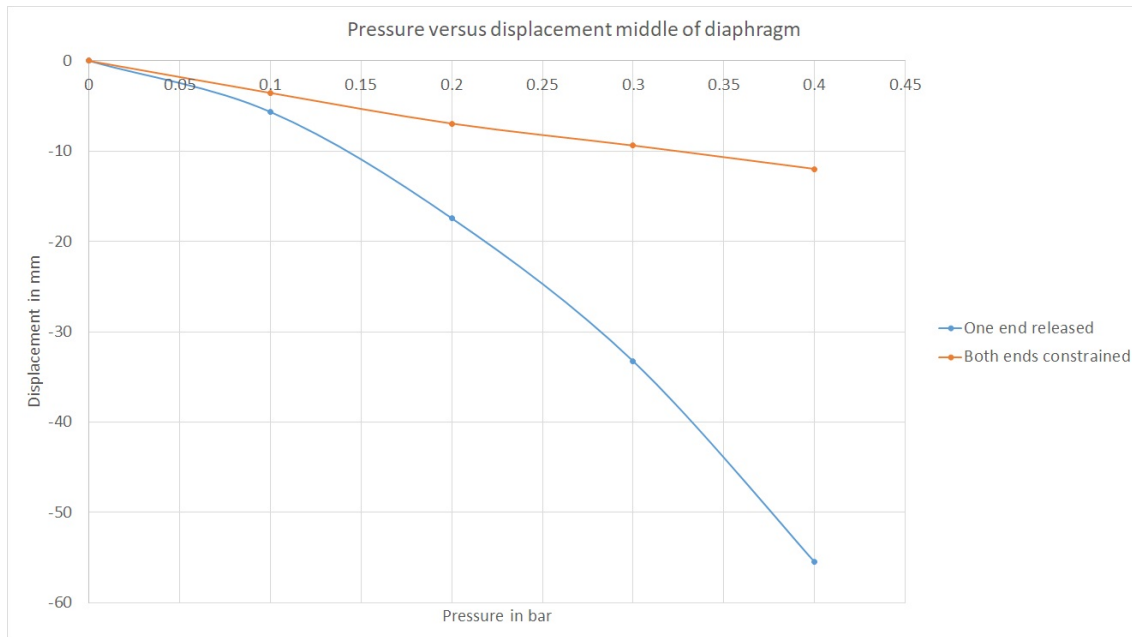


Figure 4.5: The deflection of the middle of the diaphragm. One is where both sides are constrained and the other one is where just one side is constrained, this is the situation in figure 4.4.

This first iteration was tested with nitinol wire inserted in the diaphragm and without. To easily place and remove the nitinol wire in the diaphragm pneumatic tubing has been inserted in the diaphragm to create an opening through which the wire can be inserted, the blue tubing that can be seen in figure 4.6. The nitinol wire has a diameter of 1 mm and will be cut in pieces that are slightly longer than the width of the diaphragm, so around 35 mm. It will be possible to insert 8 wires into the diaphragm. This is straight nitinol wire and should therefore give elasticity to the diaphragm in order to let it move back into its flat position. On top of that it will potentially help in bending the whole diaphragm instead of just locally at the bending actuators. These pneumatic tubes are held in place in the mold with an equal spacing. The mold for the diaphragm consist of a large bottom plate and four small sides, which allows for a large sheet to be made of 5 mm thickness on top of which the bending actuators can be attached. This can be seen in figure 4.6.

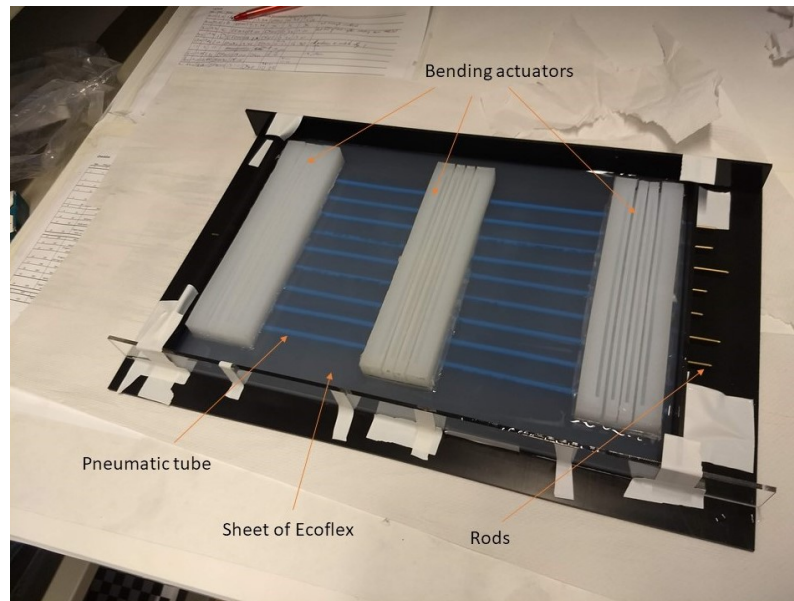


Figure 4.6: The mold for the sheet/bottom of the diaphragm. The bending actuators are on top of the sheet of Ecoflex. There are pneumatic tubes in the diaphragm to easily insert and remove nitinol wire. Rods are in the mold to keep the pneumatic tubes in place in the diaphragm, this will be extracted once the sheet of Ecoflex is cured

4.3.2 Diaphragm version 2

The second version of the diaphragm is same as the first version with the addition of the vacuum actuated muscles inspired structures. These will be inserted between the three bending actuators that are already present. A schematic drawing of this can be seen in figure 4.7. This is actually version 1 of the diaphragm that will be used again, thus after version 2 is made, version 1 cannot be tested anymore.

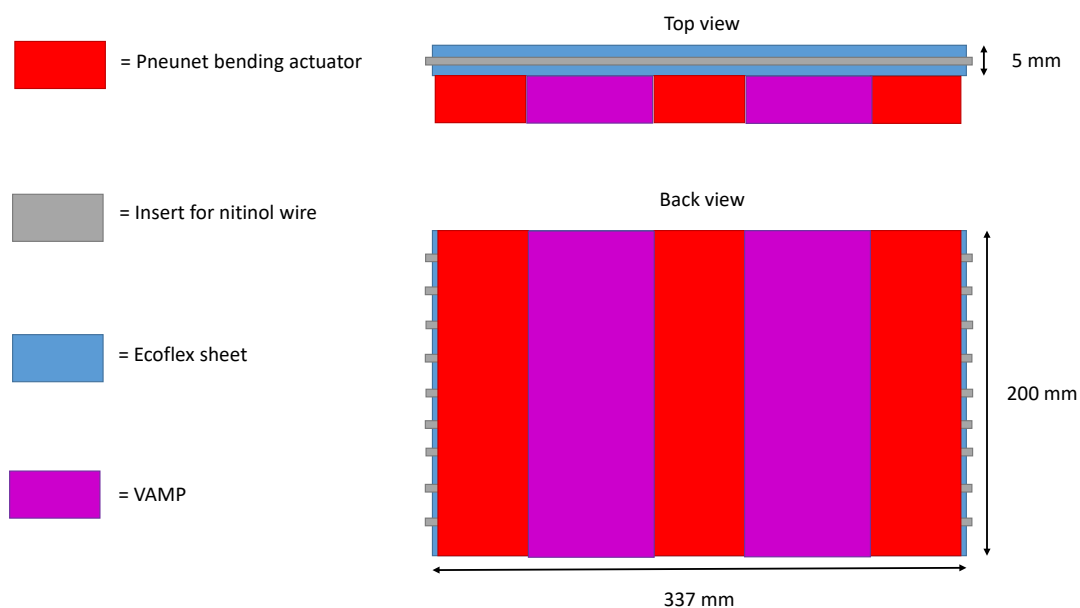


Figure 4.7: Schematic drawing of version 2 of the diaphragm, this is the diaphragm in unactuated state. The Pneunet bending actuator will bend the diaphragm into a dome shape. The VAMPS will contract the diaphragm such that it flattens. The nitinol wire will add some elasticity to the diaphragm which should help it flatten again.

Based on simulations that were performed it has been determined to attach the vacuum actuators both to the bending actuators and the diaphragm underneath it. This will lead to less 'curling/folding' of the diaphragm underneath the vacuum actuators resulting in a more natural shape, comparable to the actual human diaphragm. This can be seen on the left in figure 4.8. On the right in that figure the actuators are only attached to the bending actuators.

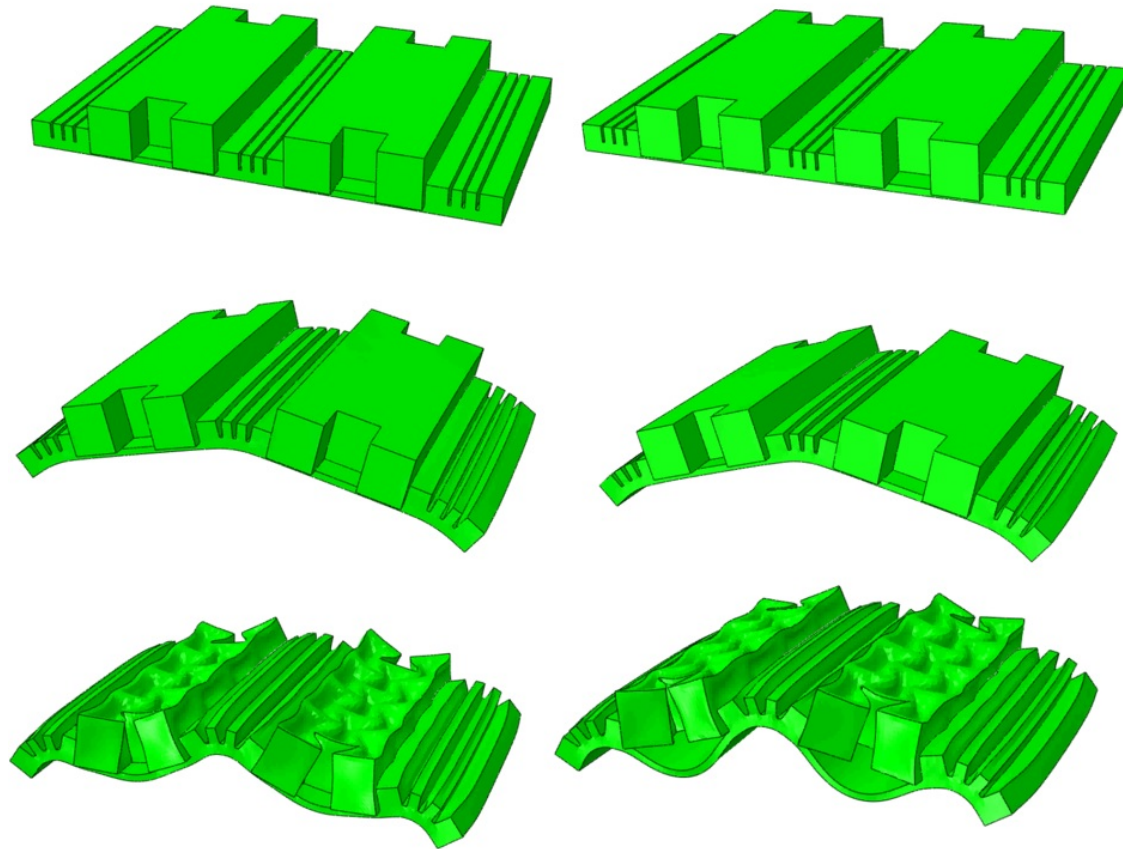


Figure 4.8: Version 2 of the diaphragm in simulation. From top to bottom, pressure is applied to the bending actuators and at the end a vacuum is applied to the vacuum actuators. Difference between left and right is that on the left the vacuum actuators are completely attached to the diaphragm and on the right they are only attached to the bending actuators.

Attaching the actuators is done by using uncured Ecoflex 00-50 as 'glue'. After one attempt the bottom of the vacuum actuators is attached, but the sides are still not well connected to the bending actuators. This can be seen in figure 4.9. Adding more Ecoflex to the gaps that can be seen solves this issue and makes sure the actuators are well attached to each other. Recreating the situation on the left in figure 4.8.

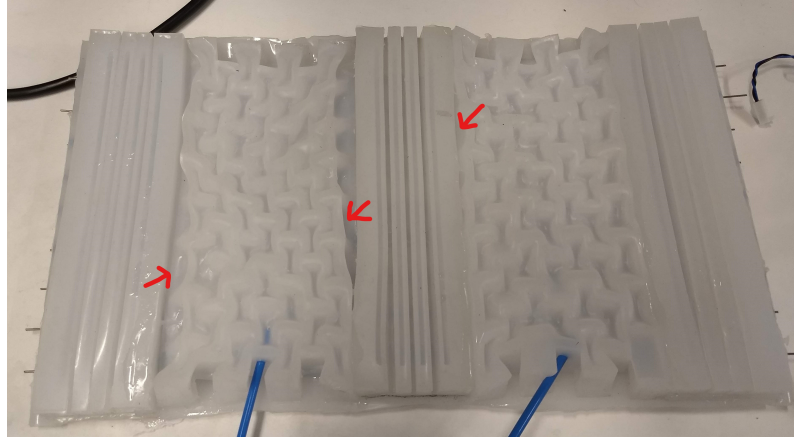


Figure 4.9: Version 2 of the diaphragm being fabricated. The vacuum actuators, in this figure a vacuum is applied to them, are still not completely attached to the bending actuators. This can be seen at the red arrows. That is fixed by adding more uncured Ecoflex at those position

4.4 Testing

In order to see what is possible with the diaphragms both versions of the diaphragm have briefly been tested to see what motion can be achieved and what the limits are. This is done to determine which version will be characterized further and whether more improvements to the diaphragm, stand of liver phantom are necessary to comply to the requirement set in section 2.1. In order to do this testing and the characterization later on a small Matlab application has been written that can control the pressure regulators via an Arduino to actuate the diaphragm. The user interface of this application can be seen in figure 4.10.

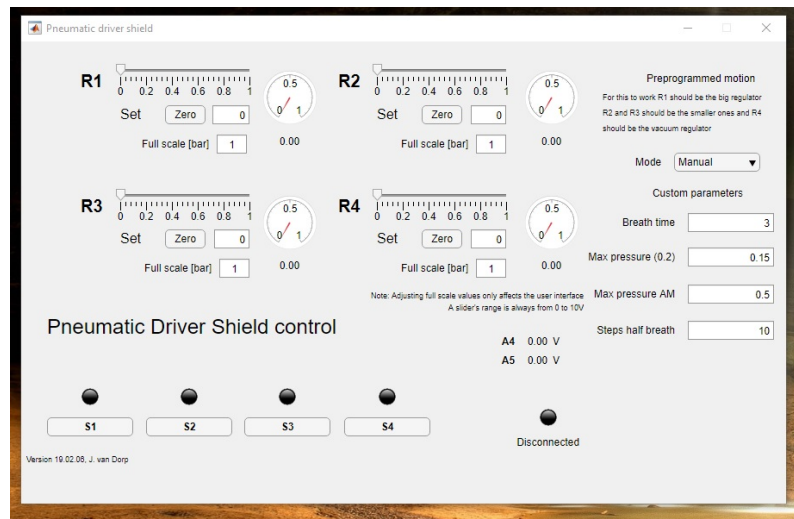


Figure 4.10: The matlab application to easily control the pressure regulators while testing. Also a 'rudimentary' breathing loop can be set with this application.

4.4.1 Diaphragm version 1

Diaphragm version 1 has first been tested unloaded. This has been done by putting an empty tray that was normally used for mixing Ecoflex against the diaphragm, actuate it and measure its displacement. The displacement is measured in SI direction compared to the neutral position the diaphragm is in when no pressure is applied to the actuators. Actuation of all the actuators has been done simultaneously with the same pressure. This has been done in the middle of the diaphragm, because the largest motion is expected there and the liver will be put

in the middle of the diaphragm. This has been tested with and without nitinol wires inserted into the diaphragm.

The results of this can be seen in figure 4.12. It is clear from this that the motion is in agreement with the requirements set for the SI motion (between 4 mm and 14 mm). At the maximum pressure, a motion of 25 mm can be seen for the diaphragm without nitinol and of 22.5 mm for the diaphragm with nitinol. This motion is reproducible within a range of 1 mm. This is in the same order of magnitude as could be seen during the test with the single bending actuator, where the unloaded case showed a displacement of almost 20 mm.

Later tests have been done with an EM-tracker. The tracker has been placed on 3 locations on the diaphragm which can be seen in figure 4.11. This allows for tracking those points on the diaphragm in 3 dimensions instead of 1 dimension as was the case with the tray. While doing this the diaphragm was hung differently in the stand. The bottom attachment to the stand was slightly higher then in previous tests, which made sure the diaphragm was never touching the bottom plate. This gave different results. With nitinol wire inserted a motion of 18 mm could be seen and without nitinol a motion of 15 mm could be seen at 0.12 bar. This shows how much influence the constraints of the diaphragm have on the motion. Both with and without nitinol a change of 8 mm maximum motion can be seen, without any changes to the diaphragm. These results can also be seen in figure 4.12. Over the whole pressure range larger motion can be seen due to the fact that the diaphragm was not touching the plate underneath it anymore. With the EM-tracker the measurements have been stopped at 0.12 bar as ballooning became an issue when kept longer at a higher pressure. This was previously not an issue, hence data for a higher pressure for the test with the tray.

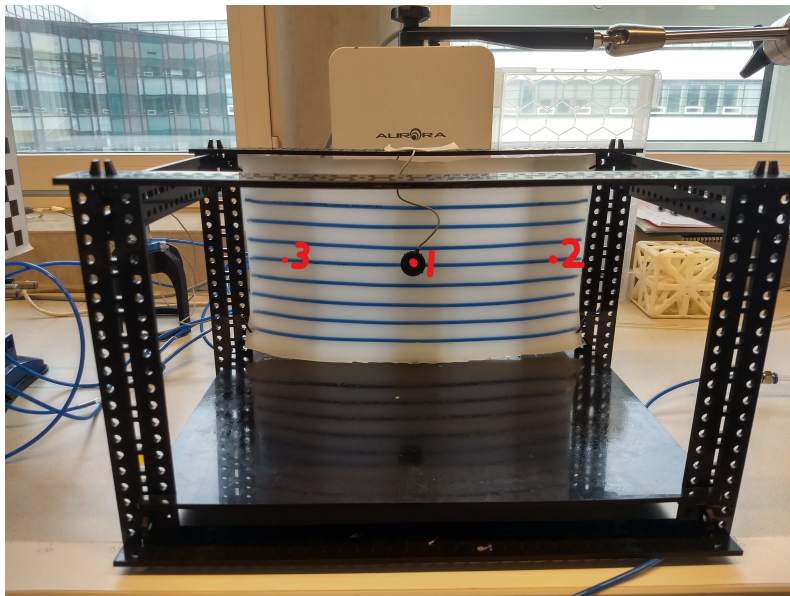


Figure 4.11: The diaphragm has been attached to the stand and an EM tracker has been attached to the diaphragm in order to track its motion in 3D. In this figure also the support plate for the liver can be seen. This is right in front of the diaphragm

After this the loaded case is tested. The phantom liver is put in front of the diaphragm and to reduce friction between the plate and the phantom liver salad oil has been put on the plate. Displacement is measured as follows: Actuators are fully actuated, the liver is placed against it and then the actuators are released. This however did not result in a significant motion of the liver phantom, while measuring with a ruler. Whether nitinol was used or not did not make a difference. The conclusion therefore was that at least with just pneumatic bending actuators the diaphragm could not generate enough force to move the liver on the plate. Instead of im-

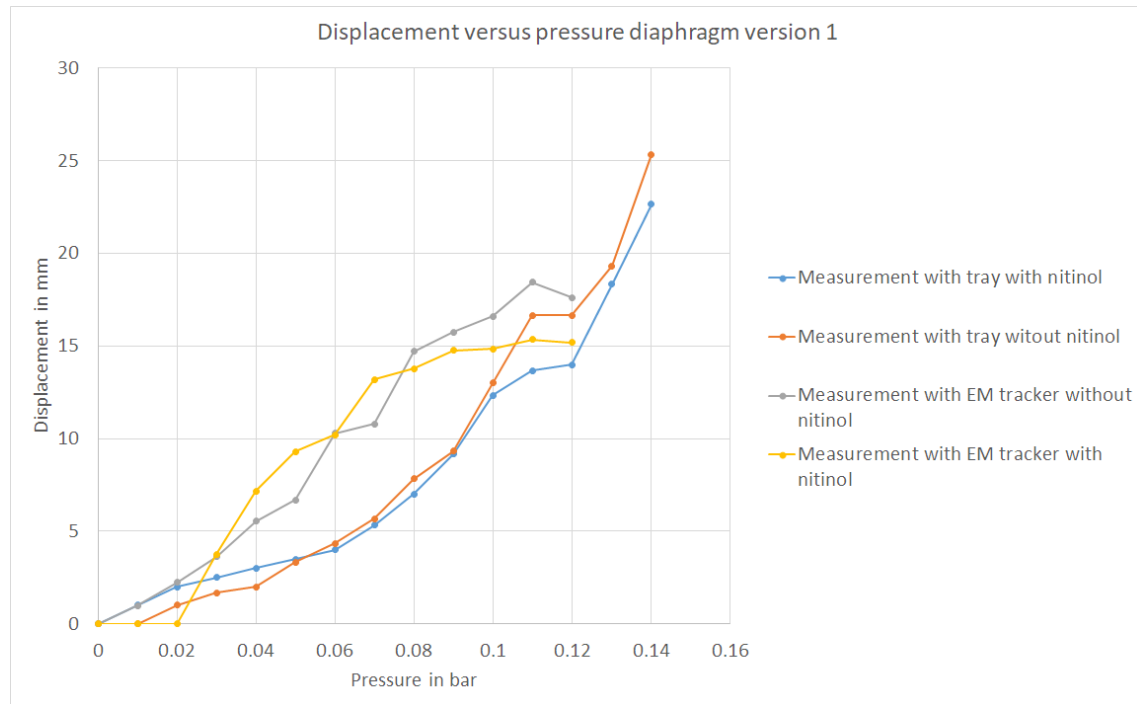


Figure 4.12: Testing of diaphragm with and without the nitinol. All pneumatic actuators are actuated with the same pressure at the same time.

proving diaphragm version 1 and the stand, which would have been an option, the decision was made to make version 2 of the diaphragm. The addition of the vacuum actuated muscle inspired structures can help generating more force, allowing for the phantom liver to be moved significantly.

4.4.2 Diaphragm version 2

The motion of version 2 has only been measured with the EM tracker. The approach was the same as for version 1. First measure the displacement of the unloaded diaphragm when actuating all bending actuators the same simultaneously. This should cause positive SI motion with a positive pressure. For negative SI motion the vacuum actuators are actuated. This is again measured on the same three points on the diaphragm, where position 1 is again most interesting as the biggest motion is expected there. These results can be seen in figure 4.13. What can clearly be seen is that motion becomes linear with addition of the vacuum actuators to the diaphragm. Due to an error in the set-up data for the vacuum actuator is not there for intermediate values. What can be said here is that motion in positive direction is slightly less with the vacuum actuators, but overall motion becomes larger. With nitinol around 28 mm and without nitinol round 40 mm. The nitinol seems to have a bigger influence on the vacuum actuator motion than the bending actuator motion, because in version 1 the difference was less clear then for version 2. The conclusion is that the SI motion has become 1.5 to 2.5 times larger when comparing version 2 to version 1 and that SI motion is well within the desired range of 8 mm to 14 mm.

The loaded case is tested next. The same as for version 1 the phantom liver has been put on the plate in front of the diaphragm. First the bending actuators are actuated after which the liver phantom is placed against the diaphragm, then pressure is released from the bending actuators and vacuum is applied to the vacuum actuators. The results of this is comparable with version 1, no significant motion could be measured.

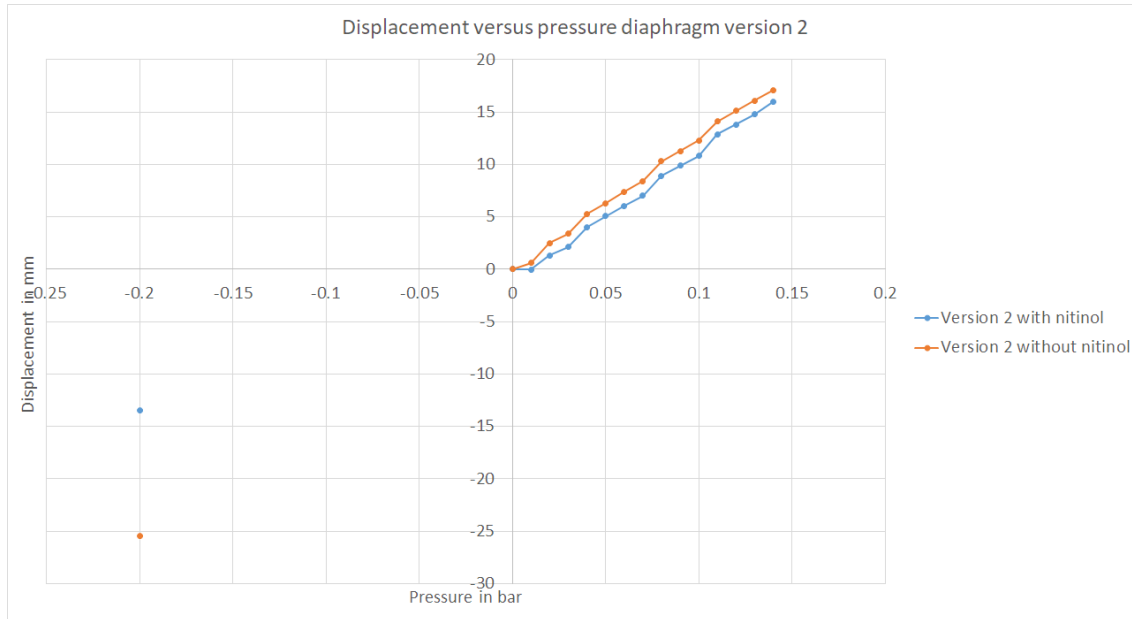


Figure 4.13: Results for displacement (SI motion) for version two of the diaphragm. With and without nitinol. Positive pressure is when the bending actuators are actuated, negative is when the vacuum actuators are actuated.

This led to the insight that either the actuators needed to be changed or the support of the liver and or diaphragm needed to be changed. The decision was not to change the actuators, thus the support of the liver and diaphragm are changed. The unloaded case showed that the SI motion could be large enough, thus with some adjustments to the stand and liver this SI motion for the loaded case will come closer to the unloaded case. Instead of placing the liver on a plate in front of the diaphragm, the liver will be hung. This will make sure there is no friction with a supporting plate of the liver, thus allowing it to move easier. Together with that a different approach for hanging the diaphragm was chosen. Eventually not only SI motion, but also AP and ML motion must be generated. By adjusting the support of the diaphragm such that it can pivot at the top the orientation (angle θ) of the diaphragm can be altered such that the displacement of the diaphragm can be used to partially cause SI motion, but also AP motion simultaneously. This set-up can be seen in figure 4.14.

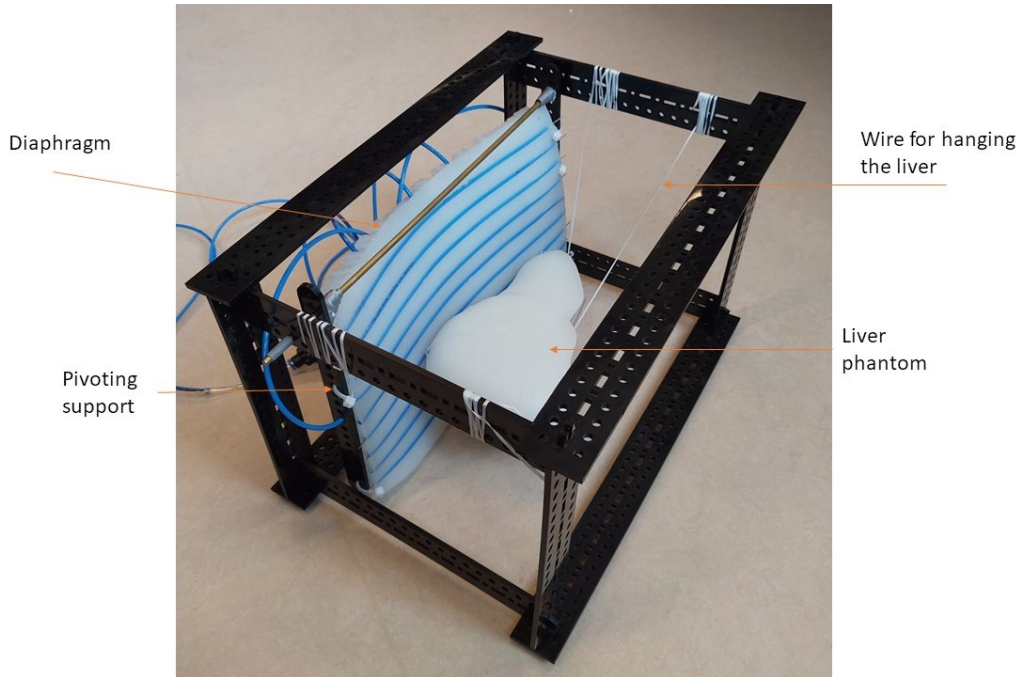


Figure 4.14: Stand with pivoting support for the diaphragm and the hanging liver phantom

4.5 Characterization for the models

In the next chapter two models will be made. For both the characterization that is done is explained next. The main difference between the characterization is the attachment of the support. The characterization that is done for model 1 is fixing the orientation of the support with tie wraps at different angles θ and in those different positions characterize what the vacuum and bending actuators do when vacuum/pressure is applied. For model 2, angle θ is altered by means of artificial muscles. These pull the bottom of the support of the diaphragm forward and up such that partially a negative SI motion is generated and a positive AP motion. The set-up with artificial muscles can be seen in figure 4.15.

The characterization has only been done without nitinol. There are two reasons for this decision. The first one is that the motion of the diaphragm without nitinol is larger, as can be seen in figure 4.13. The second reason is that nitinol might cause artefacts on an MR image and if there is no advantage in terms of motion it is better to leave it out.

The EM-sensor has been placed on top of the liver as can be seen in figure 4.15.

4.5.1 Characterization for model 1

Characterization is done for this set-up without liver phantom and with liver phantom. This is done for the diaphragm under different angles (θ). Both static characterization and dynamic characterization is done. The goal is to be able to make a simple model for control based on the characterization. The assumption is that if θ is increased the normally purely SI motion will become partially AP motion (see figure 4.16 for a visual representation of that). So SI motion would become smaller and AP motion would become bigger as θ increases. The goal eventually is to find a relation between the SI and AP motion and the pressure/vacuum in the bending and vacuum actuators. Once that relation is known the goal is to find how that changes when angle θ changes.

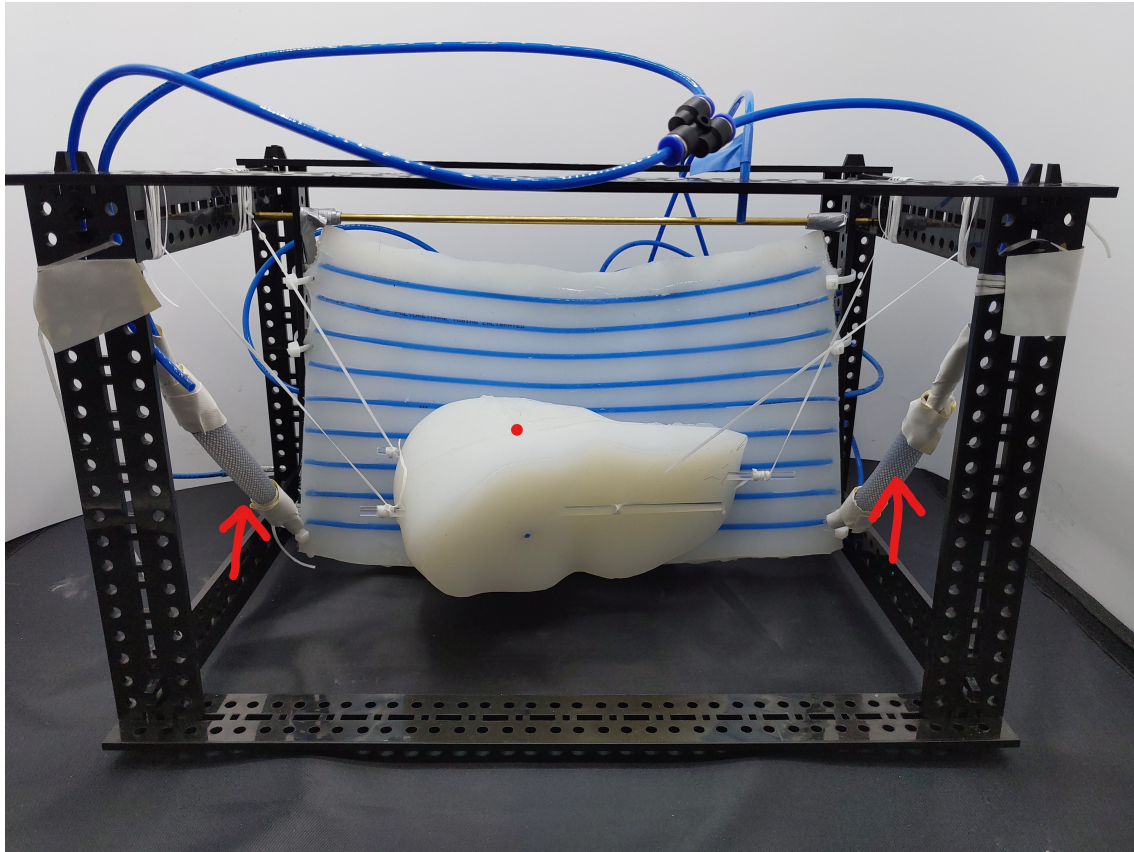


Figure 4.15: Stand with diaphragm and the artificial muscles to control angle θ . The artificial muscles are shown with the red arrows and the red dot shows the position of the EM-tracker sensor

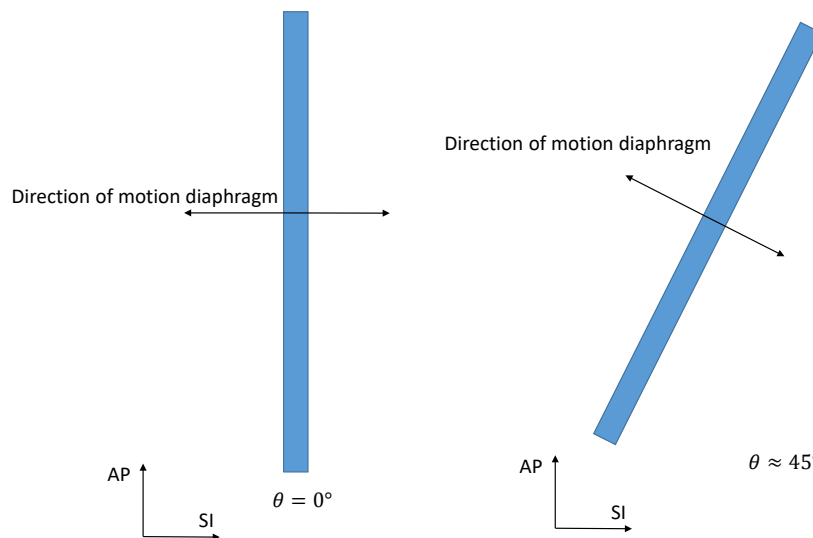


Figure 4.16: Increasing θ will change the purely SI motion in partially AP and SI motion

Static characterization

Static characterization is done by applying a pressure and waiting for the diaphragm to move to its position with that pressure applied. The position of the diaphragm is measured when it

is in equilibrium. It is kept in the same position for 10 s while the EM-tracker takes a sample every second. The average of the last five of those samples is the position that is used as result. This to mitigate the noise that is present on the EM-tracker data.

The static unloaded characterization showed that SI motion is linearly related to the applied pressure within a range from -0.1 bar till 0.14 bar and the slope of that relation decreases with a bigger θ . For AP motion this is not the case. Outside that pressure range the behaviour was not linear any more for SI motion. Next to that, AP motion did not show any significant change in motion, a maximum motion of 1 mm can be seen, nor any clear relation can be seen there between pressure and displacement or angle and displacement. This can be seen in figure 4.17.

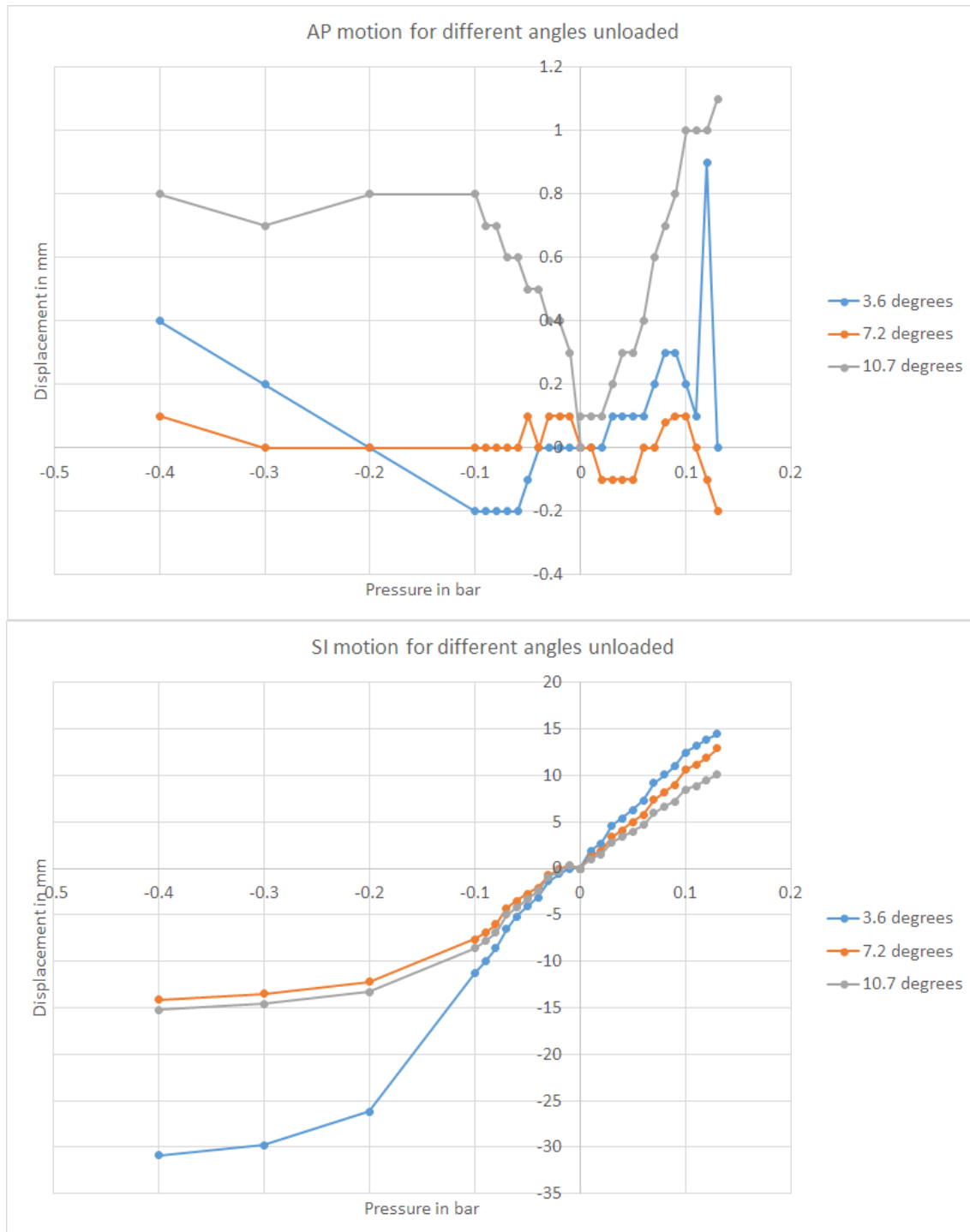


Figure 4.17: Characterization of AP and SI motion for version two of the diaphragm under different angles without a load

For the loaded case (with the liver phantom in the set-up) a more clear relation between angle, pressure and SI motion can be seen. When the angle increases the whole pressure versus displacement curve becomes less steep, as can be seen in figure 4.18. Again the AP motion is small (about 0.6 mm) and only for $\theta = 45^\circ$ a linear relation between pressure and displacement can be seen. This leads to the conclusion that it is not possible to find one angle θ where the AP and SI motion fall in the desired range that agrees with the earlier set requirements for AP and SI motion.

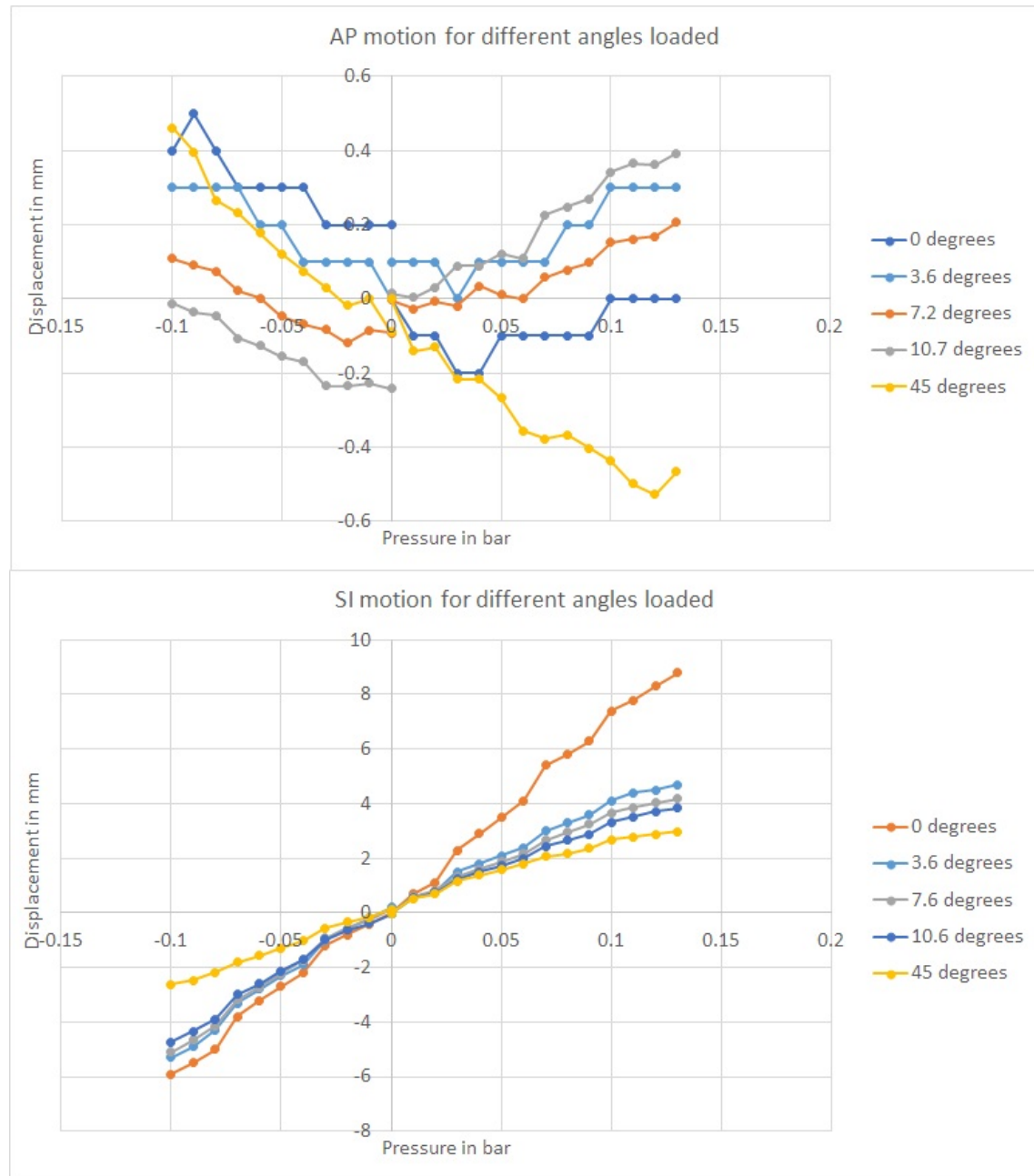


Figure 4.18: Characterization of the diaphragm under different angles while the liver is in the set-up

What can also be done to reach the desired motion in AP and SI is using the possibility that the diaphragm can pivot. If $\theta = 0$ is taken as the starting point, without actuating the actuators, but just changing the the angle of the diaphragm, a substantial motion for both AP and SI can be seen, as can be seen in figure 4.19. Using this pivoting the AP motion can be in the range that it needs to be of 8 mm at $\theta = 10.7^\circ$, this is accompanied with an SI motion. Between the diaphragm with and without nitinol only a small difference can be seen.

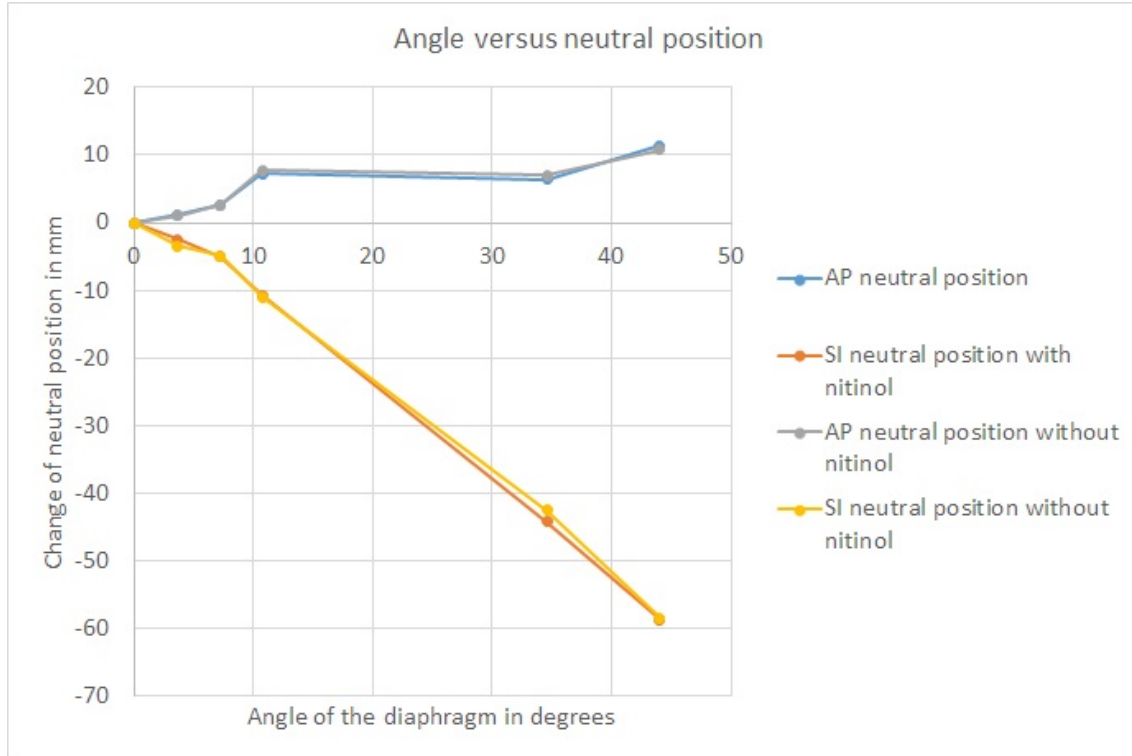


Figure 4.19: Changing θ results in an AP and SI motion. This is measured with the liver in the set-up

The relations that can be derived for AP and SI motion are equations 4.1, 4.2, 4.3 and 4.4. These will be used later on for model 1. Equation 4.1 and 4.2 give the displacement in AP or SI direction in millimetres as function of the angle of the diaphragm (θ) in degrees and the pressure in the actuators in bar. First the relation between pressure and displacement at the separate angles θ is determined with linear regression in Excel, because the data suggests this relation is linear (see figure 4.18). The part $0.405\theta^2 - 6.9187\theta + 65.497$ has been determined by determining the change of the slope of the trend lines of the data from figure 4.18 as function of θ . This is done by second order polynomial regression in Excel. All relations have an R^2 value of 0.95 or higher. This has been done with the assumption that either the bending actuator is actuated or the vacuum actuator is actuated. They are not actuated at the same time. Equation 4.4 and 4.3 give respectively the AP and SI motion as function of the orientation of the diaphragm (θ).

$$SI_{\text{bending}} = (0.405\theta^2 - 6.9187\theta + 65.497)P_{\text{bending}} \quad (4.1)$$

$$SI_{\text{vacuum}} = (0.405\theta^2 - 6.9187\theta + 65.497)P_{\text{vacuum}} \quad (4.2)$$

$$SI_{\text{neutral}} = -0.063\theta^2 - 0.306\theta \quad (4.3)$$

$$AP_{\text{neutral}} = 0.064\theta^2 - 0.0414\theta \quad (4.4)$$

Dynamic characterization

In order to see whether the static characterization holds up in dynamic motion also simple dynamic characterization has been done. In figure 4.20 the motion of the phantom liver with the diaphragm without nitinol at a 0 degree angle is shown and in figure 4.21 the motion of the

phantom with the diaphragm without nitinol at a 45 degree angle is shown. The input for this dynamic motion is a loop of 5 s where at first the bending actuators are fully actuated in 2.5 s time, after which they are released and the vacuum actuators are fully actuated in 2.5 s time. This represents a simple breathing cycle of 5 s seconds. This is done with only feed forward control for the pressure applied to the actuators and done from within the matlab application.

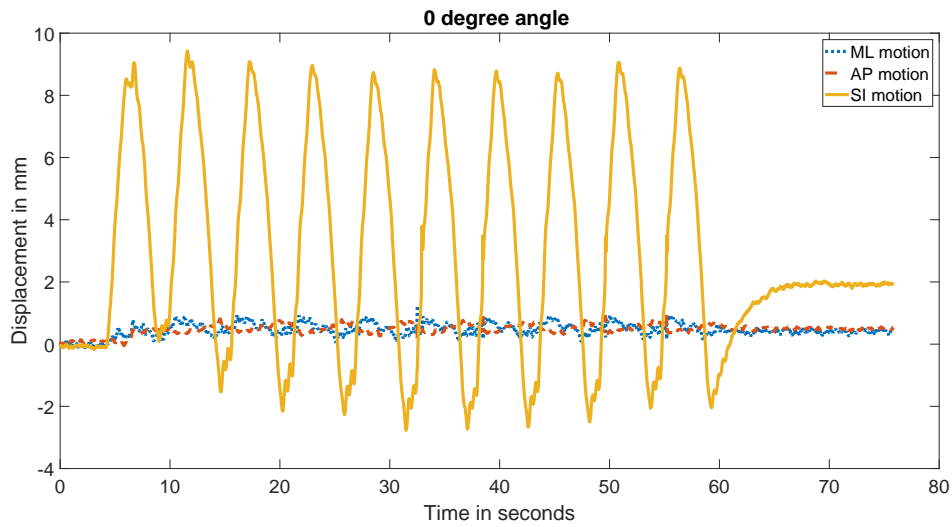


Figure 4.20: Motion at a 0 degree angle of the diaphragm with the liver in the set-up

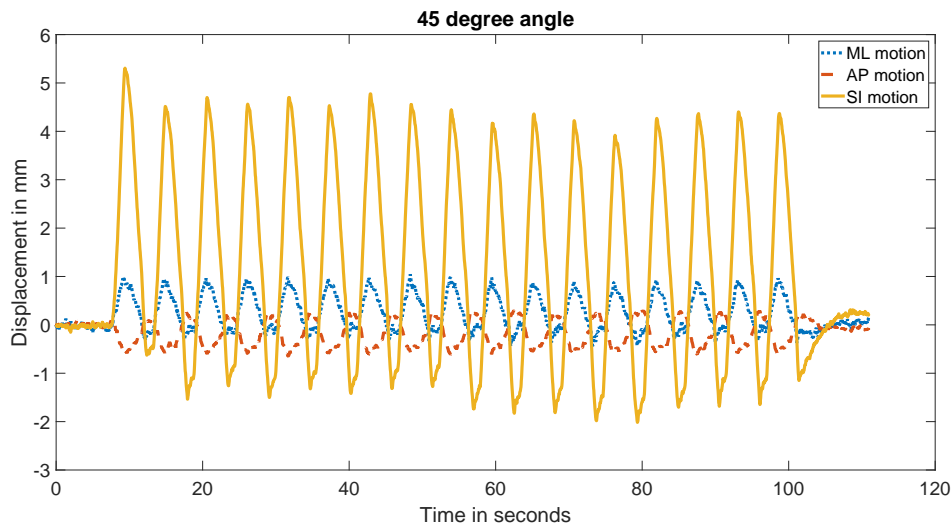


Figure 4.21: Motion at 45 degree angle of the diaphragm with the liver in the set-up

The bending actuators at a 0 degree angle are able to reach the same displacement as during the static characterization (9 mm and 9 mm from the neutral position for SI motion) and at a 45 degree angle they are able to reach an even larger displacement than during static characterization (3 mm and slightly more than 4 mm from the neutral position). This is probably due to the momentum of the liver phantom and the compliance of the diaphragm.

The vacuum actuated muscle inspired structures (for SI negative motion and for AP positive motion), however, show a smaller motion than during static testing. In both 0 degree and 45 degree orientation in the dynamic case the maximum negative motion is about half of what was reached in the static characterization. This is probably due to the fact that actuation speed of the vacuum actuators is limited by the vacuum pump.

4.5.2 Characterization for model 2

For this characterization, all actuators have been characterized for motion versus pressure while the other actuators are not actuated. This gives a good insight in what motion can be achieved with every actuator. This has been done for AP and SI motion of all actuators, but only statically. This is again measured with the EM-tracker while keeping holding the pressure the same for 10 s and taking the average of the last five samples during that period. The results of the measurements can be seen in figure 4.22, 4.23 and 4.24. The difference between this characterization is that the angle θ is not measured anymore and the support is not fixed at one angle anymore by tie wraps. The support is held in place and pivoted by artificial muscles as can be seen in figure 4.15.

A few things can be said about these results, where the first one is that all actuators individually or only able to cause a small AP motion. Next to that, the PAMS and vacuum actuators cause a negative SI motion and positive AP motion whereas the bending actuators cause a negative AP motion and positive SI motion. This is as expected and can be used when creating a model. Dynamic characterization has not been done separately for this model due to time constraints and the fact that this would not be used in model 2.

The relations that can be derived for AP and SI motion for the different actuators are equation 4.5, 4.6, 4.7, 4.8, 4.9 and 4.10. Again these pressure versus displacement relations have been determined with help of linear regression and polynomial regression in Excel. All relations are approximations with R^2 values of 0.95 or higher.

$$SI_{\text{bending}} = 29.888P_{\text{bending}} \quad (4.5)$$

$$SI_{\text{vacuum}} = 265.75P_{\text{vacuum}}^2 - 98.891P_{\text{vacuum}} \quad (4.6)$$

$$SI_{\text{muscle}} = -12.628P_{\text{muscle}} \quad (4.7)$$

$$AP_{\text{bending}} = -5.8537P_{\text{bending}} \quad (4.8)$$

$$AP_{\text{vacuum}} = 97.35P_{\text{vacuum}}^2 - 0.7008P_{\text{vacuum}} \quad (4.9)$$

$$AP_{\text{muscle}} = 1.9461P_{\text{muscle}} \quad (4.10)$$

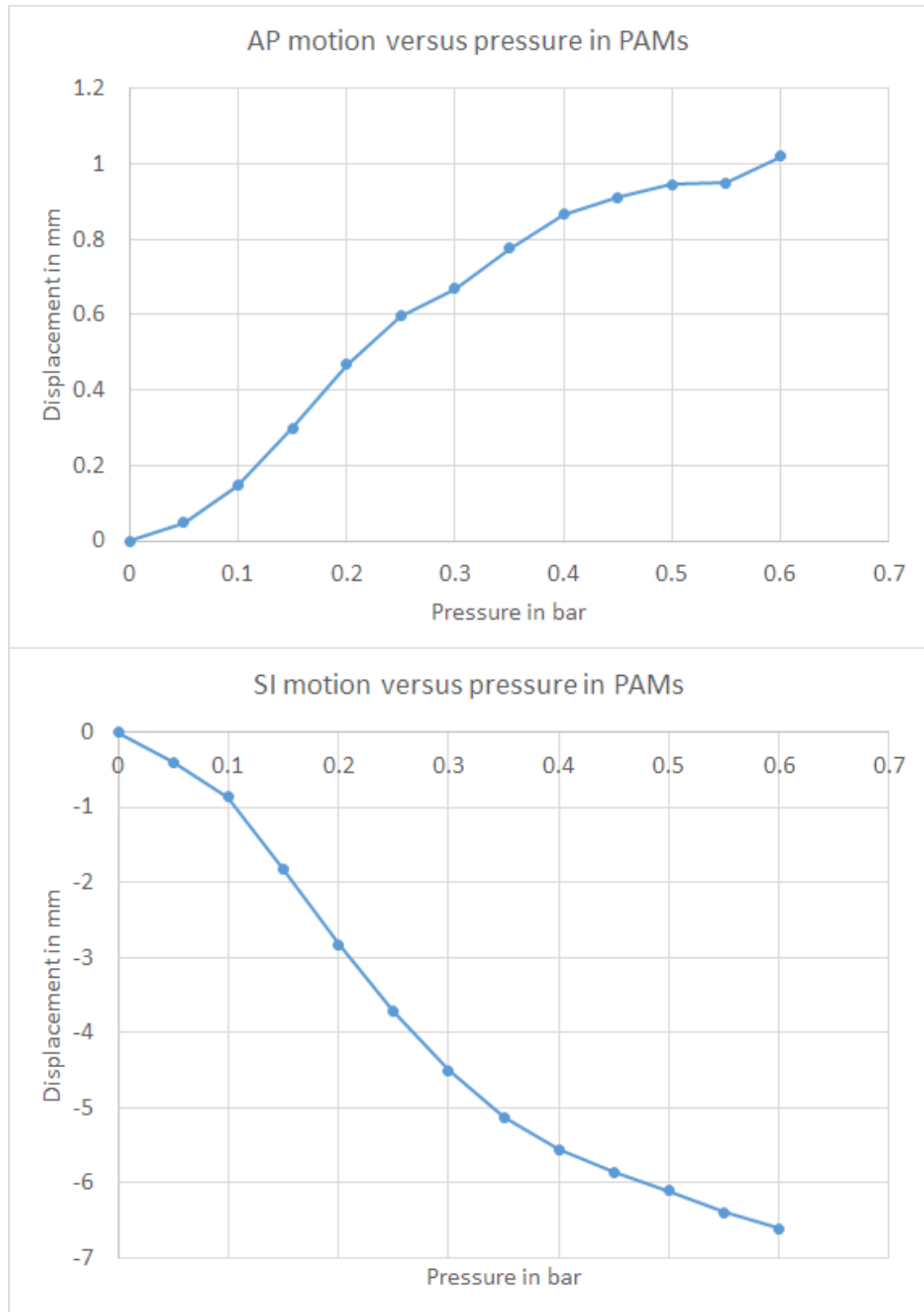


Figure 4.22: The characterization of AP and SI motion while applying different pressure to the artificial muscles

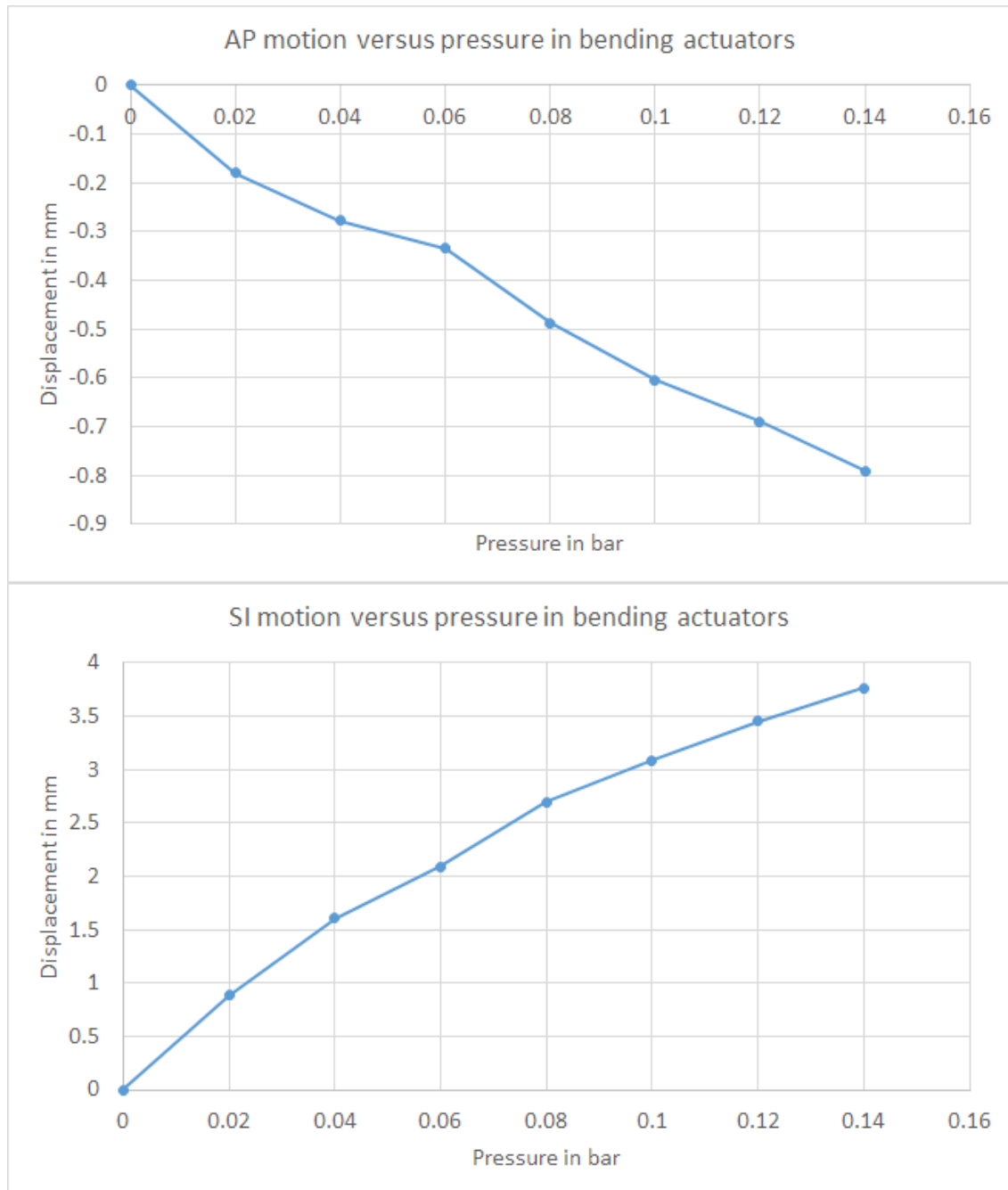


Figure 4.23: The characterization of AP and SI motion while applying different pressure to the bending actuators

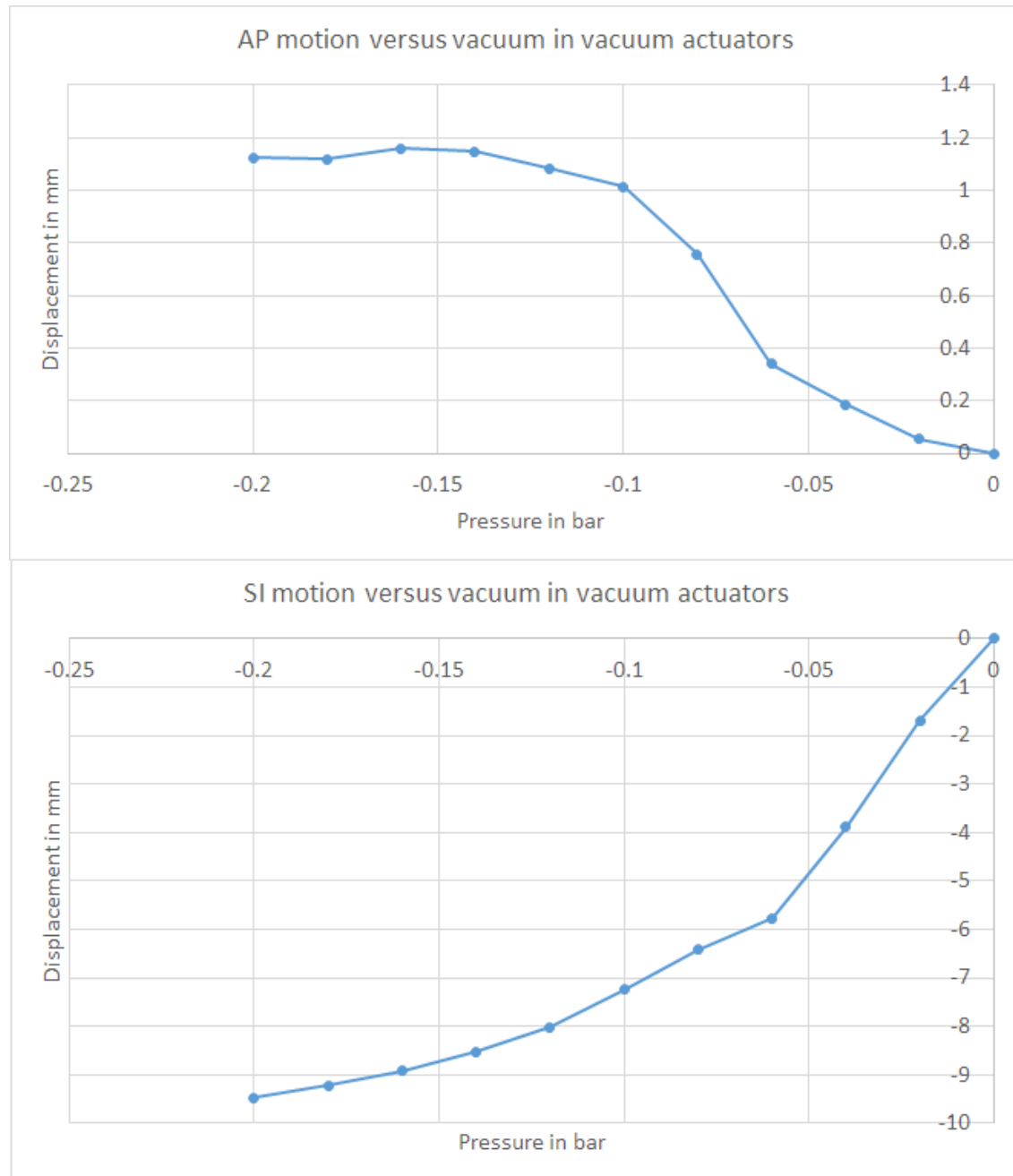


Figure 4.24: The characterization of AP and SI motion while applying different vacuum to the vacuum actuators

4.6 Summary and next steps

In this chapter 2 versions of the diaphragm have been designed and tested. A stand has been made and several modifications to the whole set-up have been done. The first version did not show the desired behaviour when loaded with the liver phantom, which was the reason to develop version 2. Version 2 did also not show the desired behaviour with the liver phantom placed in the set-up. However, after modifying the support of the diaphragm and the liver, the motion that could be achieved was within the requirements. Eventually characterization for two different models has been done and relations used for the models are derived. These models will be made and explained in the next chapter. Both characterizations show that the device can reach the desired motion for SI, but AP will be difficult.

5 Model of the diaphragm and control

5.1 Model

The models are made in 20-sim 4.7. This is a software package for mechatronics systems in which models can be made and simulations can be done. With this software it is possible to directly generate the controller code for an Arduino from 20-sim. This makes it an ideal software package to make the model and a controller in. The goal of the models is to predict the behaviour of the device and to be able to test a controller and different motion profiles for the device with the model.

Two different models of the diaphragm are made, from now on called model 1 and model 2. The models are comparable, but model 1 takes AP and SI motion to be partially decoupled. In model 2 they are not decoupled. What this means for the model will be explained later on. For both models it holds that AP and SI motion are zero when none of the actuators is actuated. All displacements that are calculated in the model are relative to the starting/initial position. So at the start of the simulations this means the displacement for AP and SI is both zero. For the measurements this is set to zero when the measurements are started. At that moment it is made sure the diaphragm is in equilibrium and none of the actuators are actuated.

5.1.1 Model 1

In this model the characterization done explained in section 4.5.1 is used to describe the relations between pressure input for the bending and vacuum actuators and the resulting displacement. For this model artificial muscles are used to change angle θ (the orientation of the diaphragm). Increasing pressure in the artificial muscles will increase the angle θ which is responsible for AP motion and part of the SI motion. The assumption is that AP motion is only generated by the artificial muscles. Because earlier characterization showed only small AP motion when actuating the bending and vacuum actuators (see figure 4.18) and significant AP motion when θ is changed (see figure 4.19). The vacuum and bending actuator only generate SI motion. This is on top of the SI motion that is already generated by the artificial muscles. The directions that are induced by actuating the different actuators can be seen in figure 5.1.

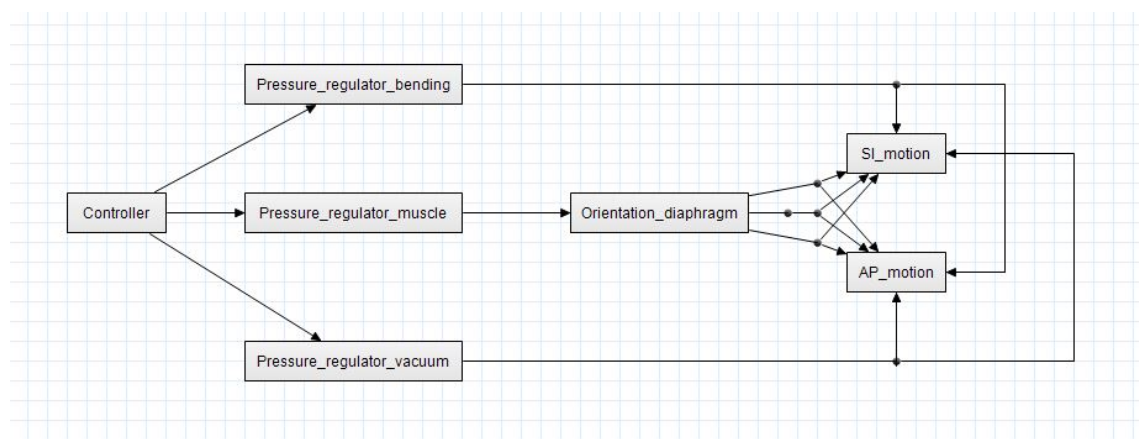


Figure 5.2: Layout of model 1 in 20-sim

As can be seen in the figure 5.2 there is a controller. This controller outputs a voltage to the pressure regulators. The pressure from *Pressure_regulator_muscle* causes the diaphragm to rotate. This causes an AP and SI motion, which is derived from the characterization as can be

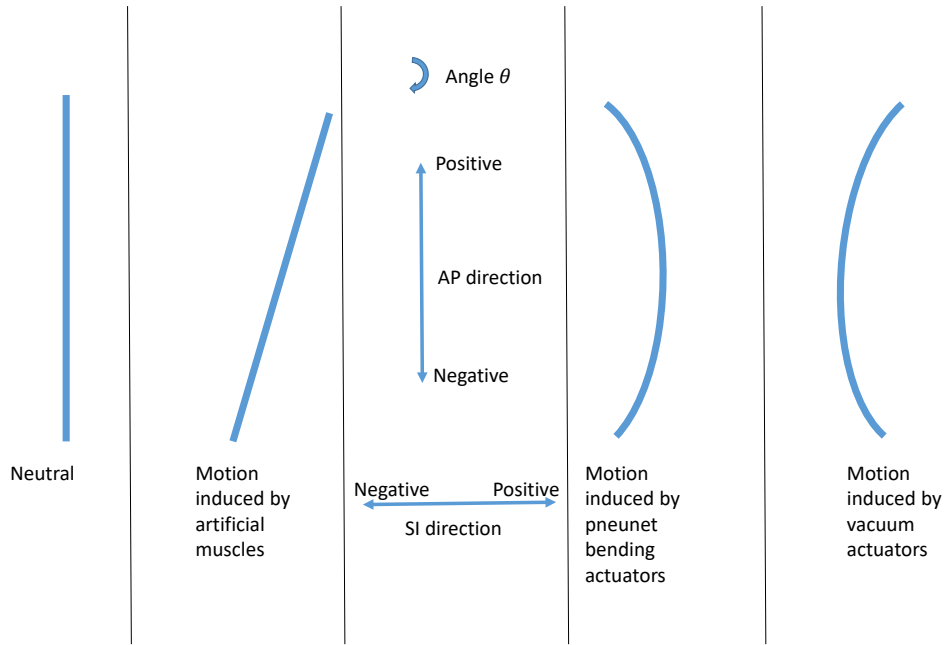


Figure 5.1: The direction of motion induced by the different actuators. The view depicted here is similar to the view in figure 4.1

seen in figure 4.19. With the input pressure the angle θ is determined and with that an AP and SI motion. The code for that can be seen next:

```
angle=10.245*P_muscle+4.3294;
AP_neutral=0.064*angle^2-0.0414*angle;
SI_neutral=-0.063*angle^2-0.306*angle;
```

These values are used to separately calculate SI and AP motion in *SI_motion* and *AP_motion*. For AP motion the assumption is that this is only caused by changing the orientation of the diaphragm as previously no clear relation was found between AP motion and the pressure in the vacuum or bending actuators. Hence in *AP_motion* only the following is done:

```
AP_motion=AP_neutral;
```

This is already the final AP motion.

For SI the motion is calculated as follows in *SI_motion*:

```
slope=0.405*Angle^2-6.9187*Angle+65.497;
bending=slope*P_bending;
vacuum=slope*P_vacuum;

SI_motion=SI_neutral+bending+vacuum;
```

Based on the angle of the diaphragm the slope of pressure versus displacement is determined. This is based on the characterization that was previously done (see figure 4.18). This slope multiplied by the pressure of the bending actuators or vacuum actuator causes an additional SI motion to the one that was already caused by rotating the diaphragm. So the final SI motion is calculated as follows: $SI_motion = SI_neutral + bending + vacuum$. This is the displacement as seen in figure 4.19 and 4.18 added or the addition of equation 4.1, 4.2, 4.3 and 4.4.

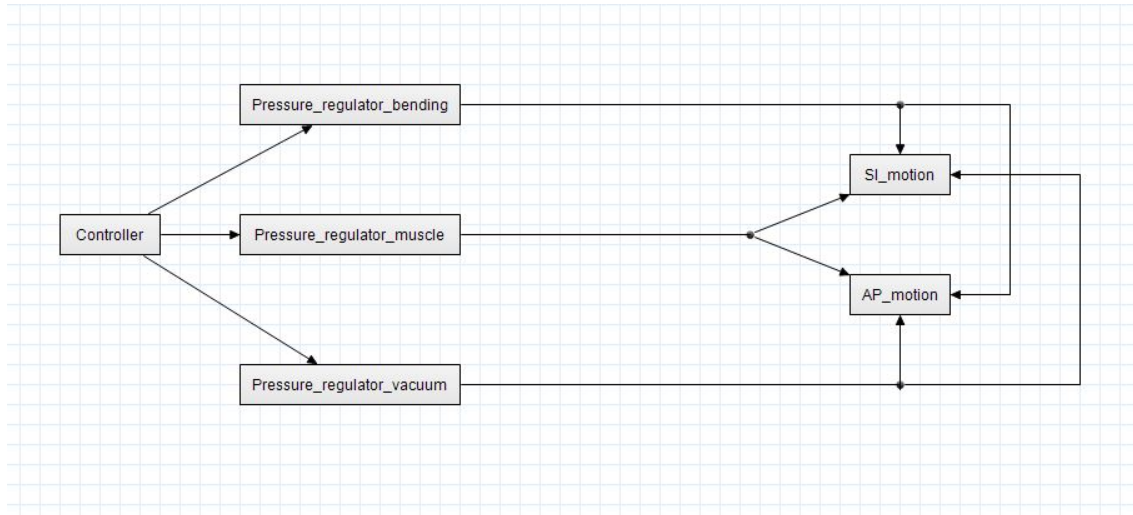


Figure 5.3: Layout of model 2 in 20-sim

5.1.2 Model 2

In model 2 the orientation of the diaphragm is not taken into account separately and the AP and SI motion are assumed to be coupled. This means that a given SI motion will always result in a certain AP motion. The characterization explained in section 4.5.2 is used here.

As can be seen in figure 5.3 the controller outputs again a voltage to the pressure regulators, these pressures are then used to calculate the SI and AP motion. The assumption is that the orientation of the diaphragm only has a small impact on the displacement caused by actuating the bending and vacuum actuators and is therefore neglected in this model. This is based on the data in figure 4.18. Only small changes can be seen for SI motion between the 3.6 and 10.6 degrees plots. Therefore the relation between pressure in the bending and vacuum actuators and their displacement does not change with a changing orientation of the diaphragm. This is the main difference with model 1 next to the AP and SI motion being coupled in model 2. In *SI_motion* the following is done:

```

bending=29.888*P_bending;
vacuum=265.75*P_vacuum^2 + 98.891*P_vacuum;
muscle=-12.628*P_muscle;

SI_motion=bending+vacuum+muscle;

```

Based on the pressure in every actuator a displacement caused by the actuator is calculated. Once that is done all these displacements are added and the result is the final SI motion.

For AP motion the same is done, but with a different characterization curve:

```

bending=-5.8537*P_bending;
vacuum=97.35*P_vacuum^2 - 0.7008*P_vacuum;
muscle=1.9461*P_muscle;

AP_motion=bending+vacuum+muscle;

```

Seperate contributions to the AP motion of the different actuators are calculated based on the pressure inside them, after which they are added and the result is the final AP motion.

5.2 Control

Two different controllers are made based on the different models that were made. Controller 1 is made for model 1 and controller 2 is made for model 2. Both controllers are purely feed forward. This allows for easy operation in an MRI machine, because next to the set-up itself no additional sensors are needed. MRI data could be used for feedback for the controller when the device is in an MRI machine, however usually the refresh rate of this is low, somewhere around 2 Hz. For this reason there is not looked into getting feedback from an MRI. Feedback from the EM-tracker that was also used for characterization is an option that is looked into, but eventually this is not pursued.

Both controllers have the same constants that can be set with which several parameters for the control of regulators can be altered. These constants are the following:

- **maxpregbending:** Maximum pressure in bar that the pressure regulator attached to the pneunet bending actuators can output, this is a specification from the regulator (default is 2).
- **maxpregmuscle:** Maximum pressure in bar that the pressure regulator attached to the artificial muscle can output, this is a specification from the regulator (default is 2).
- **maxpregbvacuum:** Maximum vacuum in bar that the pressure regulator attached to the vacuum actuators can output, this is a specification from the regulator (default is -1).
- **maxvregbending:** Maximum voltage that is applied to the regulator by the Arduino shield. 0 corresponds to 0 and 255 corresponds to 10 V (default is 255).
- **maxvregmuscle:** Maximum voltage that is applied to the regulator by the Arduino shield. 0 corresponds to 0 and 255 corresponds to 10 V (default is 255).
- **maxvregbending:** Maximum voltage that is applied to the regulator by the Arduino shield. 0 corresponds to 0 and 255 corresponds to 10 V (default is 255).
- **maxpbending:** Maximum pressure in bar that will be applied to the bending actuators. Once the controller tries to set a pressure that is above this value it is limited to this maximum value (default is 0.14).
- **maxpvacuum:** Minimum pressure in bar that will be applied to the vacuum actuators. Once the controller tries to set a pressure that is above this value it is limited to this maximum value (default is -1).
- **maxpmuscle:** Maximum pressure in bar that will be applied to the artificial muscles actuators. Once the controller tries to set a pressure that is above this value it is limited to this maximum value (default is 0.6).

For both controllers a sine is used as motion profile for AP and SI, so both breath in and breath out are the same. For breath in the AP motion will be positive and the SI motion will be negative. Breath out will have the opposite, so AP motion will be negative and SI will be positive. For this profile the breath in time and breath out time can be set in seconds with *breath_in_time* and *breath_out_time*. Also the maximum AP and SI motion in mm can be set with *max_AP* and *max_SI*. The 'standard' motion for both controllers is 8 mm for SI motion and 4 mm for AP motion. This is for AP and SI in the middle of the range stated as the requirements in section 2.1.

5.2.1 Controller 1

As explained for model 1 the SI and AP motion are partially decoupled. With the artificial muscles AP and SI motion can be controlled and with the vacuum and bending actuators SI motion can be controlled. This means that an AP motion profile can be set by controlling the artificial muscles. Next, with the vacuum and bending actuators the SI motion can be controlled to follow another profile. These then need to compensate for the SI motion that is already generated by the artificial muscles.

The internals of controller 1 can be seen in appendix 7.2.1.

setpoint_AP is the setpoint that is generated for AP motion in mm. Based on this the angle the diaphragm needs to make is determined (*setpoint_AP_degrees*). With this the pressure in the artificial muscles that is needed to reach that angle is determined (*AP_control*).

Based on the angle that was the setpoint for AP motion the new SI position is determined (*SI_neutralc*). After this the same relation as is used in *SI_motion* in model 1 is used to determine the relation between pressure in the bending and vacuum actuators and their resulting SI motion.

The setpoint for SI motion is again a sine (*setpoint_SI*). The pressure in the bending actuators (*SI_control_bending*) and the vacuum in the vacuum actuators (*SI_control_vacuum*) is calculated based on the difference between the setpoint and the SI motion that was already achieved due to the set AP motion.

At the end the output voltage is calculated for the three regulators and is limited to not exceed the previously set maximum pressure. This can cause the liver not being fully able to reach the setpoint, because a higher pressure would be needed to reach it. This can happen in both the model as well as in the real set-up.

5.2.2 Controller 2

As explained for model 2 the SI and AP motion are coupled. The consequence is that creating a motion profile for one will result in a motion profile for the other, which cannot be altered. According to the characterization that is done SI motion is the largest motion that can be controlled. Therefore it is decided to create a motion profile for the SI motion and let that result in an AP motion profile.

Controller 2 can be seen in appendix 7.2.2.

Again the motion profile given as setpoint is a sine, this is *setpoint_SI*. First the artificial muscles are used to reach the setpoint (*setpoint_SI*). In case a higher pressure in the artificial muscles is needed than allowed the vacuum actuators are used for a larger SI motion. This is where the following if-statement is for:

```

if Muscle_control > maxpmuscle then
    Vacuum_control= 0.0122*(setpoint_SI-limit(Muscle_control,0,
        maxpmuscle)*-12.628);
else
    Vacuum_control=0;
end;
```

In case positive SI motion is desired this needs to be done by the bending actuators, this output is *Bending_control*. This is always calculated, but will only result in an actual output to the regulator once the SI setpoint is above 0.

V_muscle, *V_bending* and *V_vacuum* are again the limited output to the regulators, this makes sure that the pressure in the actuators is never in the range that they might be damaged. Just

like for controller 1 this can cause the model and the real set-up to not being fully able to reach the given setpoint.

5.3 Validation of control

For both controllers the EM-tracker is used to measure the motion of the liver. This is done by placing the EM-sensor on top of the liver as can be seen in figure 4.15. The measurement data can be compared on several points with the setpoint and the model data. The first being the maximum SI and AP motion. Secondly the ability to follow the motion profile that is given as setpoint. In case the model corresponds well with the EM-tracker data it is possible to test different motion profiles in simulation, before they are actually applied to the set-up.

5.3.1 Controller 1

The given setpoint as magnitude of the motion, predicted AP and SI motion in the model and measured AP and SI motion with controller 1 can be seen in table 5.1. The given setpoint is the peak to peak distance of the sine input, so this is the magnitude of the motion. The model AP, model SI, measured AP and measured SI are the minimum and maximum value compared to the starting position of the liver.

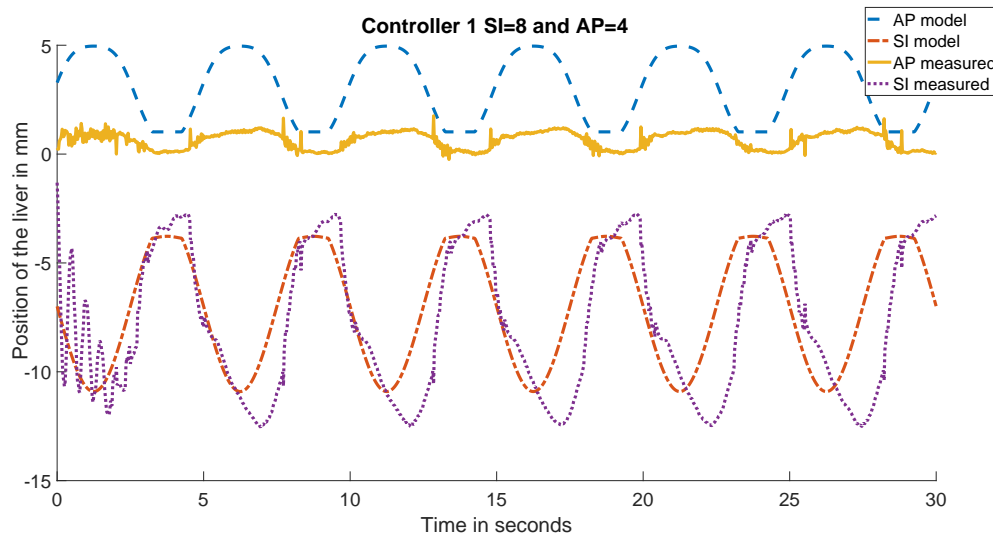


Figure 5.4: Predicted motion by the model with controller 1 and the measured motion with controller 1 of the liver

Setpoint AP	Setpoint SI	Model AP	Model SI	Measured AP	Measured SI
0	8.0	1.0 to 1.0	-11.0 to -3.7	0.5 to 0.9	-9.0 to -5.5
1.0	8.0	1.0 to 1.9	-11.0 to -3.9	0.5 to 1.0	-10.7 to -5.3
2.0	8.0	1.0 to 3.3	-10.9 to -3.8	0.5 to 1.9	-12.8 to -4.8
3.0	8.0	1.0 to 4.4	-10.9 to -3.7	0 to 1.5	-12.7 to -3.9
4.0	8.0	1.0 to 5.0	-10.9 to -3.8	0 to 1.0	-12.5 to -2.8
5.0	8.0	1.0 to 5.0	-10.9 to -3.7	-0.1 to 0.9	-11.4 to -2.6
4.0	0	1.0 to 5.0	-3.7 to -2.9	-0.5 to 0.6	-5.5 to 1.4
4.0	2.0	1.0 to 5.0	-4.9 to -3.3	-0.5 to 1.5	-5.6 to 0.5
4.0	4.0	1.0 to 5.0	-6.9 to -3.5	0 to 0.7	-7 to -0.1
4.0	6.0	1.0 to 5.0	-8.9 to -3.7	0 to 0.7	-7.3 to 1.1
4.0	10.0	1.0 to 5.0	-12.9 to -3.7	0 to 1.4	-13.3 to -4.2
4.0	12.0	1.0 to 5.0	-14.8 to -3.7	0.2 to 1.7	-14.0 to -4.6
4.0	14.0	1.0 to 5.0	-16.9 to -3.7	0.5 to 1.9	-14.0 to -4.7
4.0	16.0	1.0 to 5.0	-18.8 to -3.8	0.5 to 1.9	-14.2 to -5.1
4.0	18.0	1.0 to 5.0	-20.9 to -3.7	0.7 to 1.7	-14.3 to -5.4
4.0	20.0	1.0 to 5.0	-22.9 to 3.7	0.7 to 1.7	-14.4 to -5.6
4.0	22.0	1.0 to 5.0	-24.9 to -3.7	0.7 to 1.8	-14.3 to -5.8

Table 5.1: Setpoint AP and SI motion, predicted AP and SI motion compared to the neutral position as 0 and measurement data for AP and SI motion also compared to the neutral position. All values are given in millimetres

5.3.2 Controller 2

For controller 2 the same measurements have been done. In table 5.2 the given SI and AP setpoint can be seen together with the AP and SI range that will be reached according to the model and the AP and SI range that were reached when measured with the diaphragm.

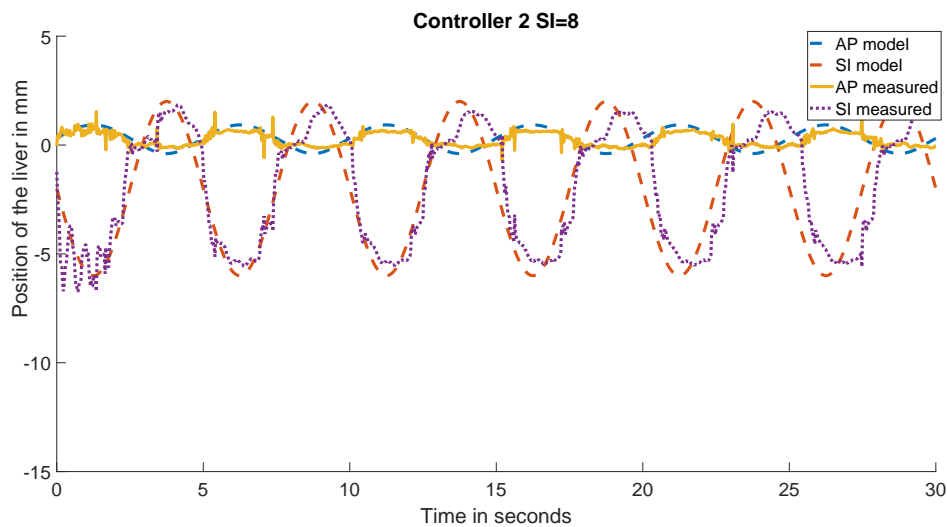


Figure 5.5: Predicted motion by the model with controller 1 and the measured motion with controller 2 of the liver

Setpoint SI	Model AP	Model SI	Measured AP	Measured SI
2.0	-0.4 to 0	0 to 1.9	-0.2 to 0.1	0.1 to 2.1
4.0	-0.4 to 0.3	-2.0 to 2.0	-0.3 to 0.2	-1.9 to 1.8
6.0	-0.4 to 0.6	-4.0 to 2.0	-0.2 to 0.5	-4.3 to 1.8
8.0	-0.4 to 0.9	-6.0 to 2.0	-0.1 to 0.7	-5.5 to 1.5
10.0	-0.4 to 1.2	-8.0 to 2.0	-0.2 to 0.8	-6.4 to 1.4
12.0	-0.4 to 1.3	-10.3 to 2.0	-0.2 to 0.8	-8.5 to 1.1
14.0	-0.4 to 1.4	-12.1 to 2.0	-0.2 to 0.9	-10.4 to 0.6
16.0	-0.4 to 1.8	-13.7 to 2.0	-0.2 to 1.0	-11.9 to -0.3
18.0	-0.3 to 2.3	-14.9 to 2.0	-0.2 to 1.1	-12.8 to -0.9
20.0	-0.4 to 2.8	-15.8 to 2.0	-0.2 to 1.3	-12.9 to -1.64
22.0	-0.4 to 3.5	-16.5 to 2.0	-0.3 to 1.5	-13.1 to -2.4

Table 5.2: Setpoint AP and SI motion, predicted AP and SI motion compared to the neutral position as 0 and measurement data for AP and SI motion also compared to the neutral position. All values are in millimetres

5.3.3 Comparison between controller 1 and 2

To be able to compare the controllers both controllers will be compared on the basis of AP and SI motion and whether they are able to keep up with different breathing times. Also the repeatability of the motion is important. Both controllers show repeatability of AP and SI motion within the error of the EM-tracker.

For AP motion only controller 2 is able to come close to the predicted motion. Up until an SI motion of 12 mm it is able to stay within 0.3 mm for the predicted motion on both sides of the motion. For larger SI motion the difference becomes larger, but still the shape is comparable. Controller 1 does offer the ability to separately set a motion profile for AP, but it is never able to reach the predicted AP motion. The maximum AP motion with controller 1 is 2 mm and for controller 2 that is 1.8 mm. So the maximum reachable motion for controller 1 is larger than for controller 2, but it is not able to predict that well.

For SI motion also controller 2 is better able to reach the predicted motion. This is within 1 mm on both sides of the motion (minimum and maximum) for SI motion magnitude up to 10 mm. For larger SI motion than 10 mm it is not completely able to reach the predicted motion anymore. For controller 1 the fact that the motion profile for AP can be set separately causes issues. This can be seen when comparing figure 5.4 to figure 5.6. Where in the first predicted SI motion and measured SI motion are comparable respectively around 6 mm and 8 mm, but in the second the measured SI motion is around 6 mm and the predicted SI motion is around 1 mm. The assumption made for model 1 that AP and SI motion are decoupled does not seem to be correct based on the measurement data from controller 1. The maximum SI motion for controller 1 is 9.4 mm and for controller 2 the maximum motion is 11.9 mm.

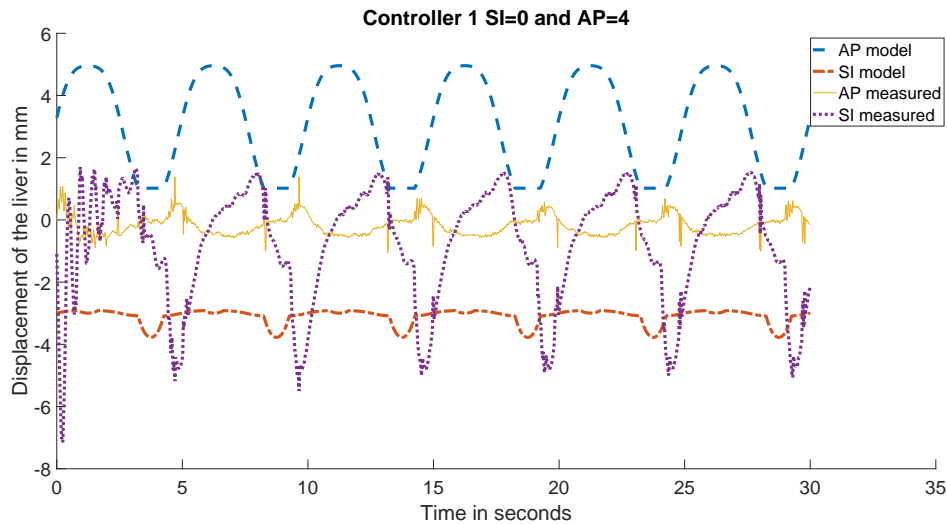


Figure 5.6: The separate motion profile for AP and SI cause the main differences between the model and the real diaphragm

For both controller 1 and controller 2 the breath-in and breath-out time of 1.0, 2.0, 2.5, 3.0, 4.0 and 5.0 s has been tested. The result was comparable for both controllers. With 1.0 s for breath in and breath out time oscillations of the diaphragm can be seen. Which are most probably due to the elasticity of the diaphragm, the weight of the liver and some flexibility in the stand. These oscillations can be seen in figure 5.7. For both controllers the SI motion that is predicted is reached or is even larger, but oscillations along the whole sine can be seen. At longer breath-in and breath-out times this is not an issue.

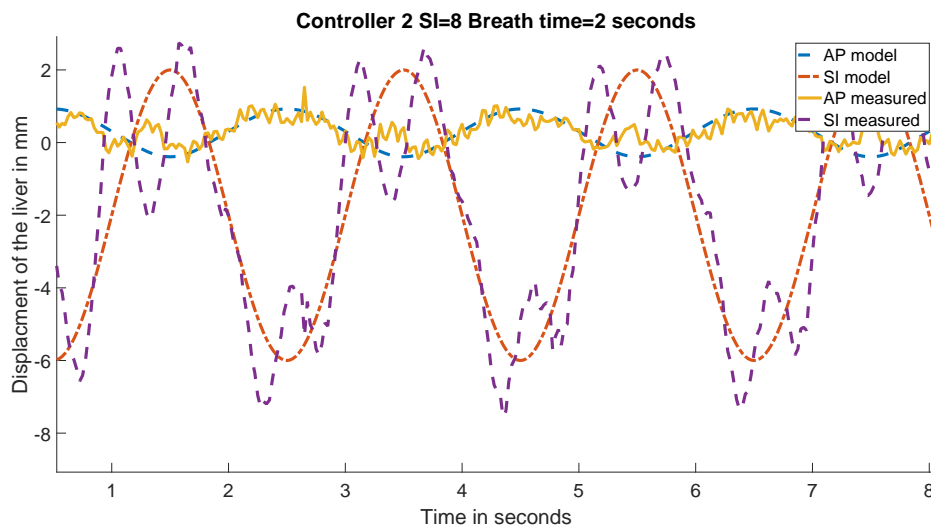


Figure 5.7: With controller 2 with a breath-in and breath-out time of 1.0 s oscillations can be seen.

5.4 Summary

In this chapter two models describing the behaviour of the device have been developed. Next to that two controllers have developed to control the device. These have been tested with the model and the actual soft robotics diaphragm. As has been explained model 1 in combination with controller 1 did not describe the behaviour of the device well, most probably due to the assumption that AP and SI motion were partially decoupled. From measurement data it is clear that AP and SI motion are not decoupled as they were assumed to be decoupled. Model 2 and

controller 2 showed good results for predicting and controlling the device for SI motion within a range of SI motion from 0 mm to 10 mm. AP motion within that range is, however, still only around 1 mm. Larger motion for AP and SI is possible, but the predictions made by the model are not reliable at that point.

6 Conclusion and recommendations

In this project a soft robotic diaphragm inspired by the human anatomy has been developed. Actuators have been designed and characterized. Based on this a diaphragm has been developed and characterized. Two models that predict the behaviour of this device have been developed. For both models a separate controller has been developed which has been tested in simulation as well as on the real set-up. Model 1 and controller 1 were not a particularly good fit. The model was not able to predict the AP motion well, because it was usually off by a factor 2 or more. On top of that the assumption made that AP and SI motion could be partially decoupled was wrong. Model 2 and controller 2 were a better fit for a range of motion up until 10 mm SI motion. AP could be predicted within 0.3 mm and SI within 1 mm in the aforementioned range. Also the repeatability of the motion was good. For controller 2 a deviation of not more than 0.3 mm between the maximum and minimum of two separate breath cycles can be seen for SI motion.

6.1 Discussion of the specifications

The requirements for the device were already given at the beginning of this report in section 2.1. They are given here again and whether the specific requirements are met is explained. Normal text is the given requirement and italic is the explanation about whether the requirement is met or not.

- The robot needs to be MR safe and sufficiently MR compatible. *All materials have been chosen such that they should not cause artefacts in an MRI. The only part that might cause issues is the brass bar that is used for the support of the diaphragm to pivot around. This might still need to be changed before testing in an MR scanner is done. As long as the pneumatic tubes are long enough to place all the electronics outside the MRI room these should not cause problems with MR compatibility. This is with the assumption that long tubes are only introducing a delay in control and no pressure waves start to occur in the tubes or actuators. Testing in an MR machine has not been done yet, but in theory the device should be MR safe and compatible.*
 - The part that goes inside the scanner bore should not cause artefacts that can obscure the region of interest. *Apart from the brass bar that is used for pivoting the support of the diaphragm there are no materials used that should cause artefacts.*
 - The system needs to fit inside a scanner with a bore of 50 cm, which is assumed to be the smallest MRI scanners that is commonly used for this application. *Although it is not tested the device should fit within a scanner bore.*
- The motion of the liver needs to be accurate *This is partially met, but perhaps more improvements can be made by tuning the controller*
 - Between 0 mm to 8 mm in left-right (ML) direction. *This has not been looked into as eventually the focus lay on SI and AP motion. However, by controlling the bending actuators and vacuum actuators all independently this should be possible.*
 - Between 4 mm to 14 mm in up-down (SI) direction. *A maximum SI motion 11.9 mm is achieved with controller 2, so 14 mm is not reached. During static characterization this was reachable, so tuning the controller might allow for a motion of 14 mm. The device is, however, able to follow a sine setpoint and to create realistic displacement in SI direction of a liver phantom.*
 - Between 2 mm to 8 mm in front-back (AP) direction with preferably the possibility of creating a difference between left and right. *A maximum AP motion of 2 mm is*

reached with the controllers, so the minimum is met. During static characterization with the liver phantom up to 10 mm was achievable. Hence, tuning the controller and some small modifications to the set-up might allow for larger AP motion. Especially the boundary conditions are important to look at.

- *Frequency that should be achievable is 0.25 Hz to 0.3 Hz. Actuation at 0.5 Hz showed to be problematic as this introduces oscillations around the given setpoint, but slower actuation at 0.25 Hz showed no issues.*
- *Optional: taking into account the motion of for example heartbeats It has been tested and it is possible to implement heartbeats by actuating the bending actuators. The data for that cannot be found in the report, but a version of controller 2 is made where the heartbeat speed and amplitude can be set.*
- *The set-up will represent a patient in supine position This is done by orientating the soft robotics diaphragm the same as the diaphragm would be of a supine patient.*
- *The design of the set-up will be inspired by the human anatomy This is done by looking at what the motion is of the human diaphragm while breathing and looking at what causes that motion. The contracting motion of the costal muscles is represented by the vacuum actuators and pneumatic artificial muscles. The elasticity of the lungs can be simulated by the pneumatic bending actuators.*
- *The user interface should be such that it is usable by clinicians. Currently there is not a graphical user interface for the control of the device. All parameters need to be set in the Arduino IDE before compiling and uploading to an Arduino is done. Even though this is not particularly user friendly with a small step by step manual most people should be able to work with it. The current implementation makes it also straightforward for people with some programming skills to adjust the controller more than just altering the maximum AP and SI motion and the breath-in and breath-out time.*

When comparing this device to other devices that have the same purpose, this device mainly distinguishes itself by its actuation. The device consists of a self-actuating diaphragm which has not been found in literature. The main advantage is that the device actuated in an way comparable to the human diaphragm, which was for example not the case for the previous set-up at the Robotics and Mechatronics group at the University of Twente. This would allow for example for integration in training dummies for clinicians, which would not easily be possible with the the previous set-up. The previous set-up did, however, show to be capable of producing larger SI (around 35 mm versus 14 mm) and AP (around 8 mm versus 2 mm) (Naghibi et al., 2018). The motion that can be generated by the soft robotics diaphragm was, however, still a larger motion than results found for another comparable device where test with human livers were done. AP and SI motion were respectively 1 mm and 11 mm there.

6.2 Recommendations for future work

Based on the discussion of the requirements that was done previously and the comparison with other devices several recommendations for future work can be done. AP motion can be improved in the future. This can be done by altering the support of the diaphragm, for example by guiding the rotational/pivoting motion at the bottom with a rail. This would make sure that the support of the diaphragm is fixed in sideways directions. Another possibility to improve the AP motion is by adjusting the diaphragm. There are several possibilities that can be looked at:

- Adjust the vacuum actuators such they can generate more force. Making the area of the vacuum actuators bigger should help achieving this

- Adjust the design of the pneumatic bending actuators. If the wall-thickness of the air-chambers is increased more pressure can be applied to them, which might allow for more force to be generated
- Making the diaphragm lighter. The thickness of the diaphragm is currently 5 mm. When this is decreased the diaphragm will become lighter. This means gravity will have less influence on the diaphragm. It will, however, also lead to a less rigid diaphragm, hence the actual implications of this design choice will be hard to predict.

Another thing that can be worked on is a graphical user interface with the Arduino from a computer. This will allow for a more user friendly experience.

What should also be improved in the future is the rigidity of the stand, because when fast breathing is simulated oscillation can be seen. This is probably partially due to the elasticity of the diaphragm, but probably also due to the flexibility of the stand.

Something else that still needs to be addressed is testing with longer pneumatic tubes, because in an MRI the pressure regulators need to be a few meters away from the diaphragm. This will cause some delay between the pressure regulators changing the pressure and an actual pressure change in the actuators. This on itself does not have to be an issue, since only feedforward control is used. What can cause issues is that pressure waves can start to arise in the pneumatic tubes, causing the pressure in the actuators to be different than expected.

Also something that can be looked into is the influence of different loads on the motion of the diaphragm and perhaps how to take that into account in the model and controller. Different loads can be different weights of liver phantoms, different ways of hanging/supporting the liver phantom, but for example also the effect of the insertion of a needle. They will most likely all influence the motion, but the effects are not known yet.

In the model potential improvements can also be made. During characterization hysteresis has been completely neglected. It is estimated that hysteresis only causes a deviation of about 1 mm in SI direction and 0.5 mm in AP direction, incorporating this into the model might still improve the accuracy of the predicted motion of the models.

Lastly, different motion profiles should still be tested. It is shown that the diaphragm can move a liver phantom reasonably well, such that it can follow a sine setpoint, but other motions have not been tested. Although it is assumed that as long as motion up to 11.9 mm in SI direction and the frequency is not higher than 0.3 Hz, it should be able to achieve that motion. Hence it should be possible to simulate patient specific respiratory motion, but this has not been tested yet.

6.3 Answers to the research questions

6.3.1 How to develop an MR compatible liver phantom that is actuated by a bio-inspired diaphragm to simulate respiratory-induced motion?

The main research question will be answered by answering the following sub questions.

6.3.2 How can the device be made MR compatible?

This can be done by choosing the right materials. By choosing pneumatically actuated soft robotic actuators there is no need for metal in the device. Also the support of the diaphragm and the liver phantom can be made from materials that are MR compatible. Next to that dimensions are such that the device should fit within an MR scanner.

6.3.3 How can the diaphragm be inspired by the human anatomy?

By looking at the function of the human diaphragm the mechanism used for the motion of the diaphragm can be determined. When actuators are chosen that can replicate this mechanism a soft robotics diaphragm incorporating those actuators can be made that can replicate this motion of the diaphragm. Two different states of the diaphragm can be identified, the flat state (inhalation) and the dome state (exhalation). Where the flattening is done by the costal muscles and the dome shape is reached because of the elasticity of the lungs. Also the ribcage helps in the respiratory motion, but this is for this project neglected.

6.3.4 What kind of actuators can be used to develop this diaphragm?

Actuators that have some compliance just like the human diaphragm are desired. For both states that have been identified actuators that enable the diaphragm to go into that state are being used. Bending actuators are used to simulate the elasticity of the lungs and VAMPS are used as the costal muscles, which contract.

6.3.5 How can a realistic respiratory motion be generated?

By characterizing the behaviour of every actuator on the diaphragm a controller is made that allows the soft robotics diaphragm to move a liver phantom in a realistic way. It is able to follow a set-point which can be altered to simulate different respiration from different patients.

6.3.6 How can the device be made useful for testing purposes of robotic systems and for training purposes of doctors/surgeons?

The motion of the liver needs to be realistic such that it is comparable to a real patient. The device itself should also fit inside an MR scanner.

7 Appendix

7.1 Schematic drawings of actuators

The following figures are schematic drawings of the actuators that were designed. The drawings of VAMP version 2 and the PAM are left out, because VAMP version 2 did not work and for the PAM only a mold has been drawn. All dimensions are given in millimetres.

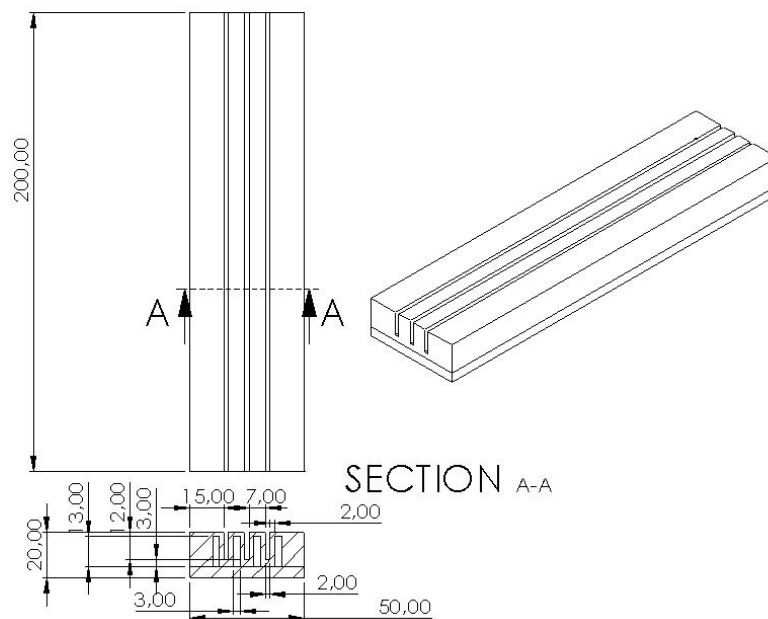


Figure 7.1: Schematic drawing of the designed Pneunet bending actuator with most important design parameters. All dimensions are in millimetres

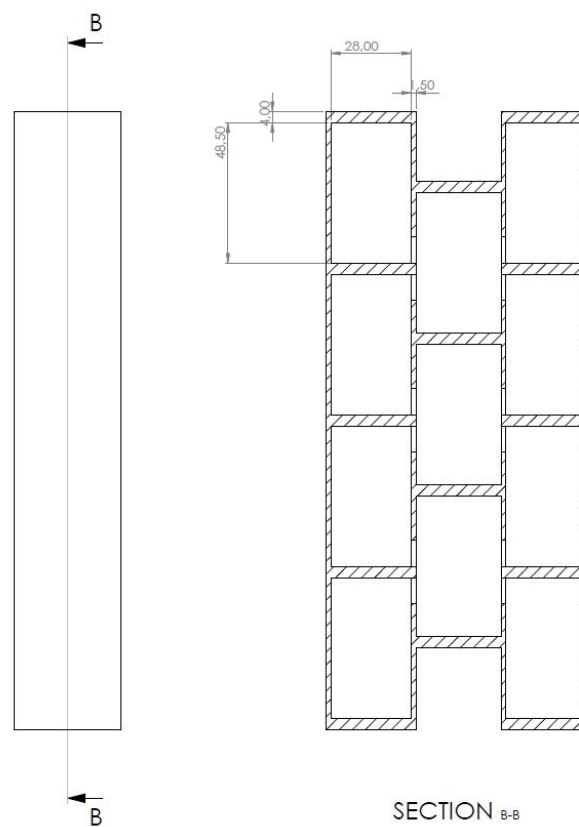
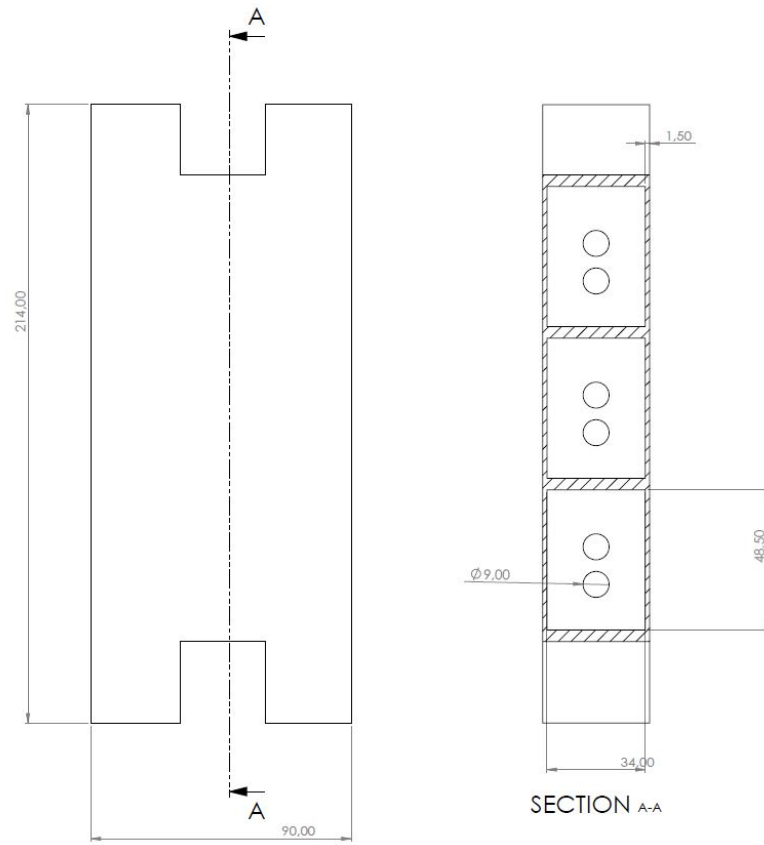


Figure 7.2: Schematic drawing of version 1 of the VAMP actuator

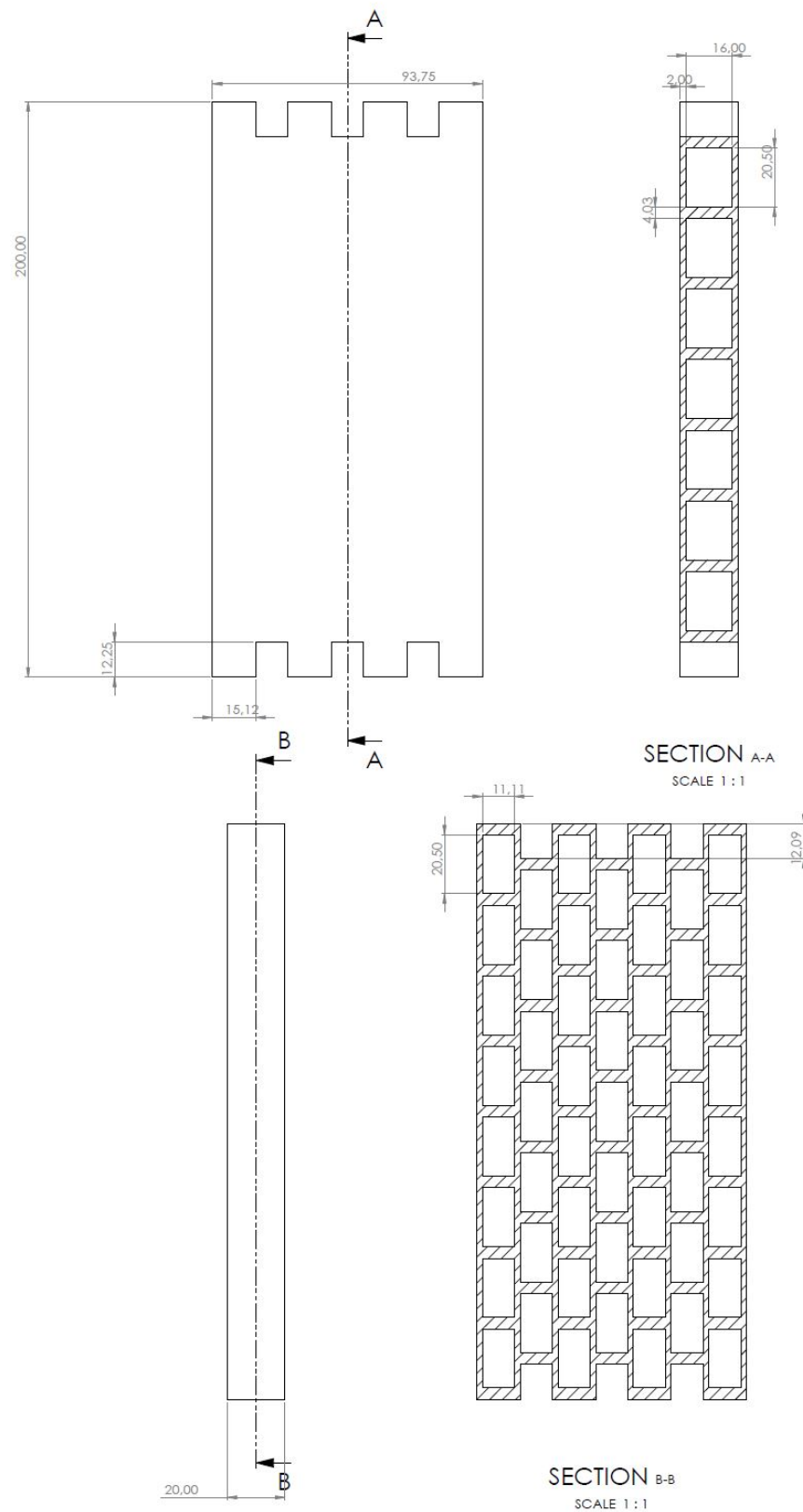


Figure 7.3: Schematic drawing of version 2 of the VAMP actuator

7.2 Code in the 20-sim controllers

7.2.1 Controller 1

```

constants
real    maxpregbending=2;// Maximum specified pressure in
        bar
real    maxpregmuscle=2;// Maximum specified pressure in
        bar
real    maxpregvacuum=-1;// Maximum specified pressure in
        bar
real    maxvregbending=255;// Maximum in arduino, 5V is 10V
        on the regulator
real    maxvregmuscle=255;// Maximum in arduino, 5V is 10V
        on the regulator
real    maxvregvacuum=255;// Maximum in arduino, 5V is 10V
        on the regulator
real    maxpbending=0.14; //Maximum control pressure of
        this regulator in bar
real    maxpvacuum=-1; //Maximum control pressure of this
        regulator in bar
real    maxpmuscle=0.6; //Maximum control pressure of this
        regulator in bar

variables
real breath_in_time; //Breath in time in seconds
real breath_out_time; //Breath out time in seconds
real max_AP; //maximum AP motion in mm
real max_SI; //maximum SI motion in mm
real SI_neutralc; //calculated neutral position of the
        diaphragm
real SI_control_bending;
real SI_control_vacuum;
real AP_control;
real setpoint_SI;
real setpoint_AP;
real setpoint_AP_degrees;
real slope;
real angle;

equations
//settings/////////
breath_in_time=2.5;
breath_out_time=2.5;
max_AP=4;
max_SI=8;

angle=setpoint_AP_degrees;
//////////

//AP Profile//////////

```

```

setpoint_AP=sin (time*pi/(breath_in_time/2+breath_out_time
/2))*max_AP/2+max_AP/2+1; // this is in mm from neutral
at 0 degree angle
setpoint_AP_degrees= -0.33*(setpoint_AP)^2 + 3.4888*
setpoint_AP; // this is in degrees
AP_control=0.0943*setpoint_AP_degrees - 0.3982; //this
needs to be in bar
//////////

//Position and characteristics calculation/////
SI_neutralc=-0.063*angle^2-0.306*angle;
slope=0.405*angle^2-6.9187*angle+65.497;
//////////

//SI Profile//////////
setpoint_SI=-sin (time*pi/(breath_in_time/2+breath_out_time
/2))*max_SI/2-(max_SI/2)-3; //This is in mm from
neutral at 0 degree angle
SI_control_bending=(setpoint_SI-SI_neutralc)/slope; //why
the factor two??
SI_control_vacuum=(setpoint_SI-SI_neutralc)/slope;
//////////

//Output

V_muscle=limit (AP_control,0,maxpmuscle)/maxpregmuscle*
maxvregmuscle; //first control this for the AP motion,
then control SI to get the desired motion
V_bending=limit (SI_control_bending,0,maxpbending)/
maxpregbending*maxvregbending; //
V_vacuum=limit (SI_control_vacuum, maxpvacuum ,0)/
maxpregvacuum*maxvregvacuum; //

```

7.2.2 Controller 2

```

constants
real    maxpregbending=2; // Maximum specified pressure in
bar
real    maxpregmuscle=2; // Maximum specified pressure in
bar
real    maxpregvacuum=-1; // Maximum specified pressure in
bar
real    maxvregbending=255; // Maximum in arduino, 5V is 10V
on the regulator
real    maxvregmuscle=255; // Maximum in arduino, 5V is 10V
on the regulator
real    maxvregvacuum=255; // Maximum in arduino, 5V is 10V
on the regulator
real    maxpbending=0.14; //Maximum control pressure of
this regulator in bar

```

```

real    maxpvacuum=-1; //Maximum control pressure of this
        regulator in bar
real    maxpmuscle=0.6; //Maximum control pressure of this
        regulator in bar

//set pam first then bend then vacuum

variables
real breath_in_time; //Breath in time in seconds
real breath_out_time; //Breath out time in seconds
real max_AP; //maximum AP motion in mm
real max_SI; //maximum SI motion in mm
real SI_neutralc; //calculated neutral position of the
        diaphragm
real Muscle_control;
real Vacuum_control;
real Bending_control;
real setpoint_SI;
real setpoint_AP;

equations
//settings ///////////
breath_in_time=2.5;
breath_out_time=2.5;
max_AP=4;
max_SI=8;

////////////////////

//SI Profile ///////////
setpoint_SI=-sin(time*pi/(breath_in_time/2+breath_out_time
        /2))*max_SI/2-(max_SI/2)+2; //This is in mm from
        neutral at 0 degree angle
//Bending_control=setpoint_SI/29.888
Muscle_control=setpoint_SI/-12.628;
if Muscle_control > maxpmuscle then
Vacuum_control= 0.0122*(setpoint_SI-limit(Muscle_control,0,
        maxpmuscle)*-12.628);
else
Vacuum_control=0;
end;

//Vacuum_control=0.1;

Bending_control=setpoint_SI/29.888;
////////////////////

```

```

//AP Profile////////////////////
//setpoint_AP= ;// this is in mm from neutral at 0 degree
    angle
//AP_control=; //this needs to be in bar
////////////////////////////////////

//Position and characteristics calculation/////
//SI_neutralc=;

////////////////////////////////////

//Output

V_muscle=limit(Muscle_control,0,maxpmuscle)/maxpregmuscle*
    maxvregmuscle; //first control this for the AP motion,
    then control SI to get the desired motion
V_bending=limit(Bending_control,0,maxpbending)/
    maxpregbending*maxvregbending; //abs(sin(time)*0.14);
V_vacuum=limit(Vacuum_control, maxpvacuum ,0)/maxpregvacuum
    *maxvregvacuum; //abs(sin(time)*0.1);

```


Bibliography

- (2008), Using MRI Safely - ismrm.
http://www.ismrm.org/smrt/files/20081210_Dutch_Guidelines_on_MR_Safety.pdf
- (2018), PneuNets Bending Actuators.
<https://softroboticstoolkit.com/book/pneunets-bending-actuator>
- Abayazid, M., T. Kato, S. G. Silverman and N. Hata (2018), Using needle orientation sensing as surrogate signal for respiratory motion estimation in percutaneous interventions, **vol. 13**, no.1, pp. 125–133, ISSN 1861-6429, doi:10.1007/s11548-017-1644-z.
<https://doi.org/10.1007/s11548-017-1644-z>
- Agarwal, G., N. Besuchet, B. Audergon and J. Paik (2016), Stretchable materials for robust soft actuators towards assistive wearable devices, *Scientific reports*, **vol. 6**, p. 34224.
- Bray, F., J. Ferlay, I. Soerjomataram, R. L. Siegel, L. A. Torre and A. Jemal (2018), Global Cancer Statistics 2018: GLOBOCAN Estimates of Incidence and Mortality Worldwide for 36 Cancers in 185 Countries, *CA: a cancer journal for clinicians*.
- Chou, C.-P. and B. Hannaford (1996), Measurement and modeling of McKibben pneumatic artificial muscles, **vol. 12**, no.1, pp. 90–102.
- Chouker, A., A. Martignoni, M. Dugas, W. Eisenmenger, R. Schauer, I. Kaufmann, G. Schelling, F. Löhe, K.-W. Jauch, K. Peter et al. (2004), Estimation of liver size for liver transplantation: the impact of age and gender, **vol. 10**, no.5, pp. 678–685.
- Daerden, F. and D. Lefeber (2002), Pneumatic artificial muscles: actuators for robotics and automation, **vol. 47**, no.1, pp. 11–21.
- Faudzi, A. A. M., J. Ooga, T. Goto, M. Takeichi and K. Suzumori (2018), Index finger of a human-like robotic hand using thin soft muscles, **vol. 3**, no.1, pp. 92–99.
- Fischer, H., B. Vogel and A. Welle (2004), Applications of shape memory alloys in medical instruments, **vol. 13**, no.4, pp. 248–253.
- Holton, A., E. Walsh, A. Anayiotos, G. Pohost and R. Venugopalan (2002), Comparative MRI Compatibility of 316L Stainless Steel Alloy and Nickel–Titanium Alloy Stents: Original article Technical, **vol. 4**, no.4, pp. 423–430.
- Hu, Y., Y.-K. Zhou, Y.-X. Chen and Z.-C. Zeng (2017), Magnitude and influencing factors of respiration-induced liver motion during abdominal compression in patients with intrahepatic tumors, **vol. 12**, no.1, p. 9.
- Jani, J. M., M. Leary, A. Subic and M. A. Gibson (2014), A review of shape memory alloy research, applications and opportunities, *Materials & Design (1980-2015)*, **vol. 56**, pp. 1078–1113.
- Kitamura, K., H. Shirato, Y. Seppenwoolde, T. Shimizu, Y. Kodama, H. Endo, R. Onimaru, M. Oda, K. Fujita, S. Shimizu et al. (2003), Tumor location, cirrhosis, and surgical history contribute to tumor movement in the liver, as measured during stereotactic irradiation using a real-time tumor-tracking radiotherapy system, **vol. 56**, no.1, pp. 221–228.
- Kratzer, W., V. Fritz, R. A. Mason, M. M. Haenle, V. Kaechele and R. S. Group (2003), Factors affecting liver size: a sonographic survey of 2080 subjects, **vol. 22**, no.11, pp. 1155–1161.
- Lee, S.-L., A. Chung, M. Lerotic, M. A. Hawkins, D. Tait and G.-Z. Yang (2010), Dynamic shape instantiation for intra-operative guidance, in *International Conference on Medical Image Computing and Computer-Assisted Intervention*, Springer, pp. 69–76.
- Li, S., D. M. Vogt, D. Rus and R. J. Wood (2017), Fluid-driven origami-inspired artificial muscles, *Proceedings of the National Academy of Sciences*, p. 201713450.

- Marchese, A. D., R. K. Katzschmann and D. Rus (2015), A recipe for soft fluidic elastomer robots, **vol. 2**, no.1, pp. 7–25.
- Marieb, E. N. and K. Hoehn (2007), *Human anatomy & physiology*, Pearson Education.
- Müller, S., L. Maier-Hein, A. Mehrabi, F. Pianka, U. Rietdorf, I. Wolf, L. Grenacher, G. Richter, C. Gutt, J. Schmidt et al. (2007), Creation and establishment of a respiratory liver motion simulator for liver interventions, **vol. 34**, no.12, pp. 4605–4608.
- Nagasue, N., H. Yukaya, Y. Ogawa, H. Kohno and T. Nakamura (1987), Human liver regeneration after major hepatic resection. A study of normal liver and livers with chronic hepatitis and cirrhosis., **vol. 206**, no.1, p. 30.
- Naghibi, H., P. A. C. Costa and M. Abayazid (2018), A Soft Robotic Phantom to Simulate the Dynamic Respiratory Motion of Human Liver, in *2018 7th IEEE International Conference on Biomedical Robotics and Biomechatronics (Biorob)*, pp. 577–582, ISSN 2155-1782, doi:10.1109/BIOROB.2018.8488115.
- Obiajulu, S. C., E. T. Roche, F. A. Pigula and C. J. Walsh (2013), Soft pneumatic artificial muscles with low threshold pressures for a cardiac compression device, in *ASME 2013 International Design Engineering Technical Conferences and Computers and Information in Engineering Conference*, American Society of Mechanical Engineers, pp. V06AT07A009–V06AT07A009.
- Pickering, M. and J. F. Jones (2002), The diaphragm: two physiological muscles in one, **vol. 201**, no.4, pp. 305–312.
- Pritts, M. B. and C. D. Rahn (2004), Design of an artificial muscle continuum robot, in *Robotics and Automation, 2004. Proceedings. ICRA'04. 2004 IEEE International Conference on*, volume 5, IEEE, pp. 4742–4746.
- Rohlfing, T., C. R. Maurer Jr, W. G. O'dell and J. Zhong (2004), Modeling liver motion and deformation during the respiratory cycle using intensity-based nonrigid registration of gated MR images, **vol. 31**, no.3, pp. 427–432.
- Shirato, H., Y. Seppenwoolde, K. Kitamura, R. Onimura and S. Shimizu (2004), Intrafractional tumor motion: lung and liver, in *Seminars in radiation oncology*, volume 14, Elsevier, pp. 10–18.
- Sun, Y., Y. S. Song and J. Paik (2013), Characterization of silicone rubber based soft pneumatic actuators, in *2013 IEEE/RSJ International Conference on Intelligent Robots and Systems*, Ieee, pp. 4446–4453.
- Suzumori, K., S. Endo, T. Kanda, N. Kato and H. Suzuki (2007), A bending pneumatic rubber actuator realizing soft-bodied manta swimming robot, in *Robotics and Automation, 2007 IEEE International Conference on*, IEEE, pp. 4975–4980.
- Suzumori, K., S. Iikura and H. Tanaka (1992), Applying a flexible microactuator to robotic mechanisms, **vol. 12**, no.1, pp. 21–27.
- Szold, A. (2006), Nitinol: shape-memory and super-elastic materials in surgery, **vol. 20**, no.9, pp. 1493–1496.
- Tondu, B. (2012), Modelling of the McKibben artificial muscle: A review, **vol. 23**, no.3, pp. 225–253.
- Trimmer, B. A., A. E. Takesian, B. M. Sweet, C. B. Rogers, D. C. Hake and D. J. Rogers (2006), Caterpillar locomotion: a new model for soft-bodied climbing and burrowing robots, in *7th International Symposium on Technology and the Mine Problem*, volume 1, Monterey, CA: Mine Warfare Association, pp. 1–10.
- Trivedi, D., C. D. Rahn, W. M. Kier and I. D. Walker (2008), Soft robotics: Biological inspiration, state of the art, and future research, **vol. 5**, no.3, pp. 99–117.
- Troyer, A. D. and T. A. Wilson (2016), Action of the diaphragm on the rib cage, **vol. 121**, no.2, pp. 391–400.

- Tsekos, N. V., E. Christoforou and A. ÖZCAN (2008), A general-purpose MR-compatible robotic system: implementation and image guidance for performing minimally invasive interventions, **vol. 27**, no.3, p. 51.
- Verma, S. K., K. McClure, L. Parker, D. G. Mitchell, M. Verma and D. Bergin (2010), Simple linear measurements of the normal liver: interobserver agreement and correlation with hepatic volume on MRI, **vol. 65**, no.4, pp. 315–318.
- Wolf, D. C. (1990), Evaluation of the size, shape, and consistency of the liver.
- Yang, D., B. Mosadegh, A. Ainla, B. Lee, F. Khashai, Z. Suo, K. Bertoldi and G. M. Whitesides (2015), Buckling of elastomeric beams enables actuation of soft machines, **vol. 27**, no.41, pp. 6323–6327.
- Yang, D., M. S. Verma, J.-H. So, B. Mosadegh, C. Keplinger, B. Lee, F. Khashai, E. Lossner, Z. Suo and G. M. Whitesides (2016), Buckling pneumatic linear actuators inspired by muscle, **vol. 1**, no.3, p. 1600055.
- Yap, H. K., F. Sebastian, C. Wiedeman and C.-H. Yeow (2017), Design and characterization of low-cost fabric-based flat pneumatic actuators for soft assistive glove application, in *Rehabilitation Robotics (ICORR), 2017 International Conference on*, IEEE, pp. 1465–1470.
- Yu, N. and R. Riener (2006), Review on MR-compatible robotic systems, in *Biomedical Robotics and Biomechatronics, 2006. BioRob 2006. The First IEEE/RAS-EMBS International Conference on*, IEEE, pp. 661–665.